Finite Element Analysis of the Wind - Uplift Resistance of Roof Edge Components

Maha Dabas

A Thesis submitted to

The Faculty of Graduate and Postdoctoral Studies

in partial fulfillment of the

thesis requirements for the degree of

Master of Applied Science

in

Civil Engineering

Department of Civil Engineering

University of Ottawa

March 2013

Abstract

Wind-induced damages on low-slope roofs are a major and common problem that many buildings located in high wind areas suffer from. Most of these damages are initiated when the metal roof edge fails first, leading to overall roof failure. This is because peak wind pressures occur at the edges and corners of low-slope roof buildings. Currently, there are not enough wind design guidelines for the Canadian roofing community to quantify the dynamic wind uplift resistance of the roof edge system. The objective of this research is to evaluate the effect of wind-induced loads on roof edges using a finite element model, verify the numerical results with those obtained from controlled experiments, and perform parametric investigations for various design variables. In this research, the overall roof edge system was modelled using the commercial finite element software package ABAQUS, by simulating the roof edge system with shell elements and applying a uniform static pressure against the face of the edge cleat or coping. Results of the modelling were compared to the experimental ones in terms of deflection of the coping under uniform pressure. The results of the numerical model and the experiments show a good agreement. Furthermore, a parametric analysis of the system was conducted under the effect of varying parameters. i.e., coping gauge, nail spacing, coping and cleat length and wind and thermal load application.

Acknowledgements

I would like to give special thanks to my supervisor Dr. Beatriz Martin-Pérez for her guidance, valuable feedback and patience throughout writing this thesis. This thesis is a better work thanks to her supervision.

I would like to acknowledge my co-supervisor Dr. Bas Baskaran for giving me the opportunity to be part of the team group at the National Research Centre (NRC). Also, special thanks to the sponsoring organizations.

I would like to express my sincere thanks to the thesis examiners Dr. Magdi Mohareb and Dr. Neal M. Holtz for taking the time to review my thesis and for their valuable comments and feedback. In addition, special thanks to Dr. Rennie Colin, the defence chair.

I would like to dedicate this thesis to my beloved father, M. Zouhair. There are no words to thank him enough for his unending love, support and encouragement. His guidance is with me in whatever I pursue. I am forever grateful to my beloved husband, Mouhcine Guennoun, for his continuous encouragement, love, understanding and valuable advices. This thesis would not have been possible without him. I am truly blessed to have the two in my life.

Table of Contents

List of Tables

List of Figures

List of Acronyms

ANSI	American National Standard Institute
ASCE	American Association of Civil Engenderers
CBC	Canadian Broadcasting Corporation
DOFs	Degrees Of Freedom
FEM	Finite Element Modelling
FM	Factory Mutual
O.C	On-Centre
NRCC	National Research Council of Canada
RCABC	Roofing Contractors Associations of British Columbia
REST	Roof Edge Systems and Technologies
RE-1 to 3	Experimental tests according ANSI/SPRI/FM 4435/ES-1
RICOWI	Roofing Industry Committee on Weather Issues
RPM	Roofing Practices Manual
SMACNA	Sheet Metal and Air Conditioning Contractors National Association
SPRI	Single Ply Roofing Industry
CSA123.21-10	Standard test method for the dynamic wind-uplift resistance of membrane-roofing systems

List of Symbols

F_1	Horizontal outward force
F_2	Uplift force
P	Wind pressure
GC_p	External pressure coefficient
C_p	Pressure coefficient
Q_{zf}	Field of roof pressure at height z
U	Displacement
θ	Angle of rotation
F_N	Reaction force
E	Young's Modulus
H_b	The back height of the coping
H_f	The front height of the coping
W_{cl}	The cleat width
H_{cl}	The cleat height
L	Length
L_{cop}	The coping length
W_{co}	The coping width
ΔP	Pressure difference
V	Velocity
ρ	Density
ΔT	Temperature change
δ_{max}	Maximum deflection
S4	4-nodes shell elements
T3D2	Three dimensional truss element of two nodes
N	Mesh size
C	Compressive forces
Q	Frictional forces
A_t	Tributary area
f_s	Nail spacing
k	Normalized nail force

Chapter 1 **Introduction**

1.1 Background

A roof edge system is comprised of a coping plate covering a cleat plate, both of which are nailed to the roof parapet using a group of single row of nails, Figure 1.1. The coping and cleat plates are connected at the bottom edge of the vertical plates by a drip-edge connection that sheds water away from the building. The roof edge acts as an effective termination and transition between the roof and other building membranes (Baskaran 2011). The roof edge is a significant roof component that protects the roof area against high-wind pressure and from moisture infiltration.

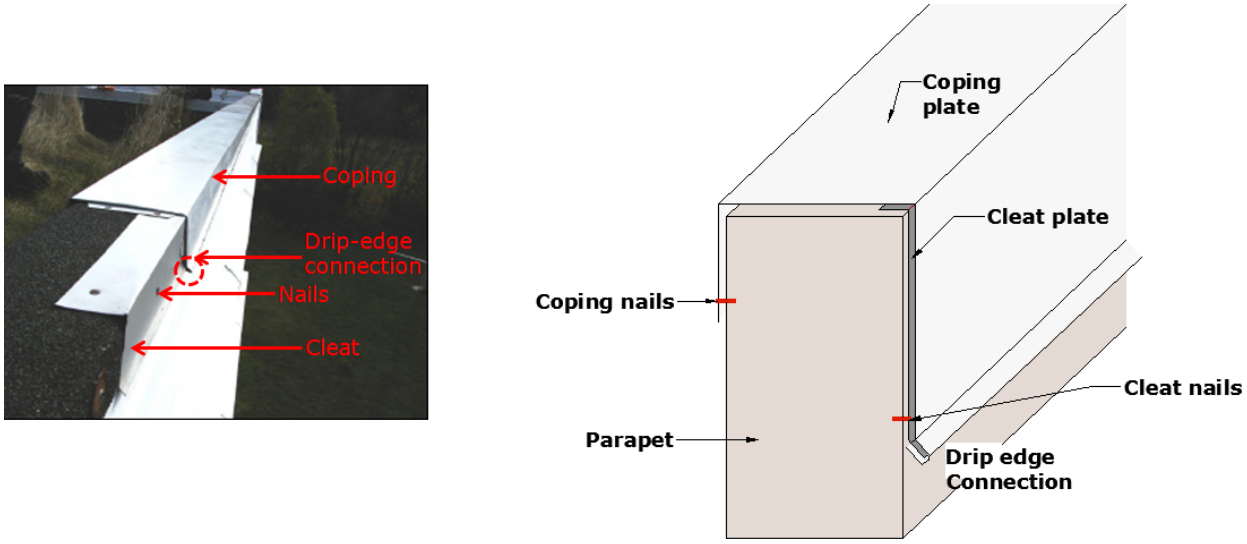

Figure 1.1 Left: An overall view of the roof edge system (reproduced from Baskaran 2011), Right: drawing of the roof edge system

Several regions in Canada experience high wind pressures from storms and even hurricanes. These extreme wind conditions are devastating to building structures, blowing off roofs and toppling buildings under construction. In 2004 and 2005, US incurred total losses of 45 and 115

billion dollars respectively due to hurricane damages. One of those hurricanes was Hurricane Charley with the highest wind speed and severe damages that resulted in 15 billion losses across Florida and South Carolina areas (Baskaran 2007). In November of 2006 a major storm of 62 mph (100 km/h) wind speed hit British Columbia, blowing roofs off buildings and causing severe damage to hydro lines. In addition, in 2007, a major storm in Alberta with wind speeds of 75 mph (120 km/h) damaged homes and other structures. And most recently, in October of 2012, Hurricane Sandy caused severe damage to building roofs, both to the roof envelope and overall roof collapses (CBC News 2012). In addition, Hurricane Sandy caused severe damage to hydro lines, toppled large trees and most importantly caused the loss of lives in both Canada and the U.S (CBC News 2012).

Damage to roof components, particularly roof edges, results from improperly installed or insufficiently designed systems. According to an FM (Factory Mutual) global loss study, it is estimated that 59% of losses on roofs are attributed to the failure of the roof perimeter (SPRI 2011). In addition, the Roofing Industry Committee on Weather Issues (RICOWI) found that most roof damage in Florida in the U.S. occurred due to roof edge failures. Failures occurred when the roof edge components of flashing and nails failed to resist the wind uplift pressures leading to a progressive failure (CRCA 2007).

Since each roof component contributes to the resistance to the wind uplift forces, all roof components must remain connected for the roofing system to remain in place and be durable. When the wind-induced pressures are higher than the resistance of any component, failure occurs. Failure of the roof edge under the effect of high wind-induced pressures exposes the roof structure to the environmental elements and leaves them susceptible to failure. The roof membrane, perimeter flashing (usually an L shaped metal sheet installed at the roof edges),

parapet coping (metal sheet enveloping the parapet) blow off under high wind pressures on low-slope roofs, as illustrated in Figure 1.2 and Figure 1.3. This is due to the highly fluctuating nature of wind pressures and high pressure peaks near the roof ridges and corners. The highest wind loads on low-slope roofs are attributed to suction (negative pressure) on the roof (Holmes 2001). Suction forces on roof edge are comprised of an uplift force on the top (F_2 in Figure 1.4) and a horizontal outward force (F_1 in Figure 1.4).

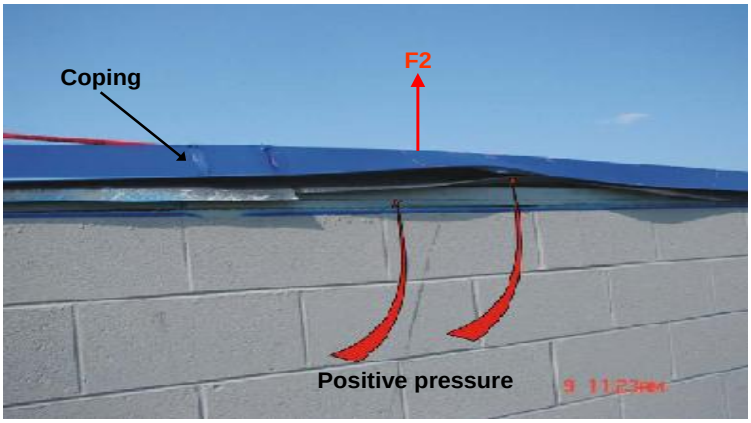

Figure 1.2 Severe deformation of the coping and cleat due to wind uplift forces (reproduced from Baskaran 2011)

Figure 1.3 Pull-out of the nail and deformation around the nail area (reproduced from Baskaran 2011)

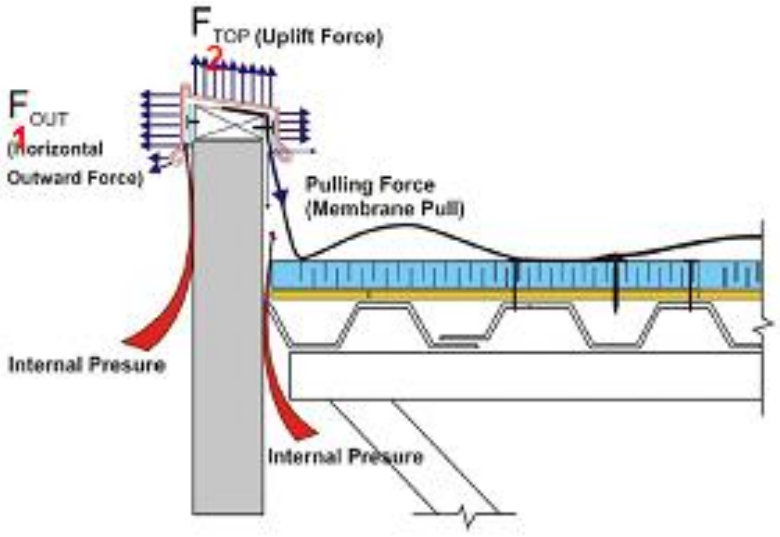

Figure 1.4 Wind induced loads on roof edge (reproduced from Baskaran 2011)

The horizontal outward force F_1 and wind uplift force F_2 can cause severe damage to the roof edge. This leaves the interior wall and roof structure of the building exposed to the weather elements. Water infiltration into the interior structure can cause water stains, corrosion and mold, slowly deteriorating the structural components of the roof. The main damage observed on roof edges caused by F_1 and F_2 are:

- Lifting of the coping,
- Deformation of the coping and cleat,
- Deformation of the coping and cleat around the nail,
- Nail pull-out failure, and,
- Deformation around the nail area.

Although roof edge damage and failure due to wind-induced loads is a common problem that many low-slope roof buildings suffer from, there is a lack of guidelines for the Canadian roofing industry to aid in the design of roof edges.

1.2 Objectives and Scope

To address the lack of evaluation standards or design procedures available to the Canadian roofing community to quantify the dynamic wind uplift resistance of the roof edge, a research partnership supported by NSERC was built between NRCC, roofing industries (SOPREMA Inc., RCABC, Menzies Metal Products, Firestone Building Products) and the University of Ottawa. Under this partnership the research team refers to the roof edge system as Roof Edge System & Technologies (REST). The aim of the partnership was to quantify the performance of roof edges both experimentally and numerically, and to establish an acceptable wind uplift standard for roof edges. The mandate of the project has been carried out through three tasks: (i) Task 1 - Experimental investigation; (ii) Task 2 - Developing a numerical model using finite-element analysis; and, (iii) Task 3 - Development of wind design guide and standards. The objective of this study is to model and predict the roof edge behaviour under wind-induced loads, and thus it falls within Task 2 in the project described above. This is achieved by analyzing the roof edge system using finite element modelling, verifying numerical results with those obtained from experimental tests (Task 1), and conducting a parametric analysis of important design variables. Thus, specific objectives of this thesis are:

- Develop a numerical model using the ABAQUS finite element software for two roof edge configurations: continuous cleat configuration (also known as on-site-fabricated) and discontinuous cleat configuration,
- Evaluate the effect of static wind-induced loads on the roof edge system using the finite element model,
- Validate the finite element model results with experimental ones; and,

- Perform a parametric analysis of the effect of various design variables, such as coping plate thickness and depth, nail spacing, and plate length on the roof edge performance.

1.3 Research Significance

Due to lack of guidelines for the roofing industry to design roof edges, it is very important to establish a comprehensive study that quantifies the wind uplift resistance of roof edges and determines the optimal system performance under variable conditions. This is to protect the public welfare against wind-induced loads that threaten insufficiently-designed roof edges, since a roof edge failure may potentially lead to an overall roof failure. Thus, the results of this study can contribute to establish new design guidelines for roof edges, which could be added to the CSA123.21-10 (Standard test method for the dynamic wind uplift resistance of membrane-roofing systems).

1.4 Thesis Outline

Chapter 2 presents a literature review of the wind effects on low-slope roofs, existing design guidelines for roof edges, and previous numerical modelling of metal edge flashings. In Chapter 3, a finite element model for roof edges is developed to predict the system behaviour under the effect of variable conditions and to determine the optimal system performance subject to wind-induced loads.

Chapter 4 presents the validation of the finite element model by comparing numerical results to those obtained in experimental tests conducted at the National Research Council of Canada (NRCC).

Chapter 5 presents a parametric analysis of the effect of several design variables on the performance of roof edges subjected to static wind-induced pressures. In addition, a brief thermal

analysis is presented to determine the effects of temperature changes on roof edge performance. Finally, the results of parametric analyses are summarized in preliminary design curves of the roof edge.

To close, Chapter 6 presents conclusions obtained from this study and recommendations for future work.

Chapter 2 **Literature Review**

2.1 Introduction

This chapter presents a brief overview of wind effects on low-slope roof buildings and wind loads on roof edge. An overview of the current roof edge systems standards and guidelines available for the roofing industry is presented and it includes the ANSI/SPRI/FM 4435/ES-1 and the Roofing Contractors Associations of British Columbia (RCABC) guidelines. It further reviews most of the available publications relevant to the topic of finite element analysis of a roof edge system. Finally, Section 2.6 addresses the existing gap in analysis and design procedures for roof edge.

2.2 Wind Effect on Low-Slope Roof Buildings

A low slope building is subjected to a steady air flow that separates at the sharp corners and edges of the structure. This is contrary to a stream type of flow where the air flow follows the contours of the structure. The separated air flow region is divided into a thin region of high shear and vortices called the free shear layer. These layers are unstable and will roll up towards the wake and create concentrated vortices. The layers will remain unstable but will reattach to the surface and form vortices along the flat surface of the rectangular building, Figure 2.1. At the upstream region, the air flow, velocity accelerates as it deflects upwards which creates a region of locally increased pressure; while the separation of the air flow downstream creates a region of locally low pressure along the roof surface. This pressure difference exerts on a structure a force of two components. One component force is perpendicular to the structure (lift force) and the second component is a parallel to structure (drag force).

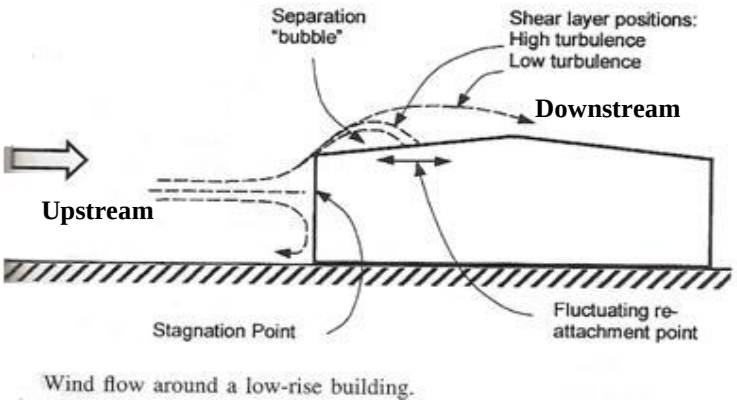

Figure 2.1 Wind flow around a low-slope roof (reproduced from Holmes 2001)

Moreover, for a rectangular building, the stagnation point (the point at which the air velocity is equal to zero) divides the structure into two regions: an upstream and a downstream region. At the upstream region the air flow is of positive velocities and high pressure, while at the downstream region there are negative velocities and low pressure, which indicates that a flow separation "bubble" has occurred, Figure 2.1. The flow of low pressure draws the vortices downstream. Therefore, wind pressures vary with both time and space along the roof surface.

From full-scale measurements on low-slope roofs, it has been observed that wind pressures and their responses fluctuate significantly on these structures (Holmes 2001). This is caused by the following:

- Pressure fluctuation induced by upwind turbulent velocity fluctuations,
- Unsteady pressures produced by local vortex shedding and other unsteady flow conditions, in the separated flow regions near sharp corners.

The dynamic wind characteristic of wind pressures consists of static and fluctuating components. The static component is the mean pressure, while the dynamic pressure is the fluctuating vc component and occurs as the random process by which the dominant frequency depends on the frequency of the upstream wind and the geometry of the building. The current study focuses on

the structural analysis of a roof edge system subject to static wind pressures only. For this study, the separation zone is of a significant interest, because it sheds light on the development of peak pressures on roof edge systems, which explains their severe effects on vulnerable roof edge systems.

2.3 Wind Loads on Roof Edges

Wind flow separates at the top of the windward elevation and reattaches further along the roof top, forming a separation zone called a bubble. The separation zone is surrounded by a free shear layer, a region of high velocity gradients and high turbulence. This layer forms vortices that shed downwind and they produce high negative peaks of pressure on the roof edge surface, Figure 2.2.

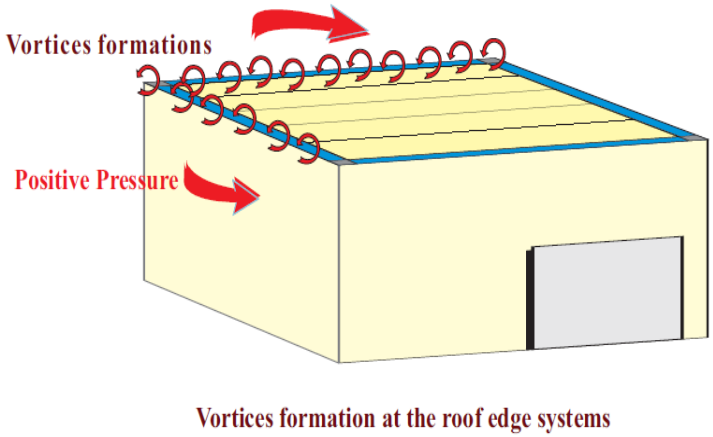

Figure 2.2 Formation of vortices at the separation zone at the roof edge systems (reproduced from Molleti 2012)

Field measurements on the roof edge have recorded peak negative pressures in the pressure separation "bubble" zone at the top elevation of the roof edge system in the vertical and horizontal direction. As a result, they are categorized into F_1 (Horizontal outward force) and F_2 (Uplift force), Figure 1.4 and Figure 2.3. Both F_1 (Horizontal outward force) and F_2 (Uplift force) act as external pressures trying repeatedly to lift the roof edge system components from outside leading to severe damage. Each roof component contributes to the resistance of the wind

uplift force. Hence, all roof components must remain connected for the roofing system to remain in place and to be durable. When the uplift force is higher than the resistance of any component failure occurs. Furthermore, from field measurements of the roof edge, high positive pressures are recognized along the windward direction of the building elevation; although these positive pressures tend to decrease gradually along the top elevation of the building particularly along the parapet elevation of the roof edge system, Figure 2.3. These positive pressures act as internal positive pressures as they leak behind and push against the system components causing further damage as shown in Figure 1.4 and Figure 2.3.

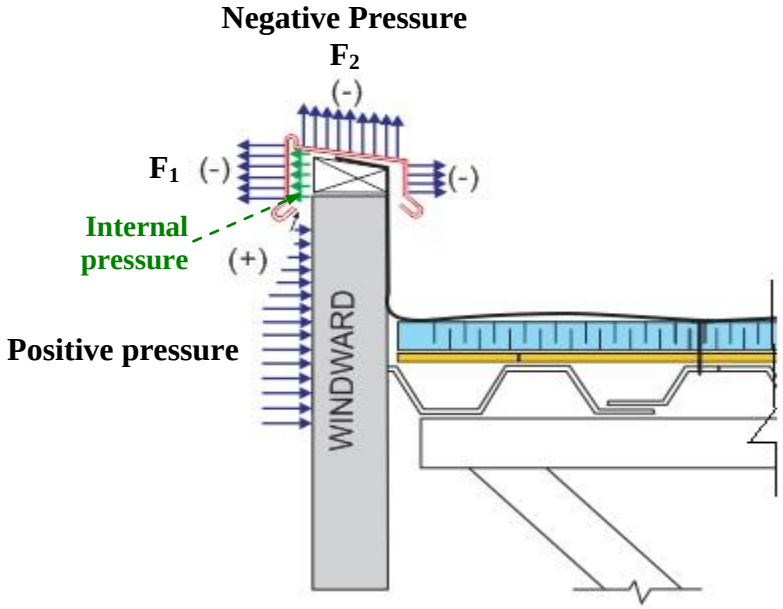

Figure 2.3 Pressure distribution for roof edge systems and technologies (reproduced from Molleti 2012)

The pressure distribution of the roof edge established from field measurements differ from the provisions of wind load application on building parapets specified by the ASCE7-2010. The ASCE7-2010 provides guidelines for the application of wind loads on the parapets of buildings with a height of less than or equal to 160 ft (49 m), as shown in Figure 2.4. This figure shows a positive and uniform distribution of wind pressure P_5 and P_1 (for a flat roof, P_1 is equal to P_5 as

specified in Table 30.7-2 of the ASCE7-2010) along the full elevation of the windward direction of the building. A negative pressure is specified only as a horizontal pressure, P_2.

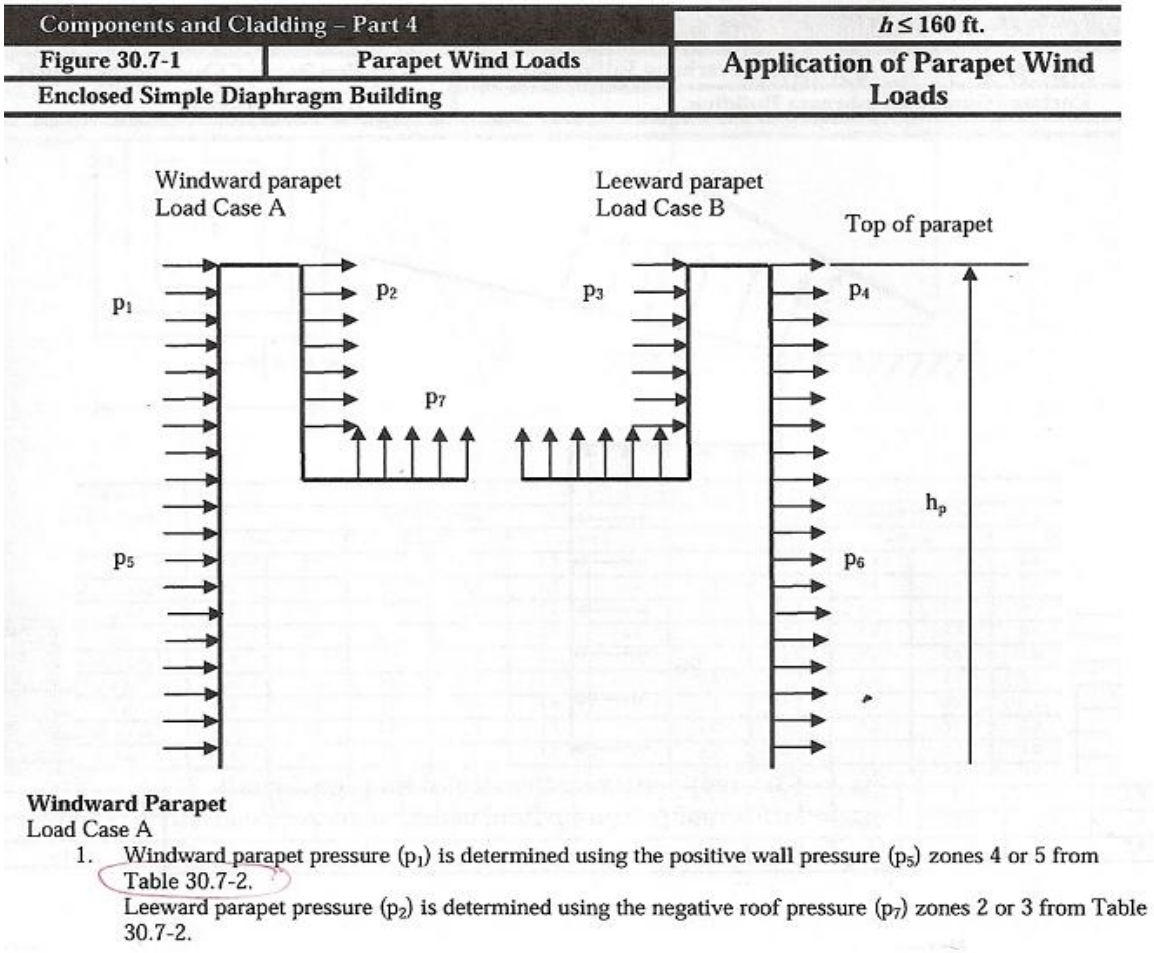

Figure 2.4 Application of parapet wind loads according to ASCE7-10 (ASCE7-2010)

A comparison between Figure 2.3 and Figure 2.4 illustrates the difference in pressure distribution of the roof edge between ASCE07-2010 and field measurements. Field measurements recorded peak negative pressures along the horizontal and vertical directions, F_1 and F_2 respectively. While on the other hand ASCE07-2010 recorded specifies negative pressure only along the horizontal direction, P_2.

2.4 Design Guidelines for Roof Edges

There are several standards available for the roofing industry for the design of roof edge systems. These include the American National Standard Institute (ANSI) Wind Design Standard used for edge system with Low Slope Roofing Systems, Single Ply Roofing Industry (SPRI), Global Mutual (GM) and Roofing Contractors Associations of British Columbia (RCABC).

2.4.1 ANSI/SPRI/FM 4435/ES-1

The wind design standard for edge systems used with low slope roofing systems, ANSI/SPRI/FM 4435/ES-1 (SPRI 2011), gives valuable information about the basic requirements for wind load resistance testing and design of roof edge systems and nails. In addition, it provides information about design requirements of metal sheet material and thickness for low-slope roof edge systems.

For the design of a roof edge system, the applied wind loads on the systems are identified and calculated based on several factors that include wind speed, building height, topography, importance factor, corner and perimeter regions and edge conditions. Subsequently, roof edge systems are tested in accordance with tests RE-1, RE-2 and RE-3, as applicable. Consequently, the resistance and material requirements of roof edge systems are determined. A brief review of the purpose, load application and failure criteria of each tests is presented here; however, detailed information of the three tests including tests set-up are available in the standard. RE-1 test, as illustrated in Figure 2.5, is concerned with testing the resistance of the membrane component of the roof edge system against a uniform tension force that is applied along the length of the membrane. Failure of the membrane is defined by disengagement of the membrane from the system to which it is mechanically attached, such that the tension force exceeds the resistance of the roof edge system.

For the RE-2 test (Figure 2.6), a uniform load is applied incrementally along the length of the vertical component of the roof edge system until failure occurs. Failure of the roof edge system is defined as nail pull out, in addition to excessive deformation that compromises the structural integrity of any component of the system.

RE1.2 Apparatus

The description of the apparatus is general in nature. Any equipment capable of performing the test procedure within the allowed tolerances shall be permitted. A schematic drawing of this apparatus is shown in Figure RE1.1. The test apparatus shall be constructed so that the performance of individual components are unaffected by edge or end constraints on the test sample. Load shall be applied and measured with calibrated load cells, each accurate to within +/-3% of full scale load cell values. Calibration shall be performed annually (minimum) and should be performed and recorded at 5%, 25%, 50%, and 75% of the expected maximum test values.

Re1.3 Safety Precautions

Proper precautions shall be taken to protect the operating personnel and observers in case of any failure.

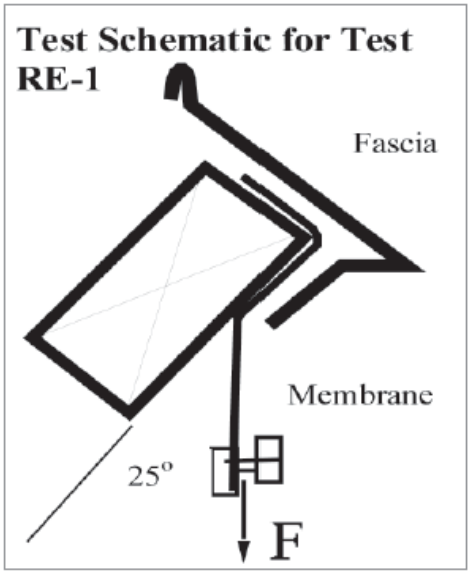

Figure RE1.1

Figure 2.5 Description and sketch of RE-1 test (reproduced from SPRI 2011)

RE-2 Test

Test Method for Dependently or Independently Terminated Edge Systems
(Exposed horizontal component 4 in. (100 mm) or less)

RE2.1 Apparatus

The description of the apparatus is general in nature. Any equipment capable of performing the test procedure within the allowed tolerances shall be permitted. A schematic drawing of this apparatus is shown in Figure RE2.1. The test apparatus shall be constructed so that the performance of individual components are unaffected by edge or end constraints on the test sample. Load shall be applied and measured with calibrated load cells, each accurate to within +/-3% of full scale load cell values. Calibration shall be performed annually (minimum) and should be performed and recorded at 5%, 25%, 50%, and 75% of the expected maximum test values. For exposed horizontal components greater than 4 in. (See Figure RE2.1) Test RE-3 is applicable.

Fascia Blow-Off Test Set Schematic
(Force at Failure x Face Area = Blowoff Resistnace)

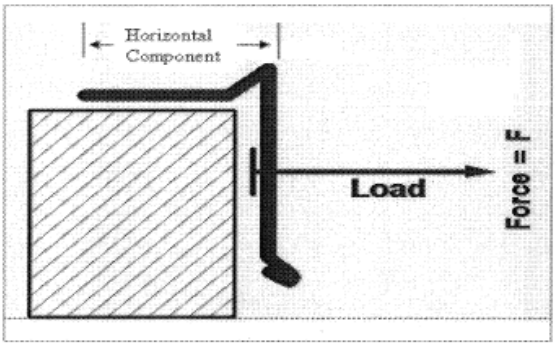

Figure RE2.1

Figure 2.6 Description and sketch of RE-2 test (reproduced from SPRI 2011)

For the RE-3 test (Figure 2.7), a uniform load is applied incrementally along the vertical and horizontal components of the roof edge system. Similar to the RE-2 test, failure of the roof edge system is defined as disengagement of any component of the system.

From those tests, it is established that each component of the system contributes to the overall system resistance to the applied loads. Therefore, loss of integrity or failure of the roof edge occurs when any of the following conditions are attained:

- Nail disengagement,
- Component disengagement,
- Metal sheet collapse due to excessive deformation.

RE-3 Test for Copings

(Exposed horizontal component exceeds 4 inches)

RE3.1 Apparatus

This description of the apparatus is general in nature. Any equipment capable of performing the test procedure within the allowed tolerances shall be permitted. A schematic drawing of this apparatus is shown in Figures RE3.1 and RE3.2. The test apparatus shall be constructed so that the performance of individual components are unaffected by edge or end constraints on the test sample. Load shall be applied and measured with calibrated load cells, each accurate to within +/-3% of full scale load cell values. Calibration shall be performed annually (minimum) and should be performed and recorded at 5%, 25%, 50%, and 75% of the expected maximum test values.

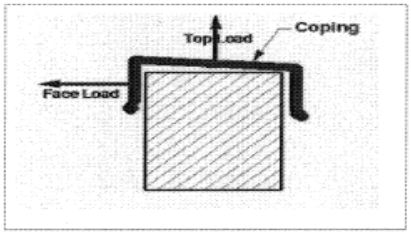

Figure RE3.1
RE3 Test—Face Leg Pull

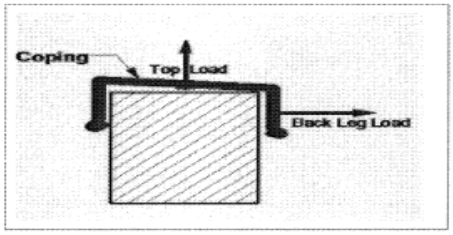

Figure RE3.2
RE3 Test—Back Leg Pull

R3.2 Safety Precautions

Proper precautions shall be taken to protect the operating personnel and observers in case of

Figure 2.7 Description and sketch of RE-3 test (reproduced from SPRI 2011)

ANSI/SPRI/FM 4435/ES-1 (SPRI 2011) provides guidelines on the calculations of wind design pressure and nail loads for roof edges in low slope roof buildings in Canada. The wind design pressure is calculated using Equation (2-1), i.e.

$$P=2Q_{zf}\,GC_p\,I \qquad (2\text{-}1)$$

where,

P Roof design pressure, psf (kPa)

GC_p External pressure coefficient, obtained from Figure 2.8,

Q_{zf} Field of roof pressure at height z (ft), obtained from Figure 2.9,

Table 2
External Pressure Coefficient[1] (GC_p)
Enclosed Building[2]

Type of Loading	Edge Location	Roof Height 60 ft. (18.3 m) or less z ≤ 60 ft. (18.3 m)	Roof Height over 60 ft. (18.3 m) z > 60 ft. (18.3 m)
Horizontal (acting outward from the building edge)	Perimeter	-0.97[3]	-0.68
	Corner	-1.21[3]	-1.25
Vertical (acting upward at the building edge)	Perimeter	-1.68	-1.57
	Corner	-2.53	-2.14

Figure 2.8 External pressure coefficient GC_p (SPRI 2011)

Table A2
Field of Roof Pressure q_{fz} psf (kPa)—Exposure B
Enclosed Building[1]

Building Height ft. (m)	Exposure B, Occupancy Category II (I=1.0) Wind Speed, 3 Second Gust, mph (m/sec)									
	85 (38.1)	90 (40.3)	100 (44.8)	110 (49.3)	120 (53.8)	130 (58.2)	140 (62.7)	150 (67.2)	160 (71.7)	170 (76.2)
0 ≤ 15 (0–4.6)	-15.3 -(0.73)	-17.1 -(0.82)	-21.1 -(1.01)	-25.6 -(1.23)	-30.4 -(1.46)	-35.7 -(1.71)	-41.4 -(1.98)	-47.6 -(2.28)	-54.1 -(2.59)	-61.1 -(2.93)
> 15 ≤ 20 (4.6–6.1)	-15.3 -(0.73)	-17.1 -(0.82)	-21.1 -(1.01)	-25.6 -(1.23)	-30.4 -(1.46)	-35.7 -(1.71)	-41.4 -(1.98)	-47.6 -(2.28)	-54.1 -(2.59)	-61.1 -(2.93)
> 20 ≤ 25 (6.1–7.6)	-15.3 -(0.73)	-17.1 -(0.82)	-21.1 -(1.01)	-25.6 -(1.23)	-30.4 -(1.46)	-35.7 -(1.71)	-41.4 -(1.98)	-47.6 -(2.28)	-54.1 -(2.59)	-61.1 -(2.93)
> 25 ≤ 30 (7.6–9.1)	-15.3 -(0.73)	-17.1 -(0.82)	-21.1 -(1.01)	-25.6 -(1.23)	-30.4 -(1.46)	-35.7 -(1.71)	-41.4 -(1.98)	-47.6 -(2.28)	-54.1 -(2.59)	-61.1 -(2.93)
> 30 ≤ 40 (9.1–12.2)	-16.6 -(0.79)	-18.6 -(0.89)	-23.0 -(1.10)	-27.8 -(1.33)	-33.1 -(1.58)	-38.8 -(1.86)	-45.0 -(2.15)	-51.7 -(2.47)	-58.8 -(2.81)	-66.3 -(3.18)
> 40 ≤ 50 (12.2–15.2)	-17.7 -(0.85)	-19.8 -(0.95)	-24.5 -(1.17)	-29.6 -(1.42)	-35.2 -(1.69)	-41.4 -(1.98)	-48.0 -(2.30)	-55.1 -(2.64)	-62.6 -(3.00)	-70.7 -(3.39)
> 50 ≤ 60 (15.2–18.3)	-18.6 -(0.89)	-20.8 -(1.00)	-25.7 -(1.23)	-31.1 -(1.49)	-37.0 -(1.77)	-43.4 -(2.08)	-50.3 -(2.41)	-57.8 -(2.77)	-65.7 -(3.15)	-74.2 -(3.55)
> 60 ≤ 70 (18.3–21.3)	-26.0 -(1.25)	-29.2 -(1.40)	-36.0 -(1.72)	-43.6 -(2.09)	-51.8 -(2.48)	-60.8 -(2.91)	-70.6 -(3.38)	-81.0 -(3.88)	-92.2 -(4.41)	-104 -(4.98)

Figure 2.9 Field roof pressure Q_{zf} (SPRI-2011)

For example, for wind exposure in the city of Ottawa, category B as given in Table 1 in SPRI (2011), and an importance factor, I=1 from (Table A1, SPRI 2011). The design pressure psf (kPa) for the perimeter of a roof edge system is calculated for a low rise building of maximum height of 60’(18 m) and for a wind speed of 100 mph (44.8 m/s) as follows:

$P=2Q_{zf}GC_pI$

$=2*26*1.68*1$

$=87$ psf (4.2 kPa)

For the perimeter region of the roof edge system, the load taken by nails at 24" (610 mm) spacing for a field pressure of 26 psf (1.24 kPa) applied against a continuous cleat configuration is calculated as follows:

$P=Q_{zf}GC_pI$

$=26*1.68*1$

$=44$ psf (2 kPa)

Therefore, the nail load is 88 lbf (391 N) for a 24" (610 mm) spacing.

2.4.2 Roofing Contractors Association of British Columbia (RCABC) - (RGC 2012)

RGC (2012) provides construction details for the design and manufacture of roof edge systems. For example, RGC (2012) provides details on the installation and assemblage of sheet metal flashing to fulfill their intended use in protecting the building from any water leakage as illustrated in Figure 2.10. RGC (2012) specifies the followings rules in the installation of sheet metal flashing:

- Only S-locks joints are allowed,
- Metal flashing must cover a completed roof membrane,
- 10' (3 m) are the maximum permitted length of flashing.

More details on architectural sheet metal are published by the Sheet Metal and Air Conditioning Contractors National Association, Inc. (SMACNA). In addition, it includes flashing details for roof edges and fascia that serve as guidelines for designers and manufacturers on the design of the roof edge as illustrated in Figure 2.11. However, this manual does not quantify the ultimate resistance of roof edge system against the wind uplift pressures.

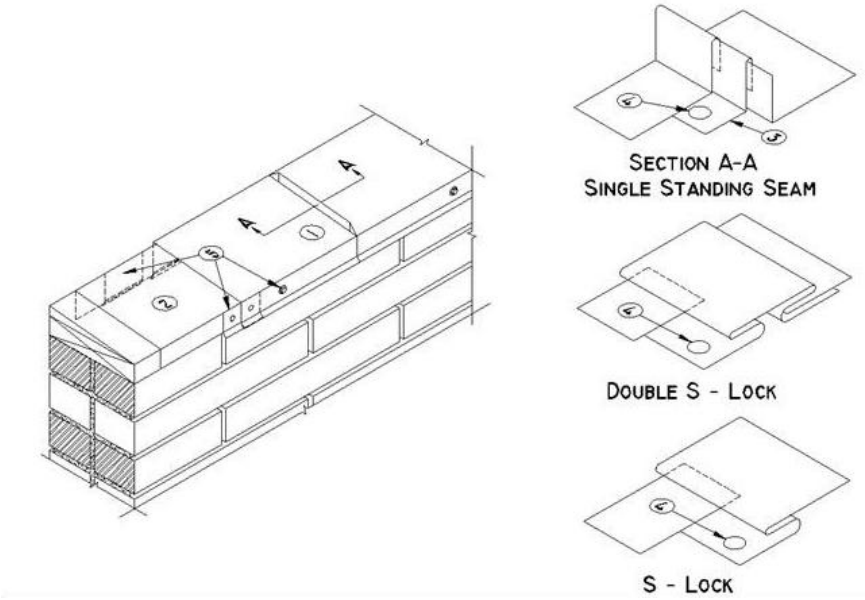

Figure 2.10 Flashing joint and joints (adapted from RGC 2012)

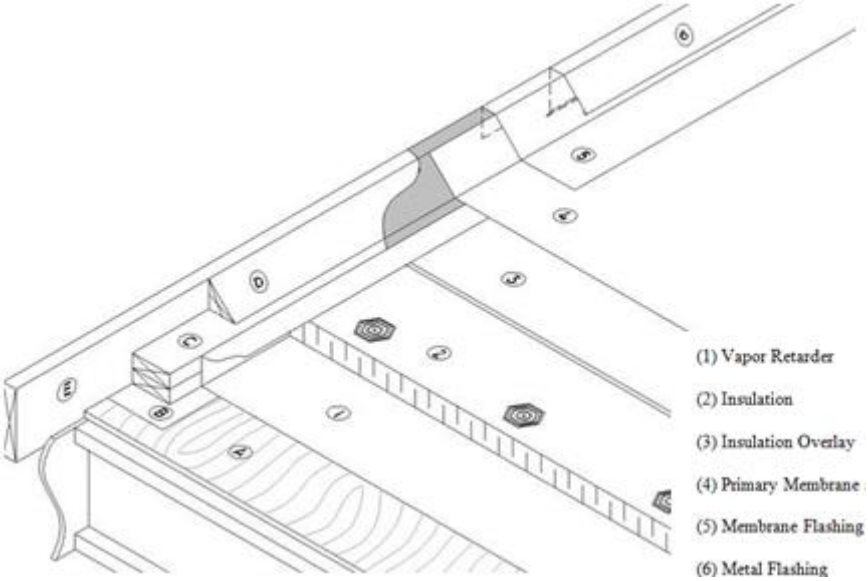

Figure 2.11 Roof edges and fascias: roof edge cant strip (adapted from RGC 2012)

2.5 Numerical Modelling of Roof Edge

There are limited published papers in the literature that investigate the effects of wind-uplift pressure on roof edge systems. The most relevant paper to date is the study conducted by McDonald et al. (1997). This paper investigates the effect of wind-induced loads on metal edge flashings using wind tunnel testing and finite element analysis using STARDYNE (TITAN Corporation USA) commercial software (McDonald et al. 1997). The objective of the study was to analyze the failure mechanism of metal edge flashing subjected to wind-induced loads.

McDonald et al. (1997) conducted finite element analyses of the roof edge with a cross section denoted as Flashing A as illustrated in Figure 2.12. The roof metal flashing, Flashing A detail, consists of 9.9 feet long by 4 inches (3.03 m by 102 mm) flashing plate fastened to the roof top with two staggered rows of roof nails spaced at 3.5" (90 mm) on-center (o.c). The cleat plate is fastened to the wall with a group of single row of cleat nails spaced at 18" (460 mm) o.c. The flashing plate thickness is 24 GA, while the cleat plate is 22 GA.

A 18" by 4" (460 mm x 102 mm) section of the overall roof metal flashing was modelled and analyzed using STARDYNE. Quadrilateral plate elements were used to simulate the flashing and cleat plates, while rigid truss elements were used to simulate all nails. The cleat nail was connected to the wall using a hinged support. On the other hand, the roof nail (flashing connection to the roof top) was modelled using a rigid support to allow for the calculation of the moment acting on the flashing. The connection between the flashing and cleat plates were modelled using a rigid link. To simplify the model analysis, the contact pressure between the flashing and cleat plates when they become in contact was neglected.

Similar to the pressure distribution established from field measurements of the roof edge referred to in Section 2.3, field measurements of the metal flashing conducted at the Texas Tech

University (TTC) Wind Engineering Research Field Laboratory (WERFL), prescribed a negative external pressure distribution along the depth of the flashing for Flashing A detail on the windward direction of the building (Wang 1995). Moreover, Flashing D, which is comprised of longer flashing depth, exhibited both negative and positive pressure distribution along the elevation of the flashing on the windward direction of the building (Wang 1995). Also, both flashing details exhibited positive internal pressure that tends to push the flashing outward. Therefore, in the finite element analysis of Flashing A a negative pressure was applied along the flashing elevation (Jiang 1995). In general, it was not clear whether the author relied on a static, dynamic or both analysis to predict the failure mechanism for the roof edge system - Flashing A configuration (McDonald 1997).

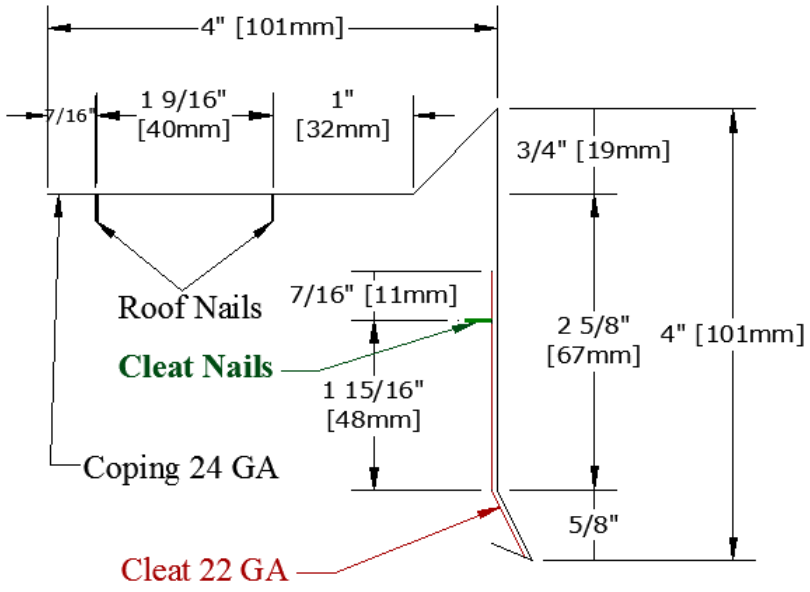

Figure 2.12 Sketch of Flashing A detail

Both wind-tunnel testing and finite element analysis of the metal edge flashing subjected to wind-induced loads determined the mechanism of failure of the system (McDonald 1997). The failure mechanism consisted of lifting and disengagement of the coping from the cleat and pull out of the nails (McDonald 1997). The maximum deflection of the flashing at the bottom edge

was estimated to be 0.002" (0.05 mm). The maximum nail reaction was calculated to be 0.4 lbf (1.78 N), and the resulting maximum von Mises stress on the sloped section of the flashing was 20,303 psf (1,020 kPa). Several conclusions were drawn from the experimental study (Jiang 1995):

- Flashing plate deflection and stresses decrease as the flashing plate thickness increase,
- Flashing plate thickness does not have a major effect of the nail reaction,
- Cleat plate, in the Flashing A detail, is an important component in resisting the applied pressure.

In addition, the following findings were observed from the finite element analyses of flashing A detail (McDonald et al. 1997):

- Stress concentration around nail area of the flashing plate, as shown in Figure 2.13,
- Disengagement of the flashing and cleat plate,
- Maximum stress value of 20,303 psf (1,020 kPa) at the sloped section of the coping plate,

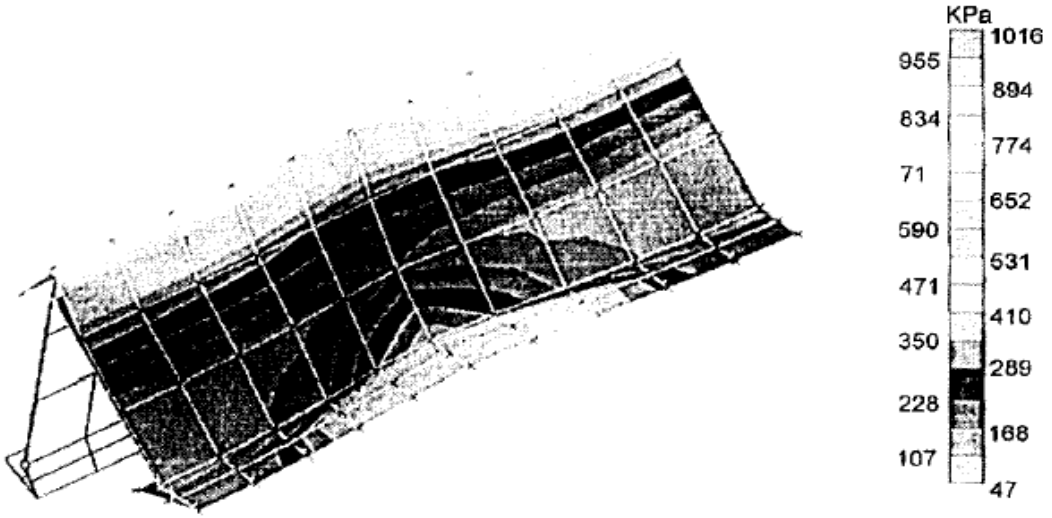

Figure 2.13 Finite element analysis of Flashing A detail (reproduced from McDonald et al. 1997)

The finite element results are summarized in Table 2.1. Note that the results provided in Table 2.2 correspond to the pressure recorded by the authors in field measurements by the 802R

pressure tap for M28N368. M28N368 is denoted by the authors to identify the configuration of the data records and to mark the data for archiving purposes (Jiang 1995).

Table 2.1 Deformation and cleat reaction force for 802R tap for M28N368 data

Tap No.	Mean	Peak min
ΔP psf (Pa)	2 (97.2)	7.7 (378)
U_z Inches (mm)	0.002 (0.05)	-
F_N lbf (N)	0.4 (1.78)	1.64 (7.29)

2.6 Gap in the State-Of-The-Art

There is a significant need to account for all wind-induced pressures in both vertical and horizontal directions according to the pressure distribution established from the field measurements in design and analyses of the roof edge. There is a lack of design guidelines or provisions, i.e. design curves, in the Canadian or American codes to quantify the wind-uplift loads to aid roof designers in the design of roof edge systems. Furthermore, there are no publications that provide comprehensive analyses on the roof edge behaviour under the effect of variable conditions, i.e., nail spacing or coping gauge, when subjected to wind-induced loads. Finite element analysis proves to be a reliable and cost-effective option to quantify the wind-uplift pressure for roof edge system under the effect of variable conditions in comparison to test experiments or field measurements. In addition, using finite element analysis wind-induced pressure in both the vertical and horizontal directions can be applied to account for the pressure distribution established from field measurements.

Chapter 3 **Finite Element Modelling**

3.1 Introduction

This chapter presents the finite element model used to conduct finite element analysis of the roof edge under sustained wind-induced pressures. Firstly, two system configurations commonly used in practice are used, and their design specifications are addressed in this chapter. The finite element model of the roof edge is described in terms of the elements used, coping gauge and boundary conditions. In addition, wind-induced loads are applied in a static analysis as uniform pressures on one and three-plane orientations against the face of the coping or cleat plates. Furthermore, sources of linearity and nonlinearity, in addition to the conditions governing their applications with regards to our problem, are discussed. Similarly, the principle of contact mechanics to simulate the contact between the coping and cleat plates as they deform is addressed. Lastly, three modelling approaches to simulate the roof edge are introduced: vertical edge, continuous edge and drip-edge connection.

3.2 Roof Edge Configurations

Current roofing practice utilizes two roof configurations: continuous and discontinuous cleat configurations. The continuous cleat configuration is comprised of two 4’ (1.2 m) and one 8’(2.4 m) segments of coping plates joined by concealed connections known as S-locks. The coping plate envelopes a two segments of 8’ (2.4 m) continuous cleat plates, which are nailed to the roof parapet by a group of nails at 18” (457 mm) spacing o.c, as shown in Figure 3.1. The discontinuous cleat configuration is comprised of two 4’ (1.2 m) and one 8’ (2.4 m) segments of coping plates also joined by S-locks. The coping plate envelopes a 40” (1 m) discontinuous cleat plate, which is nailed to the parapet by four nails at 12” (305 mm) spacing o.c, as shown in

Figure 3.1. In addition, the coping plate is fully restrained at each end. From Figure 3.2, the coping plate is nailed to the parapet at 12” (305 mm) spacing and is fully restrained at each end.

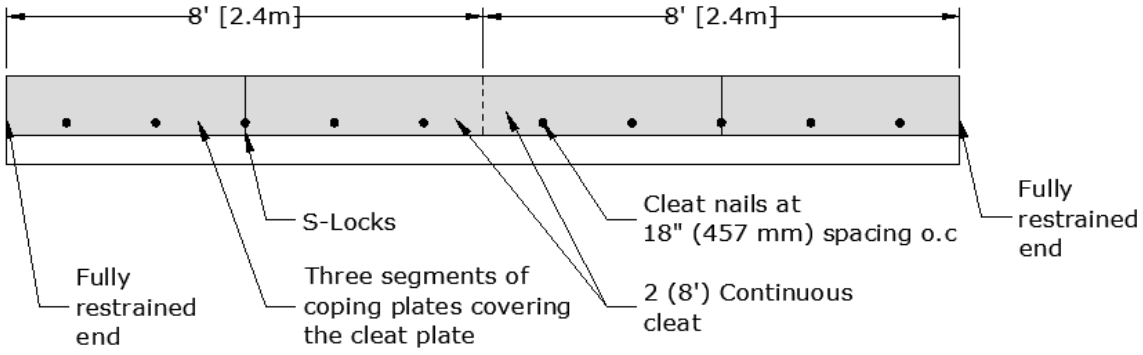

Continuous cleat configuration

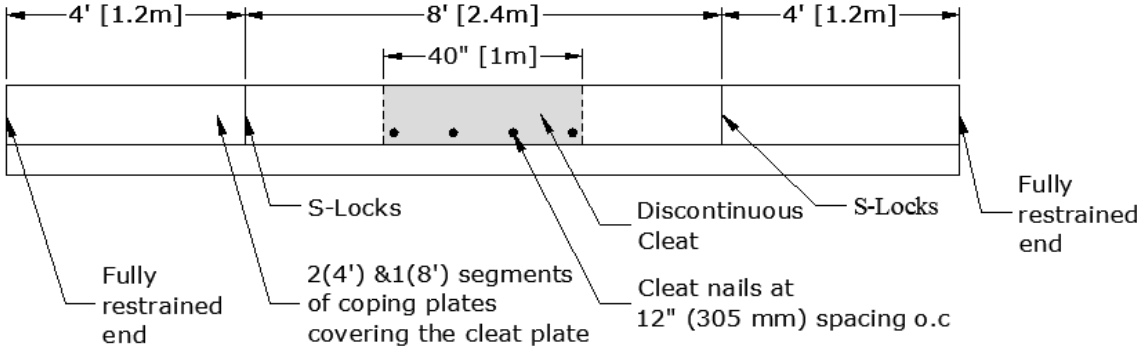

Discontinuous cleat configuration

Figure 3.1 Front view of the continuous and discontinuous cleat configurations

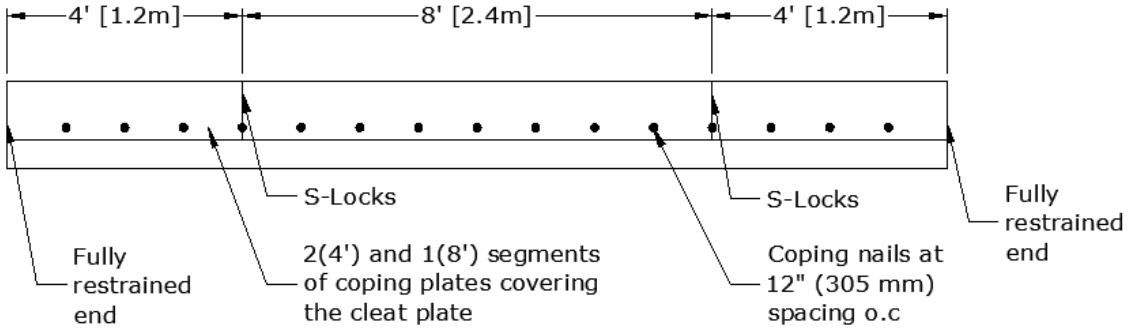

dis/continuous cleat configuration

Figure 3.2 Rear view of the continuous and discontinuous cleat configurations

Current roofing practice utilizes galvanized steel plates of variant plates’ thickness, mainly ranging from 22 to 26 GA. Table 3.1 shows the correspondence between a gauge (GA) of metal

and the thickness given in inches or mm. It is noted that as the gauge increases the thickness of the metal decreases. Throughout this study, the roof edge is modelled as a system of homogeneous material made of galvanized steel. Galvanized steel has the following physical properties that are used in this study; Poisson ratio of 0.3, Young's Modulus E= 29,000,000 psi (210 GPa) and density (ρ) of 490 lbf/ft³ (7800 kg/m^3).

Table 3.1 Plates Thickness (Rowlett 2002)

Gauge (GA)	Galvanized Steel Thickness (Inches)	Galvanized Steel Thickness (mm)
20	0.0396	1.0058
22	0.0336	0.8534
24	0.0276	0.7010
26	0.0217	0.5512

Two different geometric cross-sectional details are used to model the roof edge continuous and discontinuous cleat configurations. These two cross sections are respectively referred to as Set A and Set B. The coping of Set A has a width (W_{co}) of 10" (254 mm) and a front height (H_f) of 12" (305 mm) (see Figure 3.3 and Figure 3.4). The thickness of the coping plate in Set A is 26 GA. In Set B, the front height of the coping plate is reduced to 6" (152 mm), and its width is slightly enlarged by half inch, as illustrated in Figure 3.5. The coping plate thickness for Set B is increased from 26 GA to 24 GA.

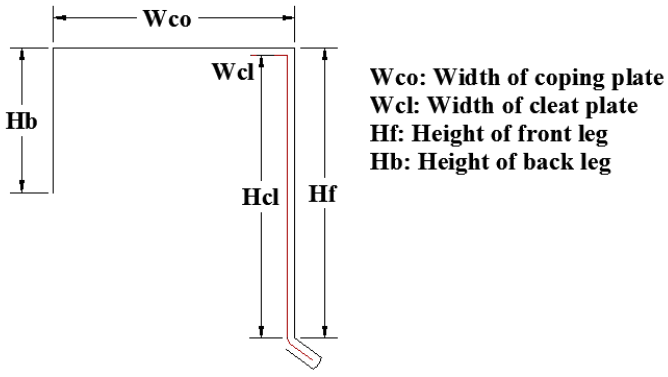

Figure 3.3 Cross-section of the roof edge system

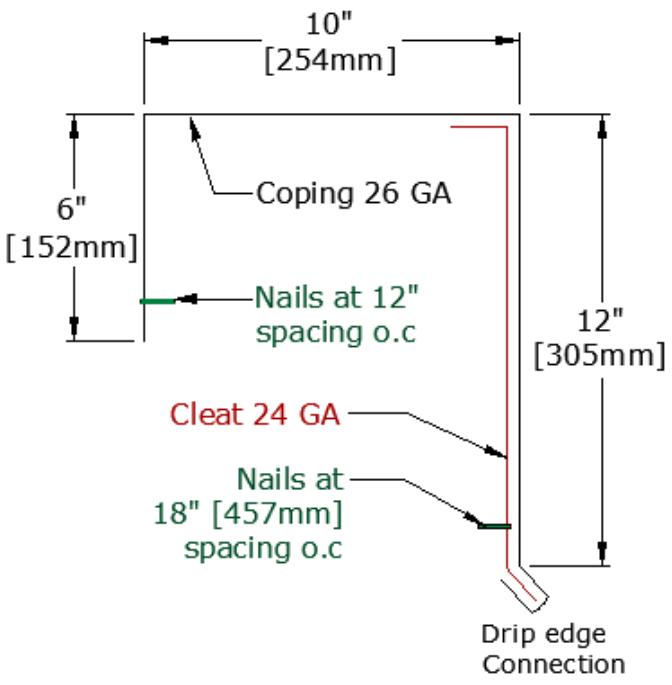

Figure 3.4 Sketch of Set A (H_b / H_f / W_{cl}): (6 / 12 / 10)

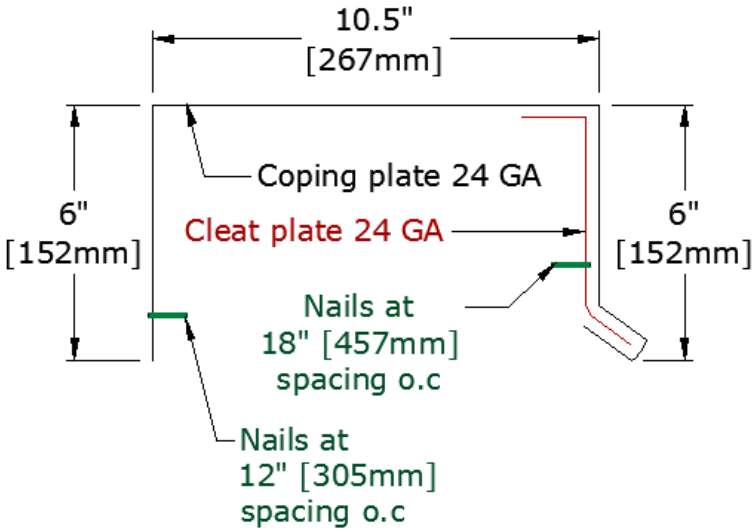

Figure 3.5 Sketch of Set B (6 / 6 / 10.5)

3.3 Finite Element Model

In this study, the commercial software package ABAQUS developed by Hibbitt, Karlsson & Sorenson, Inc, and is now acquired by Dassault Systèmes Simulia Corp., is used to analyze the roof edge. The roof edge model is simulated and analyzed using version 6.11 of ABAQUS/CAE and ABAQUS/Standard. A sample input file was developed to model the system and is included in Appendix A. In simulating a relatively complex structure such as a roof edge, it is important to represent the actual structure of the roof edge in a simpler finite element model by avoiding unnecessary details that will increase the computational effort and cost of the analysis. Unnecessary details include geometry details that represent only 1% of the overall geometry shape, e.g. nail circle holes. In addition, S-locks connections are one of those unnecessary details that do not contribute directly to the system behaviour such that their failure or their local effect does not affect the overall system behaviour; hence, they are not modelled. The physical geometry of the roof edge is idealized into a 3D mesh which is an assemblage of finite elements joined together by shared nodes, as shown in Figure 3.6. In the finite element model, the roof parapet is not modelled and it is replaced by appropriate boundary conditions. The geometry of the roof edge is defined by the continuous and discontinuous cleat configurations described in Section 3.2. The roof edge is comprised of a 16’ long, 1’ deep and 0.83’ wide (4.86 x 0.3 x 0.25 m) coping plate enveloping a 16’ (4.86 m) or 40” (1 m) long and 12” (305 mm) deep cleat plate. The cleat plate is attached to the parapet using a group of nails.

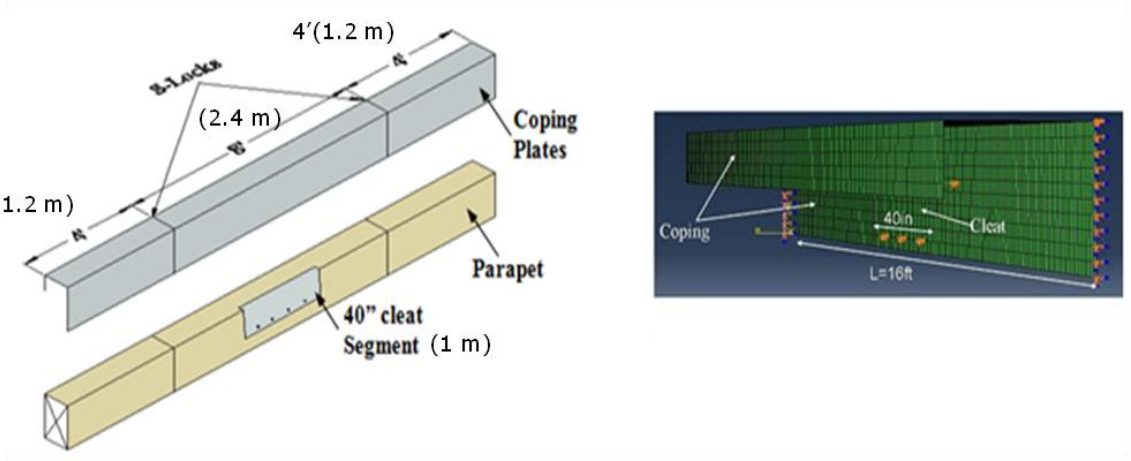

Figure 3.6 Left: roof edge geometry, Right: Finite element idealization

3.3.1 Elements

Two types of 3D elements are used in the finite element model of this study (SIMULIA (2010) :

- Shell element (denoted S4 in ABAQUS)
- Truss element (denoted T3D2 in ABAQUS)

On one hand, shell elements are selected for modelling coping and cleat plate, because they both have significantly large longitudinal size in comparison to their thickness size. In ABAQUS, there are several types of shell elements; their usage depends on the type of application and analysis. For this study, the S4 quadrilateral shell elements, which are specific to ABAQUS, are selected. This is because both coping and cleat plates are subjected to an out-of-plane pressure (P) induced by the wind loads acting on their faces Figure 3.7. This element has both three translational (U_x, U_y, U_z) and three rotational (θ_x, θ_y, θ_z), Degrees Of Freedom (DOFs) as illustrated in Figure 3.8. Furthermore, S4 accounts for thickness changes of the element, being able to simulate an increase in transverse shear deformation as the thickness decreases, which is an important factor in the parametric analysis of the roof edge discussed in Chapter 5. Another reason for selecting the shell element to model the coping and cleat plates is that it accounts for

finite membrane strains and large rotations when the roof edge experiences small deformations under high load applications (ABAQUS/CAE 2012). In addition, they are general purpose elements that are suitable to obtain stresses and deformations for both linear and nonlinear analysis.

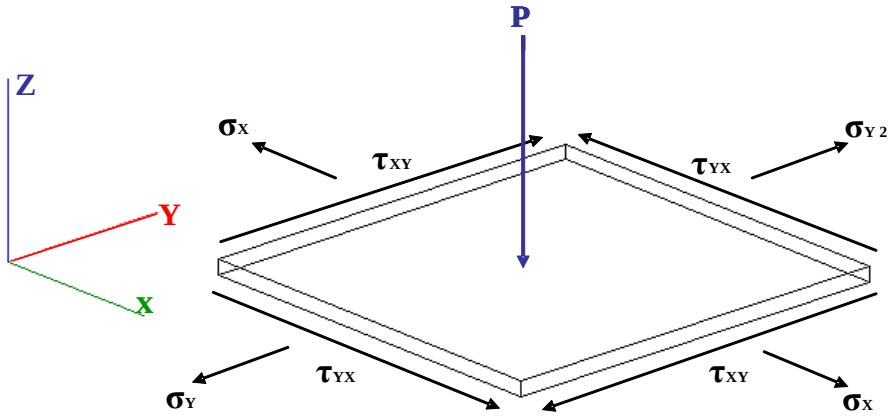

Figure 3.7 Internal stresses of shell elements under the application of out-of-plane pressure

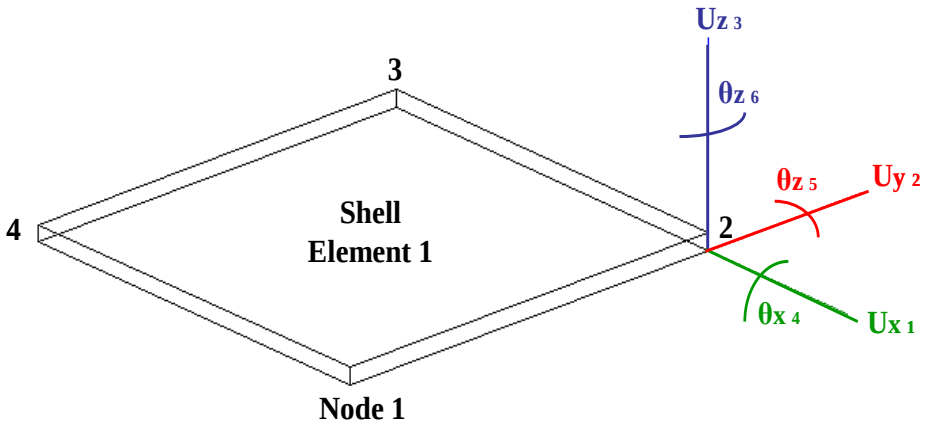

Figure 3.8 Six translational and rotational degrees of freedom at Node 2 for shell Element 1

Quadrilateral elements consist of a flat plate that does not model the curvature nature of shell elements. This in effect results in an increase of the shear stress of the analyzed element leading

to a decrease in the rate of element convergence. Consequently, the element reaches equilibrium at smaller displacements results implying a stiffer behaviour than the actual one. This phenomenon is called shear locking. In general, to avoid shear locking S4R elements are used which are general purpose shell elements with a uniformly reduced integration. In modelling the roof edge system a comparison between the displacement results of S4 and S4R elements was conducted to determine if shear locking occurs during finite element analysis of the roof edge. Accordingly, the displacements results of the coping plate taken at several pressure points for both elements S4 and S4R were found to be exactly equal; hence, shear locking is not a problem in this work; therefore, S4 is sufficient to analyze the roof edge behaviour.

On the other hand, truss elements, with one translational degree of freedom at each end as illustrated in Figure 3.9, are used for modelling the roof edge nails. This is because nails mainly transfer loads along their axial direction. In addition, there is allowance for deformation along the nail axial direction until yielding of the material is reached. In this study, yielding of the nails was considered one of the failure criteria. Furthermore, nail reactions are also calculated. It is worth mentioning that the nail head and hole in the plates are neglected in the finite element model, mainly because the nail cross-sectional area is marginal compared to the whole system area. It also takes more modelling and computational effort.

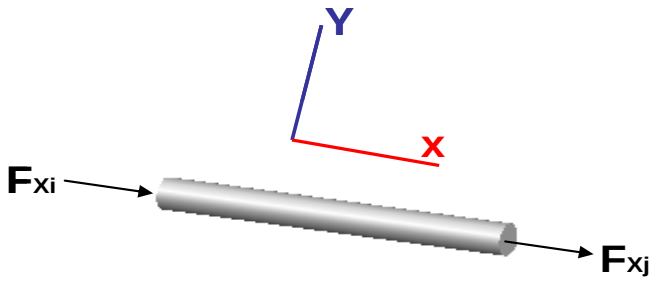

Figure 3.9 Axial forces transmitted along the length of a truss element

3.3.2 Boundary Conditions

Since the main focus of this study is to investigate deformations of roof edge plates and nail reactions, the physical roof parapet structure is not modelled in the analysis. However; the parapet is accounted for by defining appropriate boundary conditions around the roof edge, as illustrated in Figure 3.10. Translational boundary conditions (R_y and R_z) are imposed along the horizontal portions of the coping and cleat plates (W_{co} and W_{cl}) and the vertical back height (H_b) of the coping plate to avoid the roof edge system from displacing towards the physical space occupied by the parapet, Figure 3.10. Both W_{co} and W_{cl} are restrained from displacing along the negative direction of the y-axis ($U_y \geq 0$), while H_b is restrained from displacing along the negative z-axis direction ($U_z \geq 0$). Furthermore, a hinge support is defined at the end of the truss element to resemble the retraining effects of the nails attached to the parapet, as shown in Figure 3.10. In addition, the vertical legs, H_f and H_b (Figure 3.3), of the coping plate are restrained at both ends using a fixed support to resemble the restraining effects provided by clamps used in the experimental setup of the system (Alassafin 2012) as shown in Figure 3.1, Figure 3.2 and Figure 3.11.

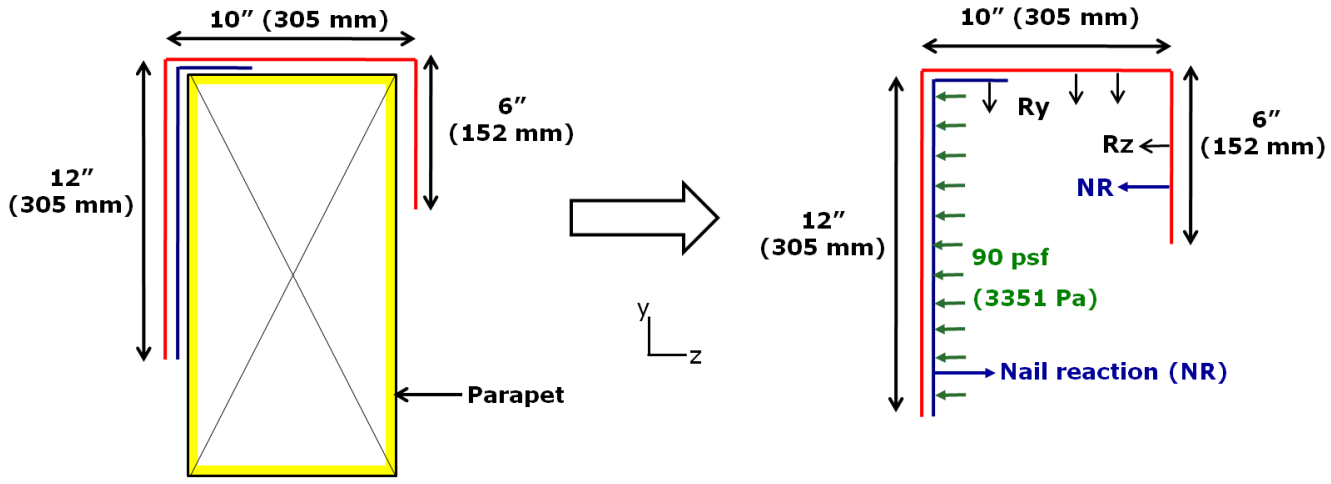

Figure 3.10 Parapet is removed and boundary conditions are imposed

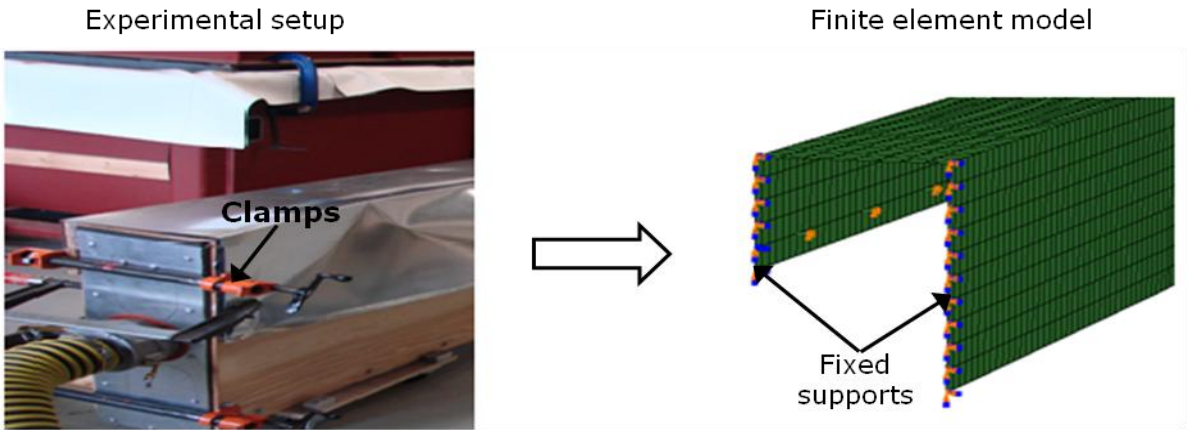

Figure 3.11 Boundary conditions of the experimental and finite element model at each end of the coping front and back vertical legs

3.3.3 Load Application

For both continuous and discontinuous cleat configurations, a uniformly distributed pressure is applied against the cleat plates on one- or three-planes. One-plane pressure is applied against the front face of the cleat plate (H_{cl}). On the other hand, for three-plane pressure the load is applied against the front and top plates (H_{cl}, W_{cl}), in addition to the top and back plates of the coping (H_b, W_{co}). Similarly, a uniformly distributed load is applied against the face of the coping plates at one-or three-planes, as illustrated in Figure 3.12. One-plane pressure is applied only against the front face (H_f) of the coping plate. On the other hand, three-plane pressure is applied against the front, back and top (H_f, H_b, W_{co}) faces of the coping plates. When the load is applied against the coping plate, translational boundary conditions (R_y and R_z) were imposed along the vertical and horizontal sections of the cleat plate (H_{cl}) and (W_{cl}) to simulate the restraining effect of the parapet against the cleat plate and also to prevent the cleat plate from displacing towards the space occupied by the parapet (U_y and $U_z \geq 0$), as shown in Figure 3.12.

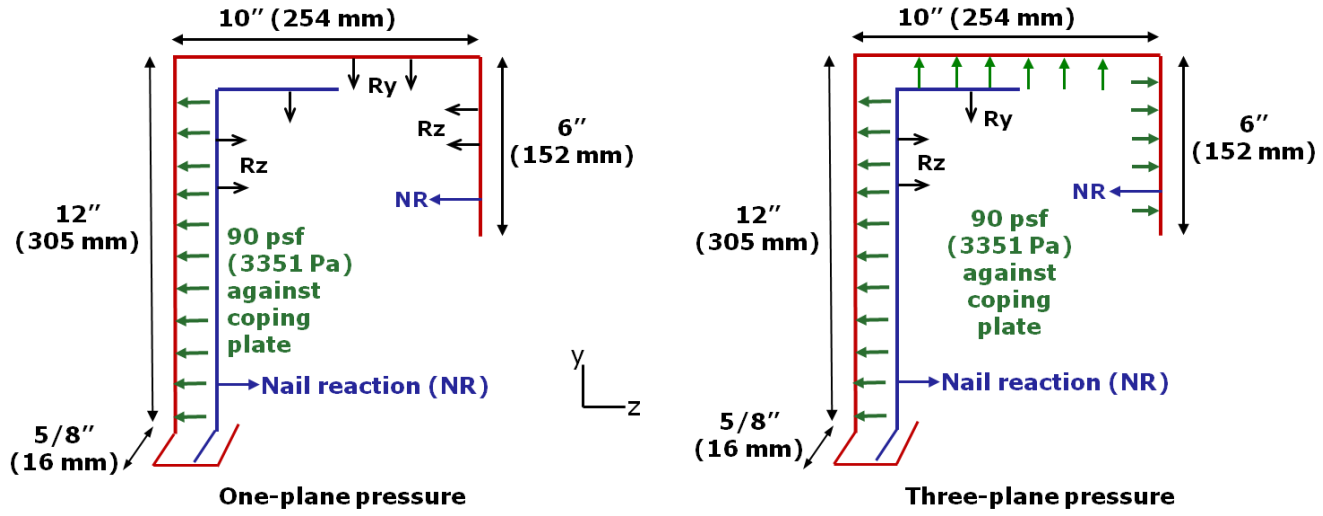

Figure 3.12 Type of load application against the roof edge on either one- or three-pressure planes

3.4 Mesh Sensitivity

To accommodate the large size of the roof edge structure of 16’ by 1’ (4.86 by 0.3 m), it is determined that a mesh of 162 elements along the full length of the coping plate, L_{cop}, and 10 elements along the vertical dimension, H_f, with an aspect ratio of 1, is reasonably adequate. This was established following mesh refinement considerations of the vertical height of the coping and cleat plates exclusively, H_f and H_{cl} where the analysis of the system stresses and displacements are at focus see Figure 3.13. Mesh refinement size is donated by N, hence, doubling the elements’ number along the vertical and longitudinal dimensions to 324 and 20 respectively yield a mesh refinement of N=½. Similarly, mesh size of N=¼ entails an elements’ number increase of 648 along L_{cl} and 40 along H_f. For both mesh sizes of N=¼ and N=½, elements are developed using an aspect ratio of 1 which results in the most accurate solution and eliminates element distortion. To create a smooth transition between different mesh densities along H_f and W_{co} (Figure 3.3) for stress and displacement analysis, transition elements of tetrahedral shell elements are created, Figure 3.14 and Figure 3.15. This smooth transition

ensures nodes and elements continuity without leaving free unconnected nodes, hence, eliminating discontinuity in the overall solution.

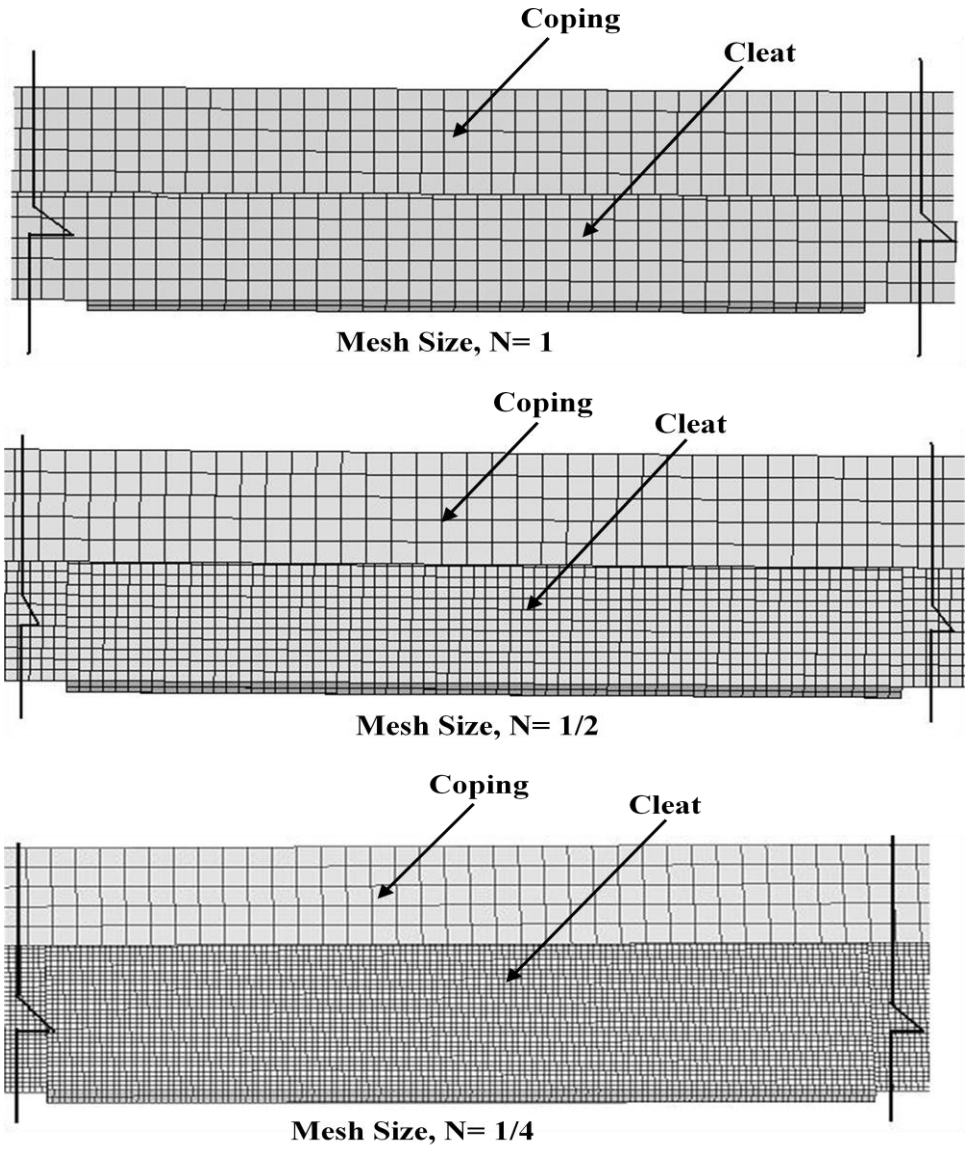

Figure 3.13 Finite element model of discontinuous cleat configuration illustrating mesh refinement of the front height (H_f) of the coping and cleat plates

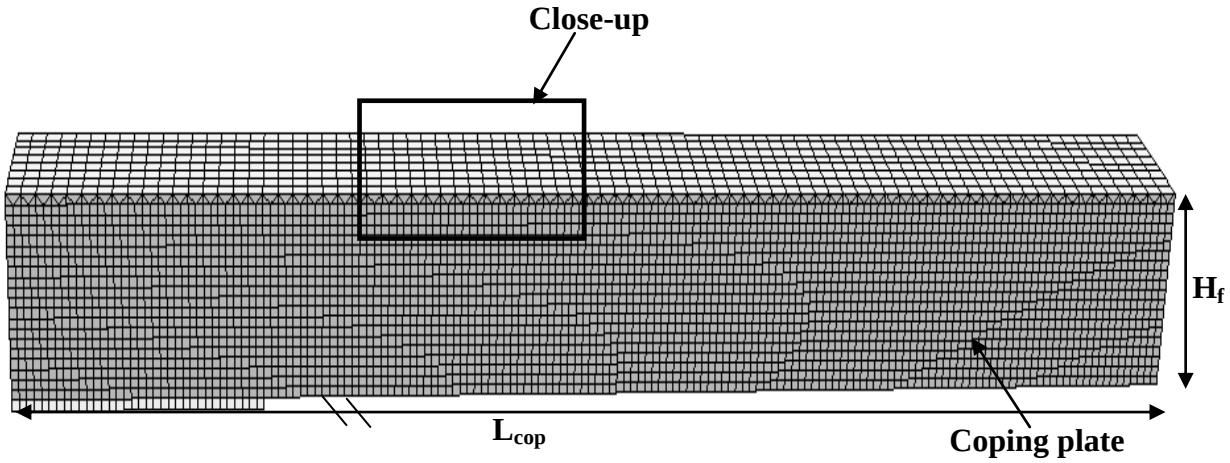

Figure 3.14 Cross –section of the finite element model

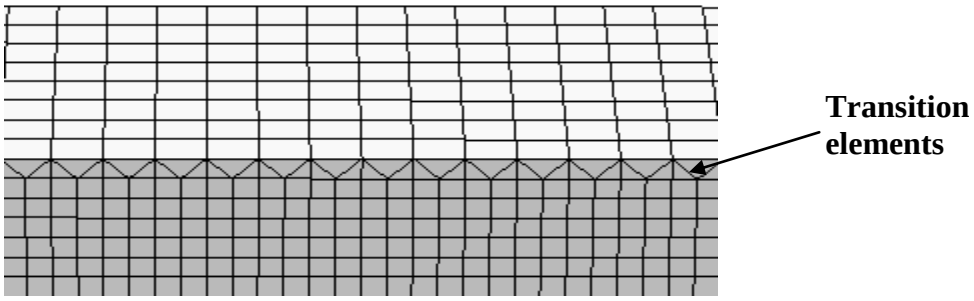

Figure 3.15 Close-up of Figure 3.14 transition elements along the coping plate length

By comparing the deflection results (δ) taken at ¼ and ½ L (Figure 3.16) and reaction forces of the cleat nails, F_N, between different meshes (Table 3.2), it is evident that further mesh refinement of the system from N=1 to N=¼ creates between 6% to 7% difference in the results, Figure 3.17. On the other hand, Figure 3.18 indicates that mesh sizes of N=¼ and N=¼ significantly increase the processing time required for running the analysis rendering the system more expensive. This is because with the increase of number of shell elements used to represent the system, more computational effort is required to reach a solution, particularly, for 3D shell elements as each shell element involves six DOFs at a node (Liu 2003). As a result, it is determined that a mesh size of N=1 is adequate and to be adopted throughout the finite element analyses.

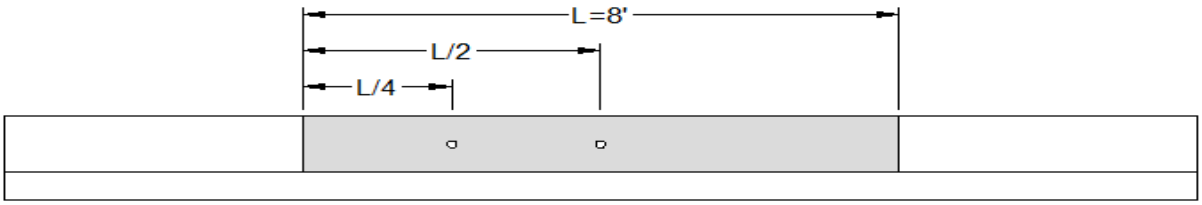

Figure 3.16 Deflection results measured at ¼ and ½ length of the coping middle segment

Table 3.2 Results of different sizes of mesh refinement of the roof edge

	Mesh Size, N		
P psf (Pa)	δ (¼) Inches (mm)	δ (½) Inches (mm)	F_N lbf (N)
10 (478.8)	0.23 (6)	0.56 (14)	13.4 (59.7)
		N= ½	
	0.24 (6.1)	0.59 (15)	12.6 (56.2)
		N= ¼	
	0.24 (6.1)	0.59 (15)	12.6 (56.2)

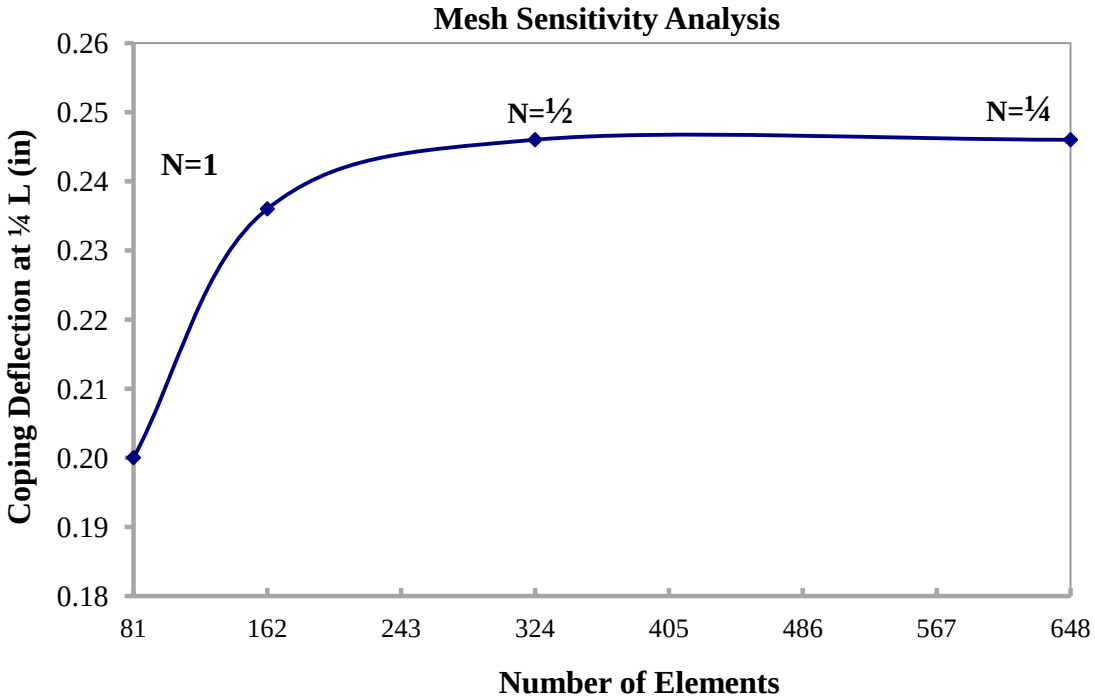

Figure 3.17 Mesh sensitivity analysis

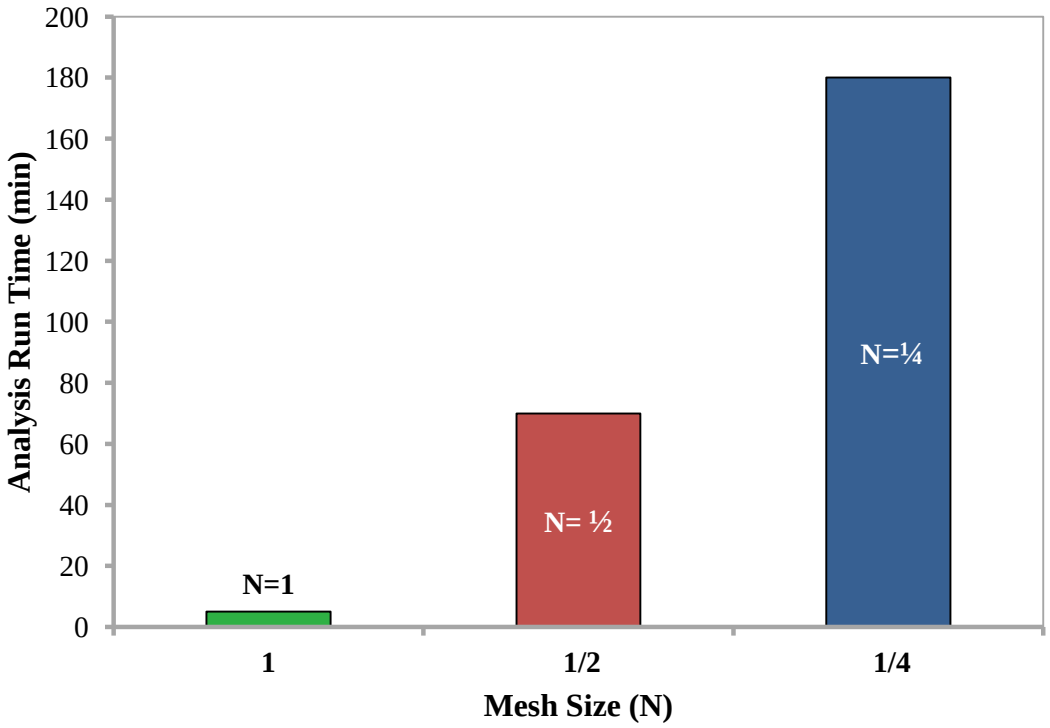

Figure 3.18 Comparison between analysis run time for the roof edge of different mesh size

3.5 Linear versus Non-linear Analysis

For a roof edge that follows linear behaviour, a linear analysis provides quite accurate results. However, this analysis is not valid after yielding of the material or when the system exhibits nonlinear behaviour (Reddy 2004). Therefore, it is very important to determine which type of analysis needs to be conducted to better predict the structural response of roof edge under the applied wind pressure.

A linear-elastic analysis is sufficient to determine the behaviour of the roof edge subject to wind-induced loads when small or non-permanent deformations take place. This is the case for stiff systems, e.g., continuous cleat configurations with cross sections Set A subjected to a one-plane pressure applied against the cleat plate and Set B subjected to a one-plane pressure applied against the coping plate. In general, this is true for systems subject to small loads. Basically, the application of loads does not change the overall geometry and configuration of the structure.

Furthermore, a linear analysis is appropriate to use when the boundary conditions of the system are uniform throughout the application of the load. For example, there is no contact between the surfaces of the structure; no additional constraints from those determined initially exist after the application of load that restricts the structure deformation. In summary, a linear-elastic analysis is usually adequate for the analysis of roof edge that exhibits the following conditions (Fish 2007):

- Deformations are small,
- Material response is linear,
- Boundary conditions are constant and there is no contact between the surfaces of the structure; and,
- Geometric shape is constant.

Although nonlinearity requires more computational effort by ABAQUS, the analysis yield a more realistic and accurate response of the system depending on the assumption used for a particular case. Linear analysis may potentially overestimate deflection of the system under the applied load, which is a serious problem when the failure criterion is based on deflection of the coping plate. There several sources of non-linear behaviour:

- Material,
- Boundary,
- Geometric.

Material nonlinearity arises when the material yields at large strains. At low strains the material response is linear; the stress versus strain relationship is linear. However, once the material is stressed beyond the yield stress, plastic deformation takes place. Boundary nonlinearity is caused when the boundary conditions of the roof edge change during the analysis, for example, the

coping and cleat plates come into contact with each other. Geometric nonlinearity occurs due to geometry changes that result from large deformations and rotations of the structure. As a result, the stiffness of the structure varies. Geometric nonlinearity should also be considered in the simulation even with relatively small displacement values due to significant changes in stiffness values as the system deforms. A nonlinear analysis takes more computational effort. However, when it is applicable as discussed above, it yields more accurate results.

3.6 Contact of Plates' Surfaces

In this study, contact mechanics is a very important concept when trying to simulate the cleat and coping plates in contact. The structural response of the roof edge accounting for the contact interaction between the two plates is completely different than when this interaction is omitted. Under the application of a normal uniform pressure, two or more plates come into contact resulting in force and moment transmission. Contact of non-deformable surfaces result in motion, sliding or rolling; however, contact of deformable surfaces result in surface deformation. In this study, contact of the deformable shell plates representing the coping and cleat metal sheets results in surface deformations. This surface interaction changes the boundary conditions of the structural system by introducing a new constraint upon contact. Also, when surfaces separate, the constraint is removed. This in effect changes the structural response; therefore, it is very important to analyze and detect when a structure's surfaces come in contact. At a contact point the resultant force transmitted from one surface to another is comprised of a normal compressive force C and a tangential frictional force Q (Johnson 1985). In addition, moments are transmitted at the point of contact. Forces and moments acting on a surface area S are transmitted by surface traction, normal traction (pressure) p and tangent traction (friction) q (Johnson 1985). Since the roof edge is comprised of deformable steel plates subject to out of plane pressure,

normal contact between the two plates will result in surface deformation. In addition to normal contact, there exits some relative motion in the tangential direction due to friction and boundary conditions imposed on parts of the roof edge (Valentin 2010). To reduce computational costs, friction forces are ignored in this study, since roof edge plates are smooth, made of similar material and most importantly to be conservative.

ABAQUS software does not recognize that two or more structural surfaces may potentially come into contact unless otherwise defined. Ignoring this contact mechanism gives unrealistic behaviour, because surfaces that may potentially come into contact will penetrate each other, as shown in Figure 3.19. In order to define the interaction between the two plates in the roof edge, a contact option is defined between the long legs of the coping and cleat plates and between the surfaces of the coping / cleat drip-edge connection, Figure 3.20. A general contact (surface-to-surface interaction with hard over-closure relationship) is defined which is specific to ABAQUS software. Based on this type of contact a nonlinear penalty method is used for contact constraint enforcement. This method improves the accuracy of the results and reduces the number of iteration required to achieve a solution.

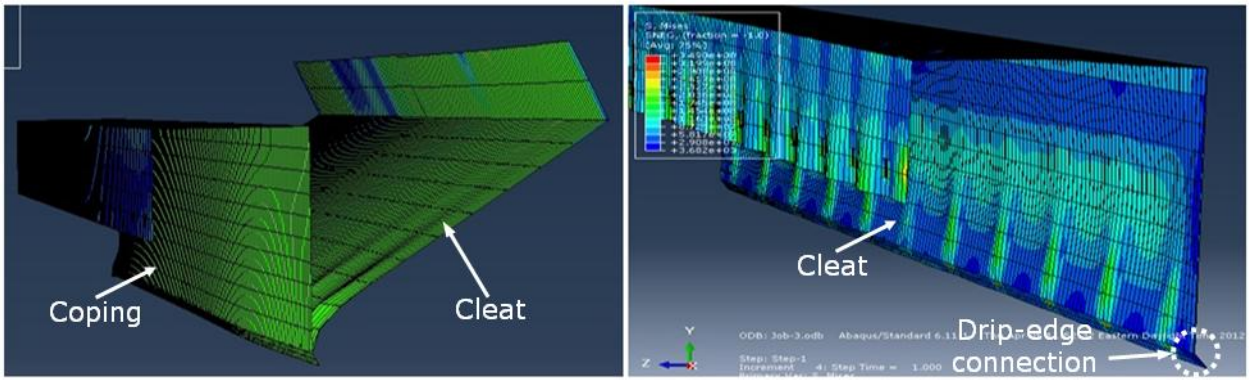

Figure 3.19 Left: contact concept is not defined in ABAQUS. Right: contact concept is defined.

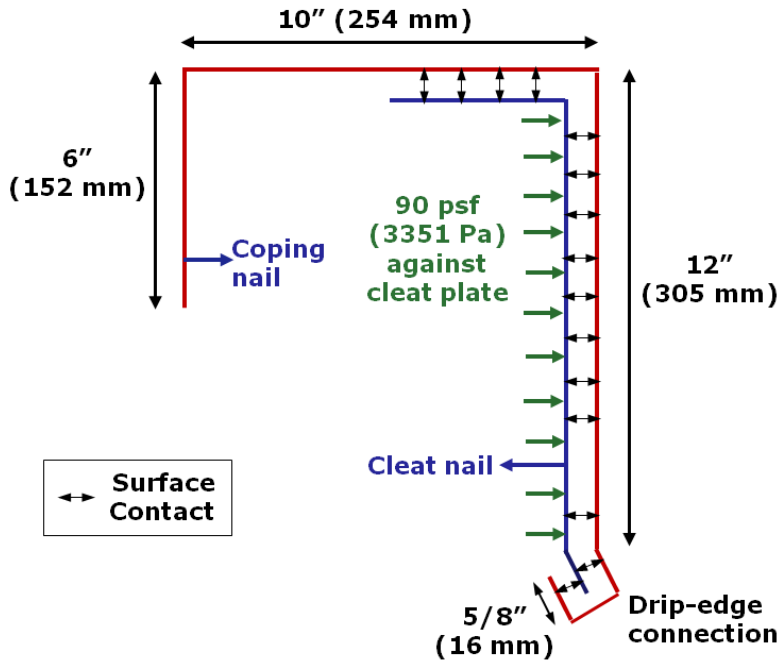

Figure 3.20 Contact is defined between coping and cleat plates

3.7 Three Modelling Approaches

To predict the behaviour of the roof edge, two system configurations are used, discontinuous and continuous cleat configurations, as previously discussed in Section 3.2. Modelling the drip-edge connection between the coping and cleat plate can be a challenging problem, because it requires advanced ABAQUS functions to be defined such as the contact function. Therefore, for each configuration, three modelling approaches are used: 1) modelling the full system with vertical cleat/coping edges, which are not connected; 2) modelling the full system with a sealed drip edge, i.e., the coping and cleat are continuous; and, 3) modelling the full system with a drip edge, i.e., a contact interaction is defined for the coping/cleat ends. These three modelling approaches are illustrated in Figure 3.21 to Figure 3.23. The three approaches are compared to each other to determine the optimal approach in predicting a reasonable structural behaviour of the roof edge.

Furthermore, this serves to understand the structural effect of the cleat/coping drip-edge connection on the overall structure performance.

3.7.1 Approach 1 - Vertical edges

The full roof edge is simulated except for the drip edge connection between the coping and cleat plates. The plates' edges on the long leg, 12" (305 mm), are kept free, as shown in Figure 3.21.

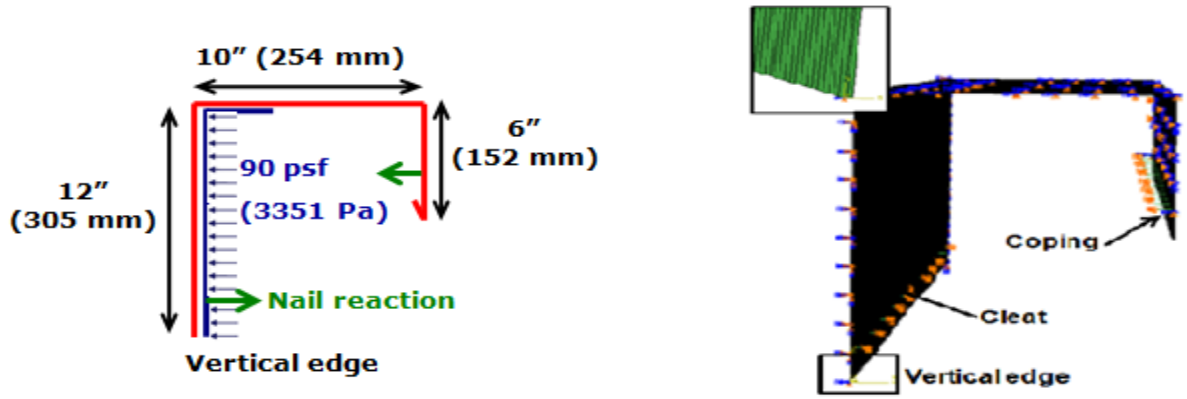

Figure 3.21 Sketch and ABAQUS FEM of the continuous cleat configuration with modelling approach 1

3.7.2 Approach 2 - Continuous edge

In this approach, the drip edge connection between the coping and cleat plates is continuous, i.e., the drip edge of the coping and cleat is simulated as one-piece, as shown in Figure 3.22.

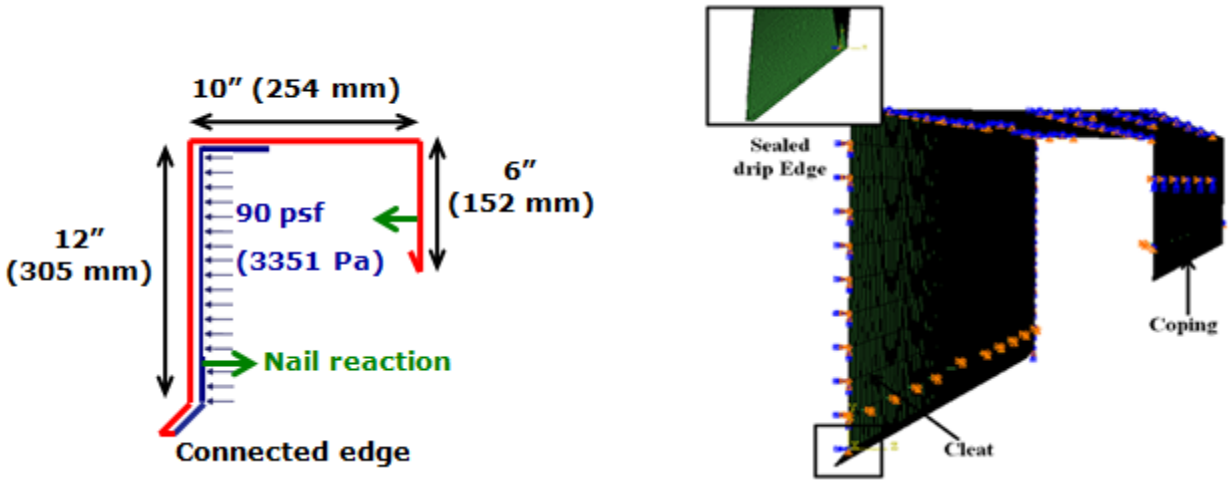

Figure 3.22 Sketch and ABAQUS FEM of the continuous cleat configuration using approach 2

3.7.3 Approach 3 - Drip edge

In this third approach, the full roof edge model is simulated to resemble roof edge in real life, particularly; the drip-edge connection between the coping and cleat plates is modelled as an interaction between the two surfaces. In this approach, the cleat drip edge is tightly sandwiched between the coping drip edge, but it is not sealed, as illustrated in Figure 3.23

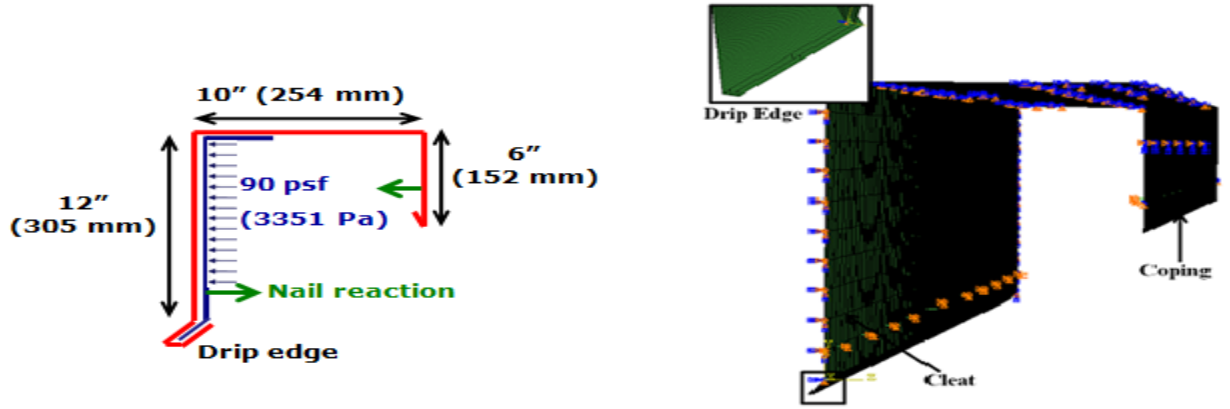

Figure 3.23 Sketch and ABAQUS FEM of the continuous cleat configuration using approach 3

3.8 Summary

This chapter has introduced the geometric details of two roof edge configurations that are used in the finite element analysis: continuous and discontinuous cleat configurations. For the continuous configuration, two sets of cross sections, Sets A and B are simulated. For discontinuous cleat configuration, only cross section Set A is modelled. A uniform pressure is applied against the face of the coping and cleat plates on one- or three-planes. Chapter 4 will present the results of the finite element model verifications, in which analysis results are compared to experimental tests conducted at NRC (Alassafin, W 2012), as outlined in Table 3.3. The coping deflection at ¼ and ½ length of the middle segment are compared to those obtained from test experiments.

Table 3.3 Outline of finite element modelling

Configuration Type	**Edge Size (H_f / H_b / W_{co}) Inches**	**Pressure Plane**	**Load Application**	**Experimental Verification**
Continuous cleat	**Set A** (12/6/10)	One-plane	Cleat Coping	Yes Yes
		Three-plane	Cleat Coping	Yes
	Set B (6/6/10.5)	One-plane	Coping	Yes
Discontinuous cleat	**Set A** (12/6/10)	One-plane	Cleat Coping	Yes
		Three-plane	Cleat Coping	

Chapter 4 **Finite Element Model Validation**

4.1 Introduction

In this chapter, the finite element model presented in Chapter 3 is validated against numerical results presented in McDonald et al. (1997) and experimental tests conducted at the National Research Council of Canada (NRCC) (Alassafin 2012). The finite element analyses conducted by McDonald et al. (1997) were performed on a section detail referred by the authors as "Flashing A detail" and illustrated in Figure 2.12. Experimental tests were conducted on both continuous and discontinuous cleat configurations under two different load applications: one-plane pressure and three-plane pressure against the cleat and coping plates. Data used in the comparisons are the coping plate deflection and the nail reaction. During the experimental tests, the deflection of the coping plate was monitored through laser sensors at mid-height at ½ and ¼ length (L) of the middle coping segment, as indicated in Figure 4.1. These values were compared to the deflection results of the finite element model at the same locations.

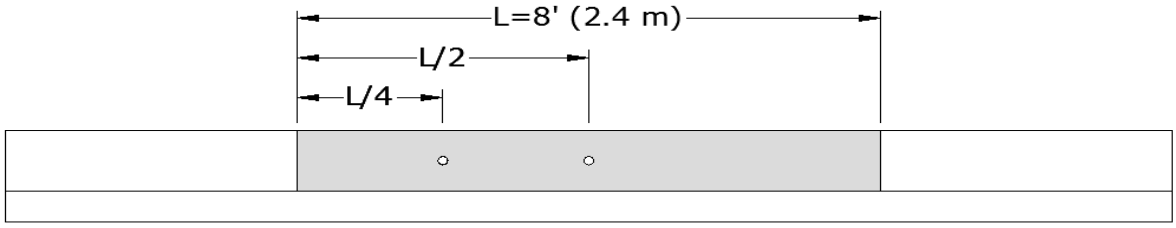

Figure 4.1 Location of laser sensors that measure deflection points at ½ and ¼ L along the longitudinal plane of the coping plate

The maximum reaction forces (F_{Nmax}) of the cleat and coping nails were also monitored as the applied pressure was increased in the finite element analysis. It is noted that the mechanism of nails pulling out from the roof edge assembly is not explicitly modelled in ABAQUS, but it is rather a measure of the reaction force that holds the truss element used to simulate the nails.

In the finite element model, failure of the system is local yielding of the plates around the nail area due to excessive stress concentrations, permanent deformation of the cleat or coping, and disengagement of the coping / cleat drip-edge connection. Based on industry experience (Baskaran 2012), in this study severe deformations refer to plate deformations that exceed 1" (25 mm), moderate deformations refer to deformations that exceed ½" (12 mm) and, finally minor deformations refer to deformations below ½" (12 mm), Figure 4.2 outlines the analysis cases used in ABAQUS to validate the finite element model of the roof edge. Both the continuous and discontinuous cleat configurations were analyzed when the pressure was applied on one-plane against either the cleat or the coping. In addition, the continuous configuration was also analyzed for a three-plane pressure applied against the cleat.

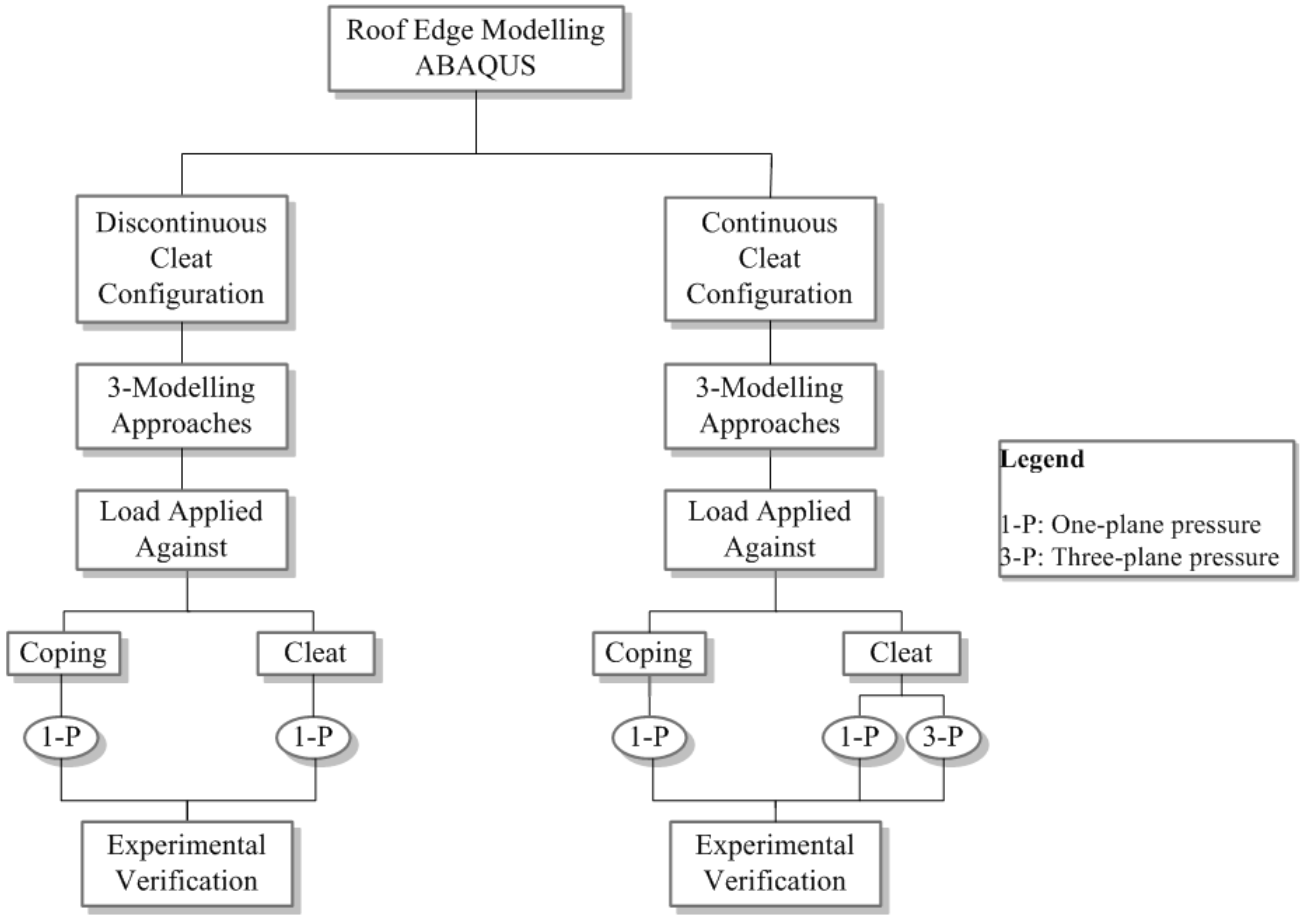

Figure 4.2 Validation outline of the roof edge system

4.2 Numerical Results – Flashing A Detail

McDonald et al. (1997) conducted finite element analysis on a metal roof edge section of 18" by 4" (460 mm x 102 mm), as illustrated in Figure 2.12. The same section was modelled and analyzed using the ABAQUS finite element software. The cleat is attached to the parapet with one nail, while two staggered rows of roof nails at 3.5" (90 mm) spacing o.c. are used on the top of the coping. The cleat and coping were modelled using quadrilateral shell elements. The cleat nail was modelled using a truss element connected to the parapet wall with a hinged support. On the other hand, the roof nails connecting the flashing to the roof top were modelled using a fixed support to simulate the same boundary conditions. Symmetry boundary conditions were imposed along the vertical ends of the flashing and cleat plates to simulate continuity of the roof edge (i.e., vertical displacement was allowed while horizontal displacement along the length of the section was restrained), Figure 4.3. A uniform and static wind pressure was applied against the face of the cleat plate and the top flange of the flashing plate as illustrated in Figure 4.3. This pressure was calculated from pressure coefficients obtained from pressure taps data obtained by the authors in experimental tests (McDonald et al. 1997). For the analysis presented here, the data recorded by pressure tap 802R, with values shown in Table 4.1, was chosen to calculate the pressure to be applied in the finite element model. This pressure ΔP was calculated from:

$$\Delta P = C_p \frac{1}{2} \rho V^2 \qquad (4\text{-}1)$$

where C_p is the pressure coefficient , ρ is the air density, ρ = 0.08 lbf/ft^3 (1.29 kg/m^3), and V is the wind speed. Reported data for record M28N368, which was used here to calculate ΔP, has a mean speed of V= 42 ft/s (12.8 m/s). The resulting ΔP applied in the finite element analyses based on the mean and peak min pressure coefficients, Table 4.1, are 2 psf (97 Pa) and 8 psf (388 Pa) respectively.

Table 4.1 Pressure coefficients C_p at the top roof tap:

Tap No.	Mean	Peak min
802R	0.92	3.67

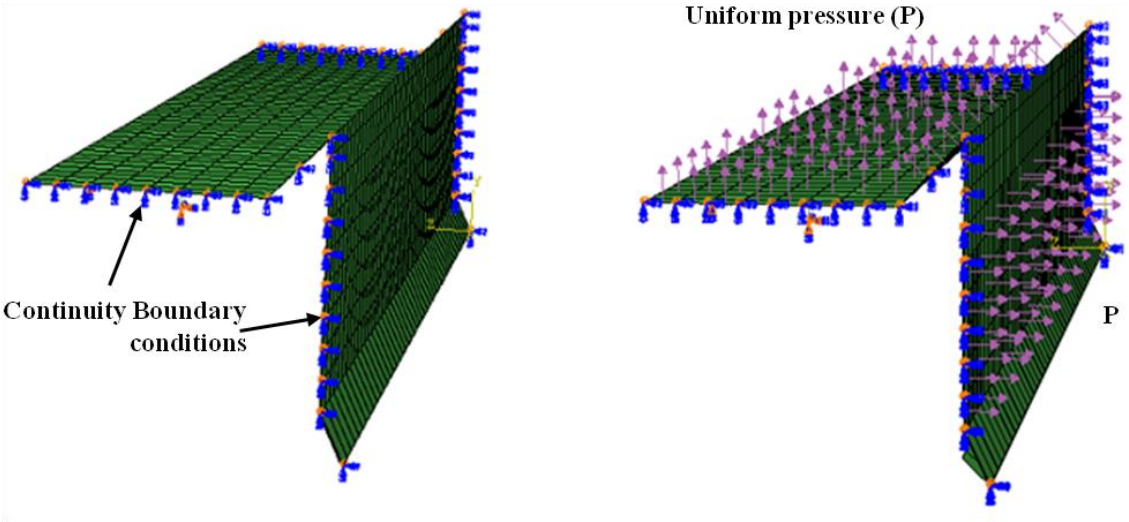

Figure 4.3 Boundary conditions imposed on Flashing A (Left) and a uniform static pressure applied against cleat and flashing plates (Right)

The von Mises stress contours (in MPa) on the coping and cleat plates resulting from the finite element analyses are respectively shown in Figure 4.4 and Figure 4.5. From these figures it is observed that:

- Localized stress concentrations occur on the top flange of the flashing around the nails areas, also shown in Figure 4.4;
- Maximum stresses of 29,240 psf (1.4 MPa) on the metal flashing occur at the top flange, as shown in Figure 4.5;
- A localized stress concentration (of almost 125,313 psf (6 MPa)) occurs on the cleat plate around the nail area, as illustrated in Figure 4.5.

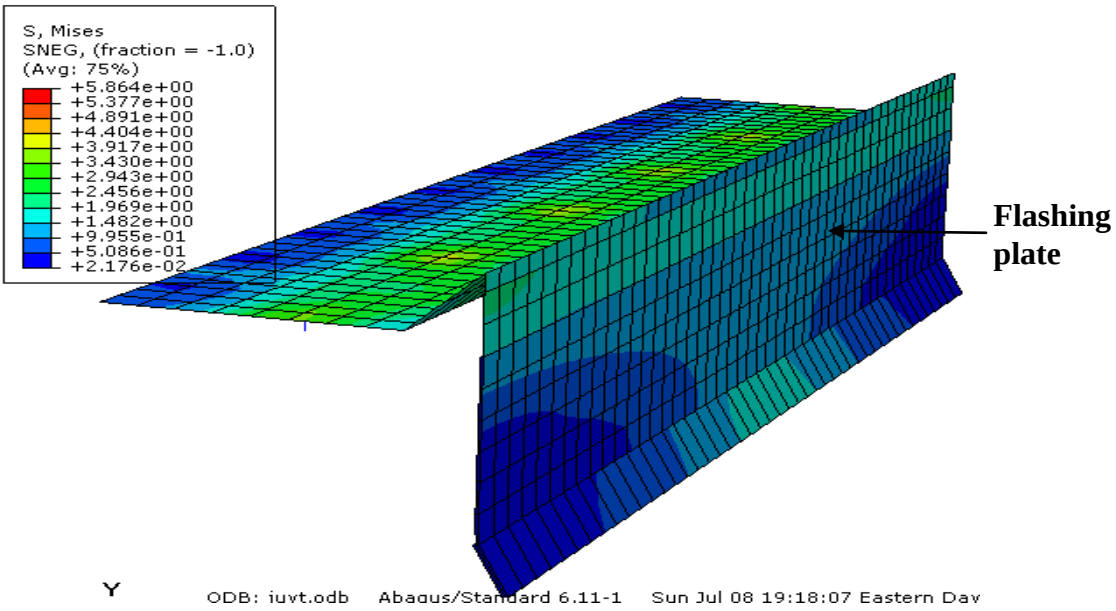

Figure 4.4 Stress contour of the flashing plate subject to uniform pressure for record M28N368 (ABAQUS Scale 1:1)

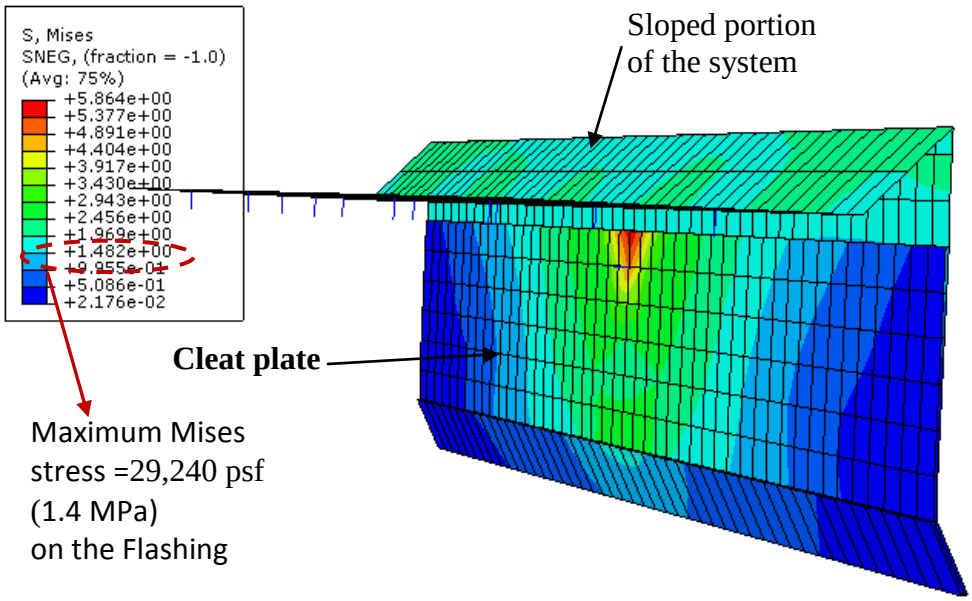

Figure 4.5 Stress contour of the cleat plate around the nail area subject to uniform pressure for Tap No 802R mean pressure data (ABAQUS Scale 1:1)

- Based on finite element modelling of the system using the ABAQUS software, the nail reaction of the cleat and the maximum deflection of the flashing plate are given in Table 4.2.

Table 4.2 Comparison between deformation and cleat reaction force for 802R tap for M28N368 data calculated by both ABAQUS and STARDYNE software

	ABAQUS		STARDYNE	
Tap No.	**Mean**	**Peak min**	**Mean**	**Peak min**
$\boldsymbol{\Delta P}$ psf (Pa)	2 (97.2)	7.7 (378)	2 (97.2)	7.7 (378)
$\mathbf{U_z}$ Inches (mm)	0.012 (0.3)	0.047 (1.2)	0.002 (0.05)	-
$\mathbf{F_N}$ lbf (N)	0.4 (1.78)	1.6 (7.1)	0.4 (1.78)	1.64 (7.29)
Maximum stress psf (MPa)	29240 (1.4)		21303 (1.02)	

McDonald et al (1997) modelled the roof edge system Flashing A using the finite element analysis. The behaviour and results of the finite element analyses for both ABAQUS and STARDYNE are compared in Table 4.2. In ABAQUS, a static analysis was used to predict the behaviour of the system and obtain coping deflection and nail reaction forces. On the other hand, in STARDYNE, the analysis consisted of two parts static and dynamic one. In general, both analyses calculate maximum stress concentrations on the sloped portion of the flashing, Figure 2.13 and Figure 4.4. From the results in Table 4.2 it is found that the nail reaction of the cleat using ABAQUS is the same as the nail reaction determined by STARDYNE. On the other hand, the ABAQUS analysis predicts a higher deflection value of 0.012" (0.3 mm) in comparison to 0.002" (0.05 mm) for STARDYNE. This could result from the different assumptions made in imposing the boundary conditions on the system and from defining the surfaces' interaction between flashing and cleat plates. For example, in the ABAQUS analysis a contact mechanism between the interacting surfaces of the cleat and flashing plates were accounted for to better define the system behaviour, while in STARDYNE the contact mechanism was neglected for

simplification purposes. More importantly, the variation in deflection results could result due to the different nature of load application (static or dynamic) on the system between the two analyses.

Finally, from the overall finite element analysis, the results from ABAQUS support the same finding previously established by the STARDYNE analyses where the cleat plate is established as an important component of the roof edge in resisting the applied wind pressure. Whether the load is applied against the cleat or flashing plates, the cleat plate stiffens the overall roof edge and provides additional strength to the overall roof edge.

4.3 Continuous Cleat Configuration – Set A

The Continuous cleat configuration is comprised of a continuous cleat (two segments of 8' (2.4 m) cleat plates) nailed to the parapet with a group of single row of nails spaced every 18" (457 mm). In the finite element analyses, the wind-induced pressure was applied on one- and three-planes against the face of the cleat and coping plates, respectively, as shown Figure 3.10. The roof edge performance was analyzed in terms of the coping plate deflection at mid depth at ¼ and ½ L of the middle segment (see Figure 4.1) and in terms of the nail reactions. Cross section Set A has the following geometry dimensions 12" / 6" / 10" (H_f / H_b / W_{co}), as illustrated in Figure 3.3 and Figure 3.4. Three different modelling approaches, as presented in Chapter 3, were utilized in the analyses to simulate the connection between the coping and the cleat plates, namely, vertical edge (approach 1), sealed edge (approach 2) and drip edge (approach 3). The results of the three modelling approaches were compared to each other in terms of the coping plate deflection to determine the optimal approach in predicting the roof edge behaviour.

4.3.1 One-Plane Pressure Applied Against Cleat Plate

The continuous cleat configuration Set A was analyzed under a uniform static pressure applied on one plane against the face of the two 8' (2.4 m) cleat plates (Figure 4.6). The pressure was increased from 10 to 90 psf (479 to 4,309 Pa) at an increment of 20 psf (958 Pa). The following assumptions were made during the analysis: (i) the pressure is applied only against the face of the cleat plate, and (ii) the coping plate is installed snug-tight to the parapet structure, hence, boundary conditions are imposed on the coping plate as illustrated in Figure 4.6.

Since the pressure is applied against the cleat plate, contact is defined between the front height of the cleat and coping plates (H_f and H_{cl}) for all three modelling approaches used. In addition contact is defined between the coping and cleat plates at the continuous and drip-edge connections for both approaches 2 and 3, respectively. Figure 4.7 shows the deflection of the coping plate at ¼ of the length against the applied pressure for the three modelling approaches of the coping/cleat connection. By comparing the three approaches, it is noted that both the continuous and drip-edge connections, approaches 2 and 3, respectively, stiffen the overall system behaviour, whereas the results for approach 1 show a softer response. The deflections of the coping plate at ¼ L and ½ L are significantly reduced for approaches 2 and 3 in comparison to that of approach 1, Figure 4.7. Furthermore, approach 2 is slightly stiffer than approach 3, since the connection between the coping and cleat plates is continuous and both plates act as one piece.

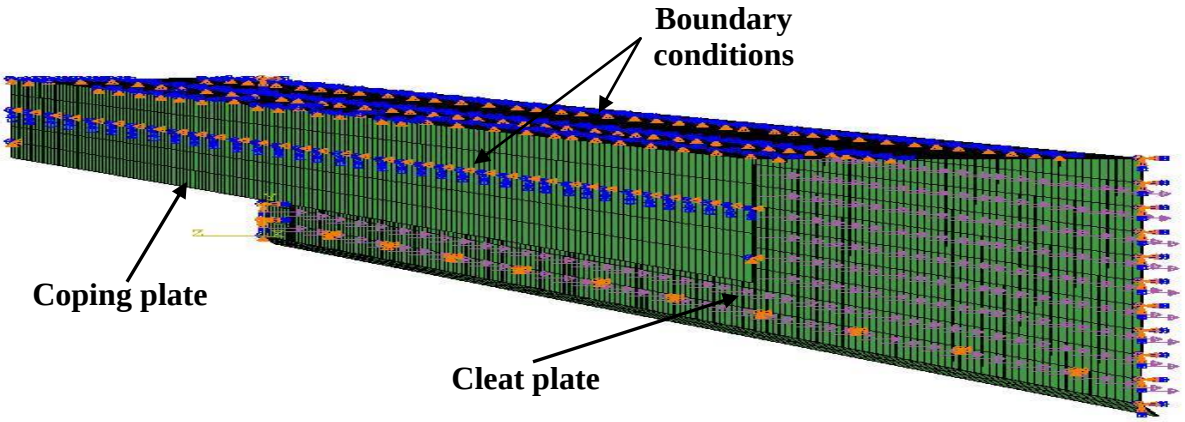

Figure 4.6 One-plane pressure is applied against cleat plate (approach 3)

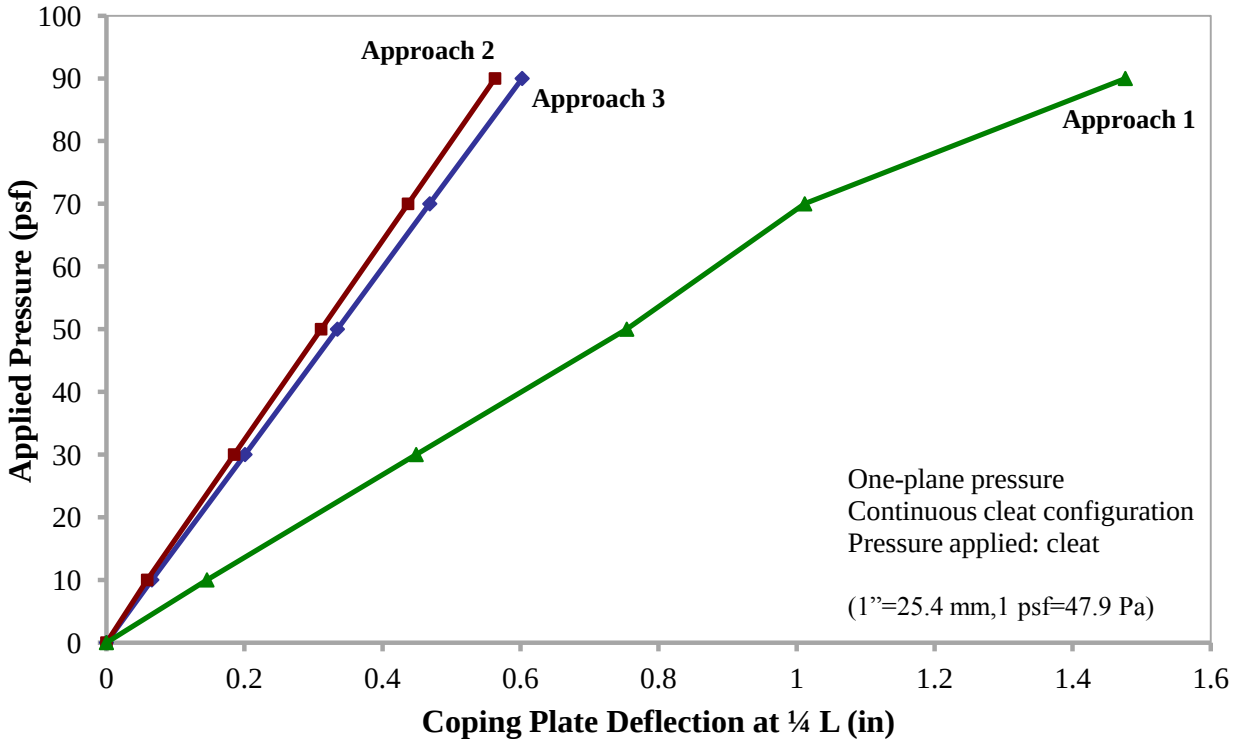

Figure 4.7 Coping plate deflection at ¼ L for the three approaches for one-plane pressure applied against the cleat plate for the continuous cleat configuration

Figure 4.8 shows the coping deflection at one quarter of the length of the plate against the coping plate depth. From the figure, it is observed that the coping plate deflection follows a parabolic pattern for approach 3, with a maximum deflection at mid depth. On the other hand, the deflection results for approach 1 show that the coping plate experiences severe outward deflection, with maximum deflection at the bottom edge of the plate. The drip-edge connection between the coping and cleat plates stiffens the overall performance of the roof edge and

prevents excessive deflection of the bottom edge of the coping plate at the maximum pressure of 90 psf (4,309 Pa). Because modelling approach 3 best resembles the actual physical response of the roof edge, it is chosen to simulate its performance when subjected to one-plane pressure against the cleat plate, in order to validate the model against experimental results.

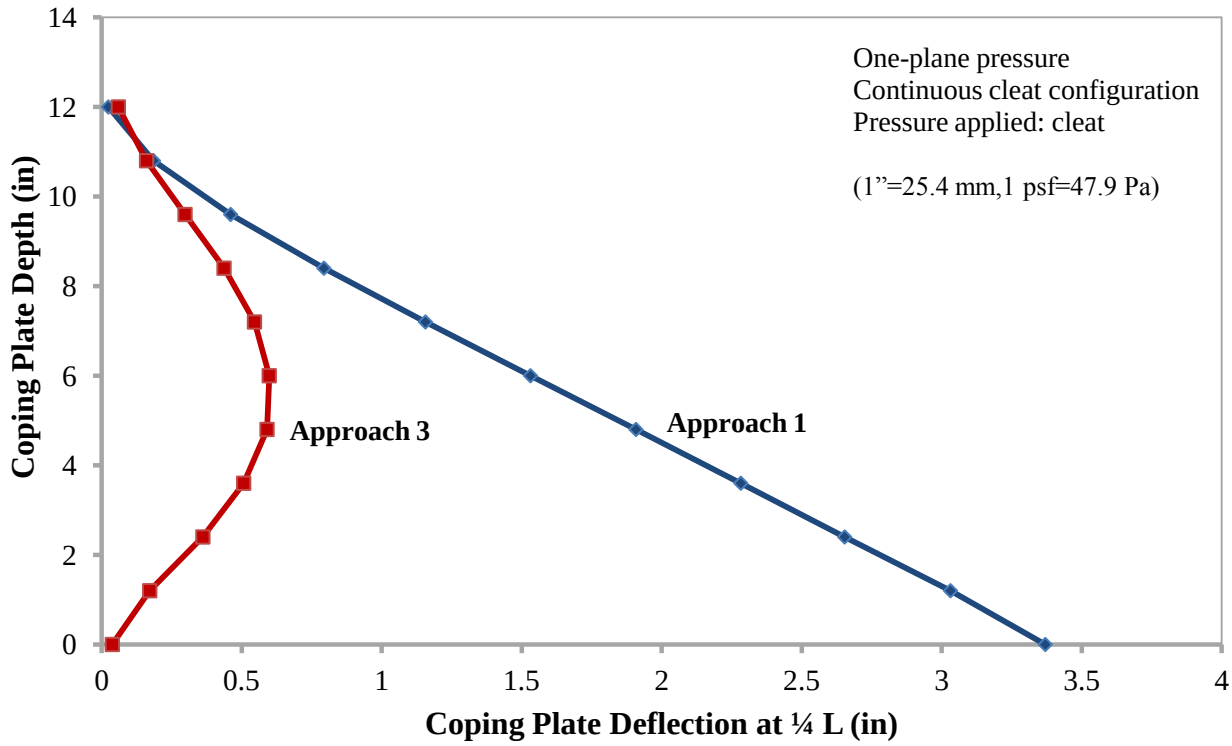

Figure 4.8 Coping plate deflection at ¼ L against the coping depth for modelling approaches 1 and 3 for one-plane pressure of 90 psf (4,309 Pa) against the cleat plate for continuous cleat configuration

Figures 4.9 and 4.10 show the resulting von Mises stress contours on the cleat and coping plates, respectively, when the cleat plate of the continuous cleat configuration is subjected to a one-plane pressure of 90 psf (4,309 Pa). From the figures, it is observed the following:

- Moderate stress concentrations and deformations of the cleat and coping plates around mid-depth of the plates, Figure 4.9 and Figure 4.10,
- Moderate stress concentrations and localized deformation of the cleat around the nail area, Figure 4.9; and,

- Deformation and minor lifting (less than ¼" (6 mm)) of the drip-edge connection without connection disengagement, as shown in Figure 4.8.

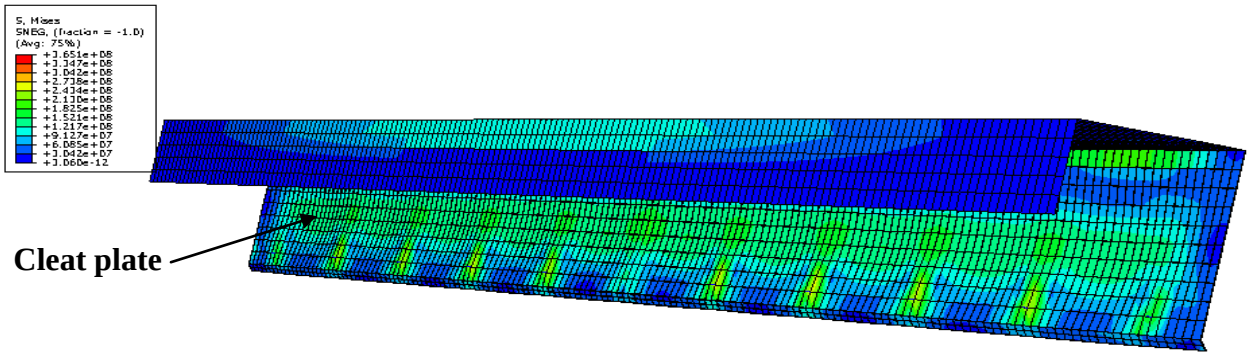

Figure 4.9 Stress contours (Pa) on the cleat plate at 90 psf (4309 Pa) pressure (approach 3)

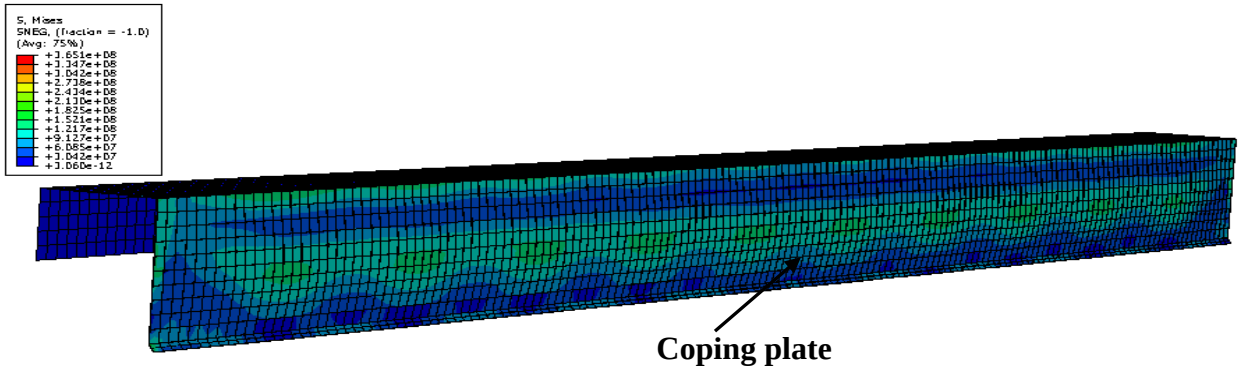

Figure 4.10 Stress contours (Pa) on the coping plate (approach 3)

Figure 4.11 shows the deformation of the coping plate in the experimental tests conducted under the same conditions (Alassafin 2012). Figure 4.12 shows a diagram illustrating the deformation pattern under the applied pressure. The deflection profile along the depth of the coping plate and at mid-length of the roof edge resulting from the finite element analysis is illustrated in Figure 4.13. This figure shows a similar pattern as that observed in the experiment, in which the maximum deflection of the coping plate occurred at mid depth. The comparison of deflection values at ¼ and ½ of the length of the coping plate between the experimental and numerical results is presented in Figure 4.14. The comparison between the two sets of results show very good agreement.

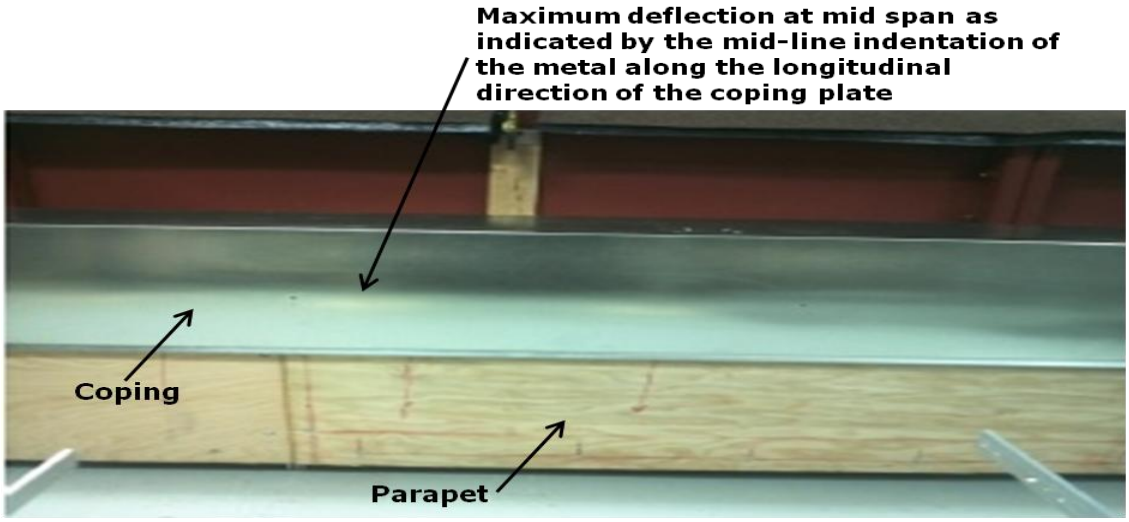

Figure 4.11 Maximum deformation of the coping plate at mid-depth (Alassafin 2012)

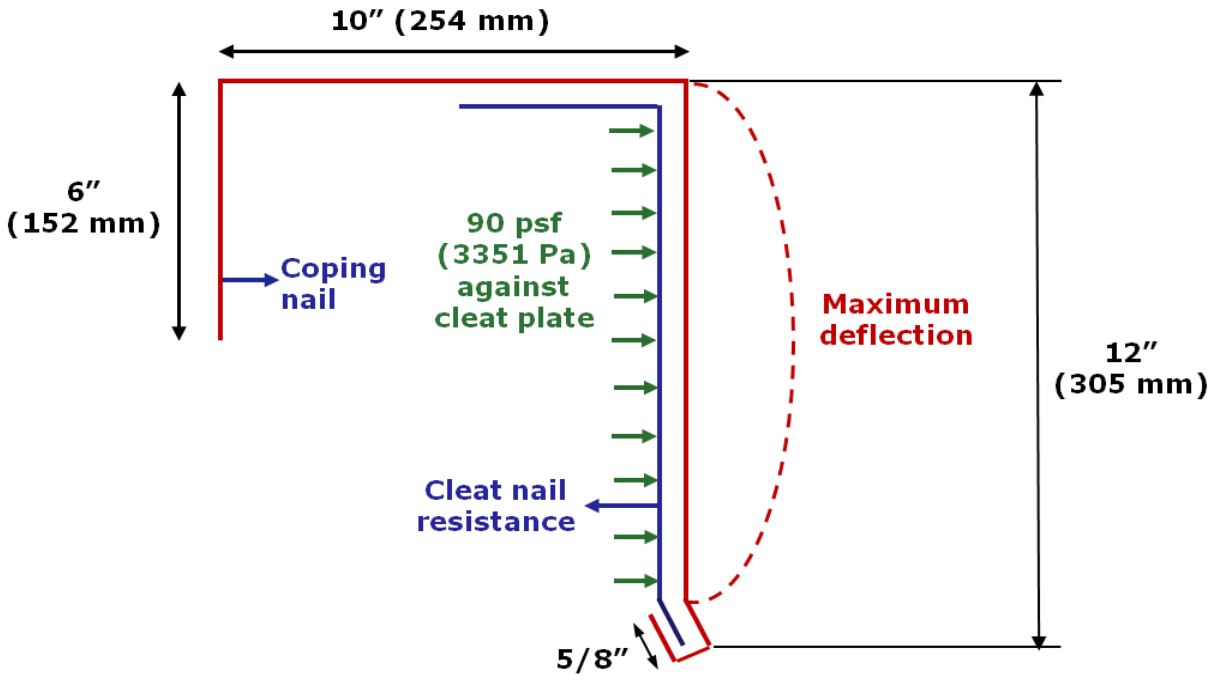

Figure 4.12 Deformation of the coping plate at ½ L along the front height depth H_f for one-plane pressure against the cleat plate for continuous cleat configuration (approach 3)

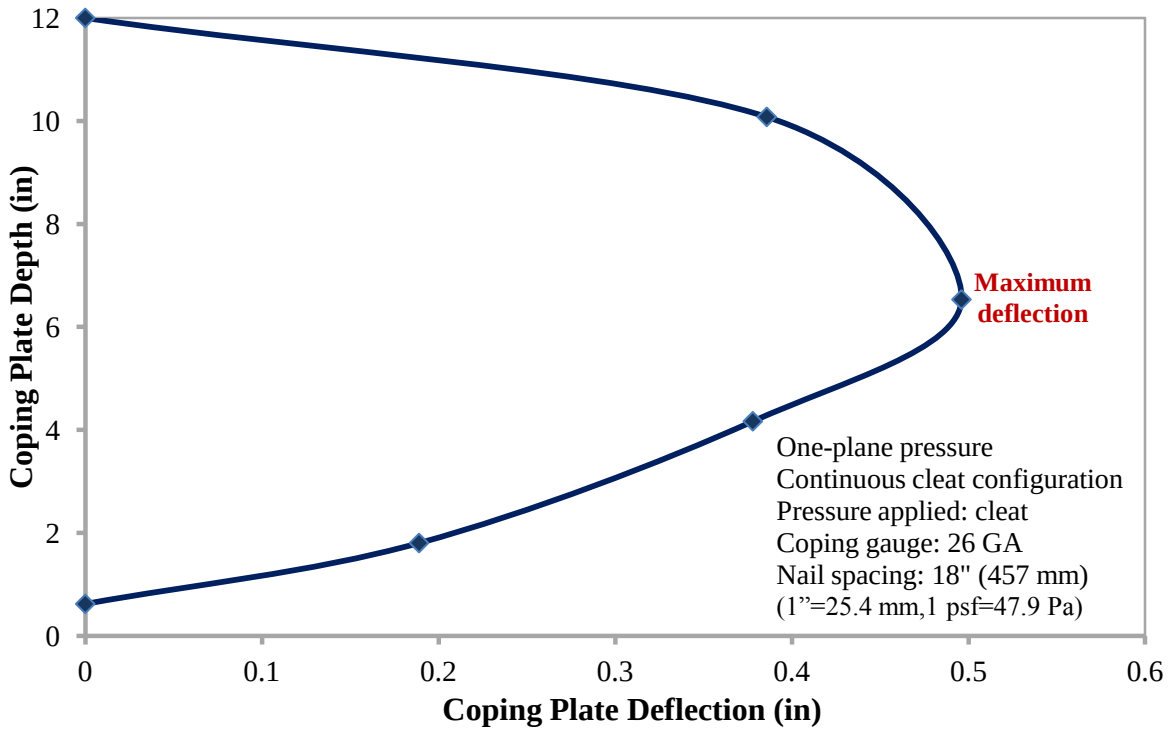

Figure 4.13 Deflection of the coping plate at ½ L along the front height depth H_f for one-plane pressure applied against the cleat plate for continuous cleat configuration (approach 3)

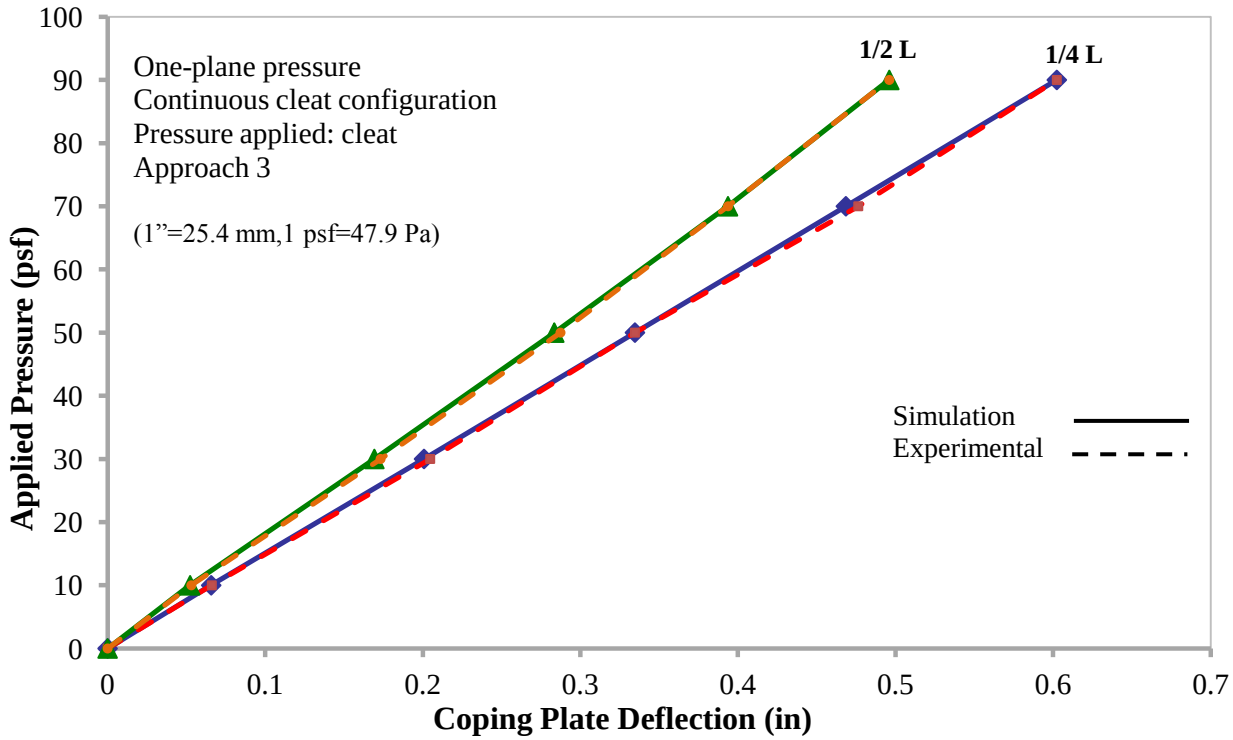

Figure 4.14 Comparison of the finite element deflection results at ¼ and ½ L for the continuous cleat configuration (approach 3) against experimental values

The assumption of linear analysis is further explored by running the same configuration under both assumptions, i.e., linear and nonlinear analyses. Figure 4.15 shows the coping plate deflection from both analyses against the experiment's results. In this case, it is evident that linear analysis is sufficient to model the roof edge behaviour. This is because the roof edge does not undergo large strains or rotations under the effect of the applied pressure. In addition, the material behaviour is within the elastic range. Although boundary conditions are not constant as the pressure is increased, since the pressure applied against the cleat plate pushes the cleat against the coping plate, this source of nonlinearity is accounted for in the definition of the contact interaction between the two surfaces. Therefore, a linear analysis proves sufficient to predict the system behaviour under the applied one-plane uniform pressure.

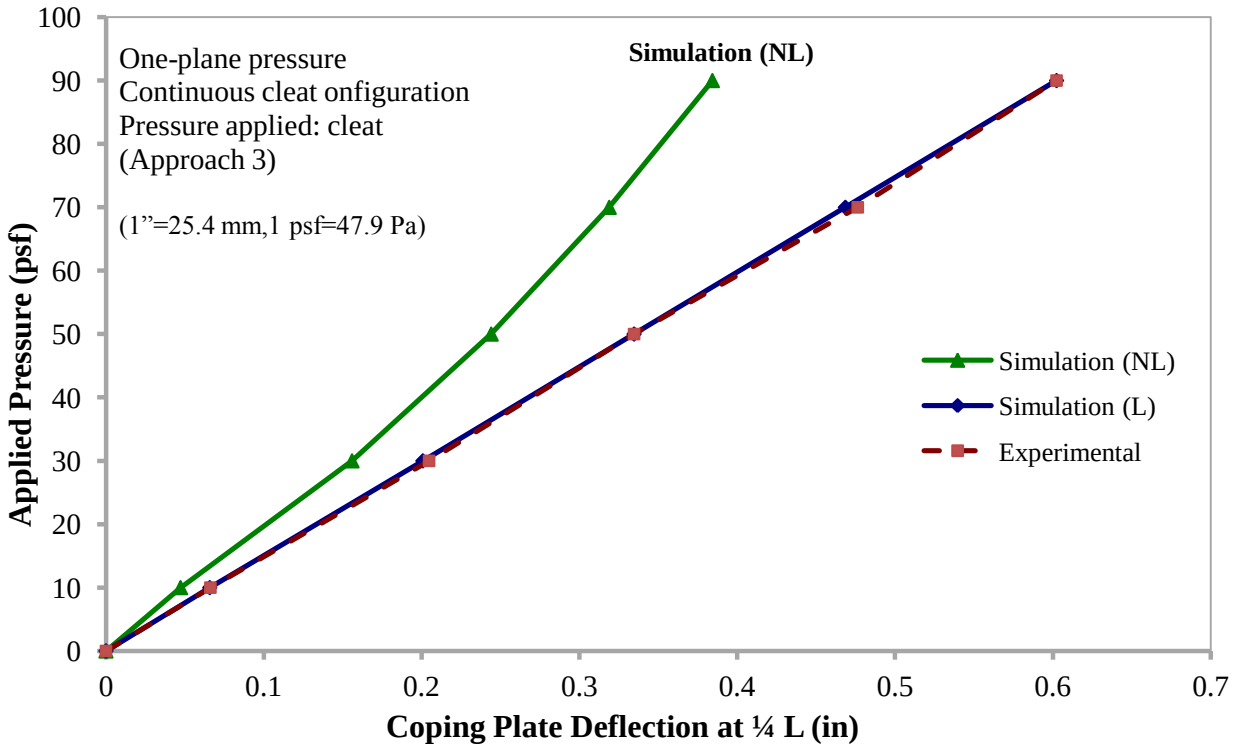

Figure 4.15 Comparison between linear and nonlinear analysis of finite element deflection results at ¼ L for one-plane pressure applied against the cleat plate for the continuous cleat configuration with the experimental ones

Figure 4.16 shows the finite element results for the nail reaction as a function of the applied pressure. As expected this relationship is linear, with a nail reaction of 62 lbf (276 N) at a maximum applied pressure of 90 psf (4,309 Pa).

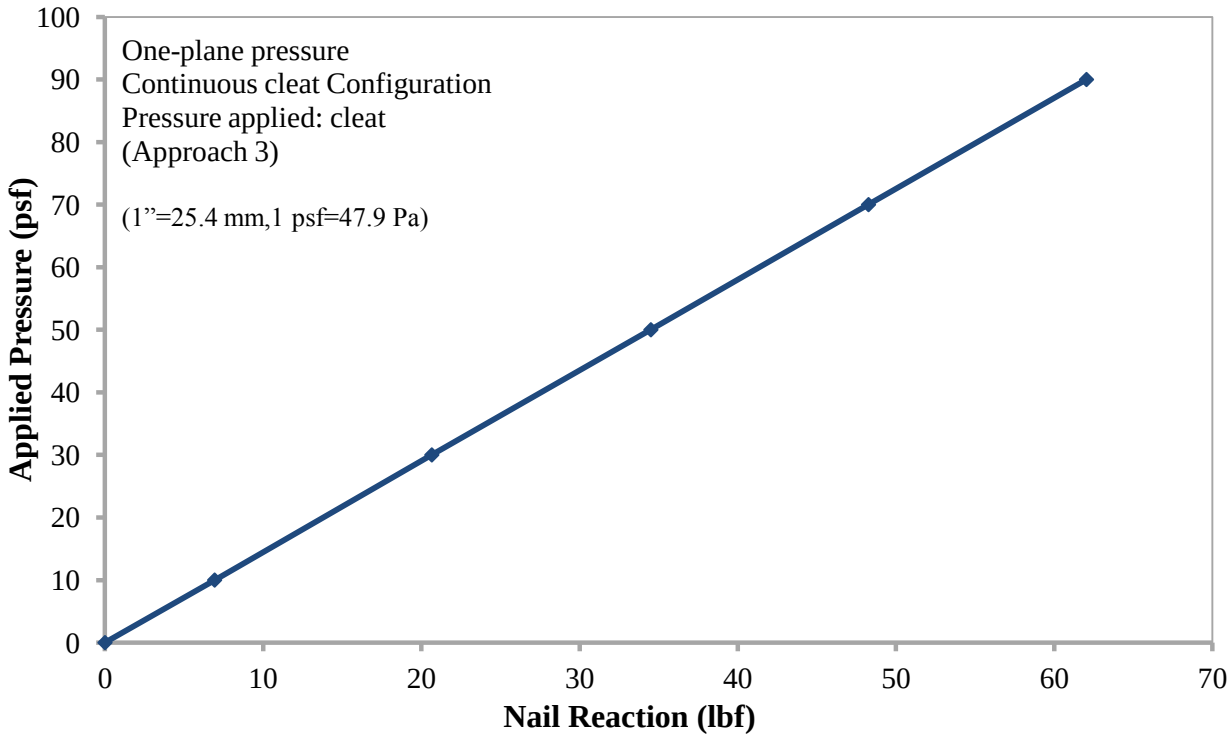

Figure 4.16 Nail reaction response to one-plane pressure applied against the cleat plate for continuous cleat configuration (approach 3)

4.3.2 Three-Plane Pressure Applied Against Cleat Plate

Three-plane pressure refers to a uniform static pressure that is applied against the full system, i.e., against the 12" (305 mm) face of the cleat plates (H_{cl}) and against the top 10" (254 mm) coping plate (W_{co}) and 6" (152 mm) short leg of the coping plate (H_b) as illustrated in Figure 3.5 and Figure 4.17. Coping plate deflection results at ¼ and ½ L were also analyzed and verified with those obtained from test experiments. In addition, nail reactions were monitored at five pressure points at an increment of 20 psf (958 Pa) from 10 to 90 psf (479 to 4,309 Pa).

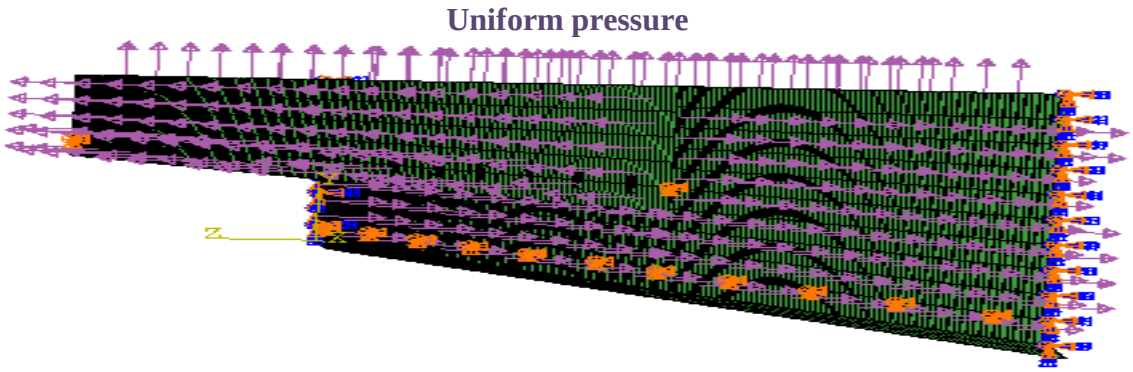

Figure 4.17 Three-plane pressure applied against the full system

For the analysis where a three-plane pressure applied against the cleat plate, the following findings are observed:

- Moderate stress concentration at mid-depth of the cleat plate as shown in Figure 4.18;
- Stress concentrations around the nail area of the cleat plate as illustrated in Figure 4.18;
- Stress concentration around the nail area of the coping short leg (H_b) of the coping plate also seen in Figure 4.18;
- Minor stress concentrations of the coping plate at mid-depth of the long leg (H_f) as illustrated in Figure 4.19; and,
- Minor stress concentrations on the top of the coping plate. This corresponds to approximately $\frac{1}{3}^{"}$ (9 mm) at mid width.

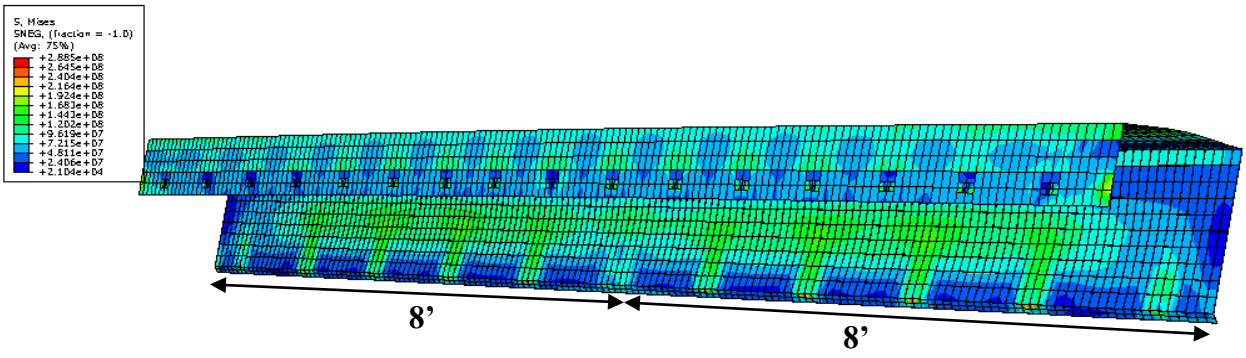

Figure 4.18 Stress contour (Pa) of the cleat plate at 90 psf (4,309 Pa)

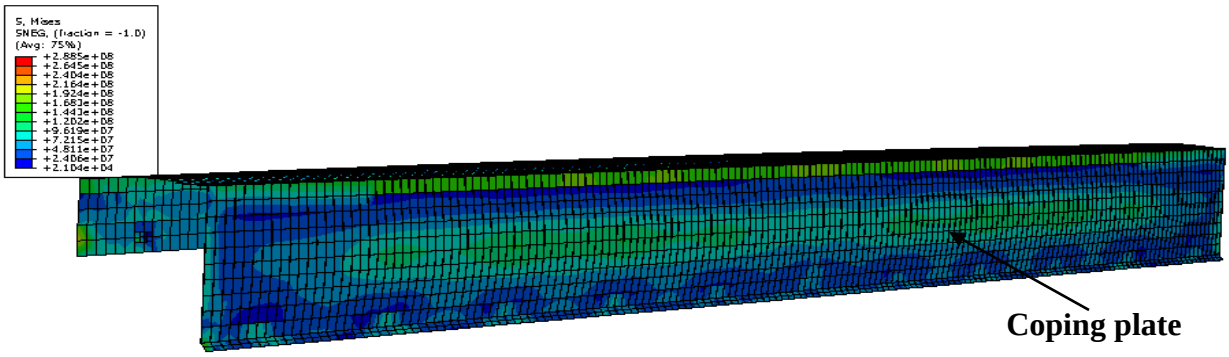

Figure 4.19 Stress contour (Pa) of the coping long leg

Similar to the one-plane pressure, for three-plane pressure applied against the cleat plate, three modelling approaches were used to simulate the roof edge model. For approach 2 and 3, the coping plate deflection results are in close agreement contrary to approach 1, where the system experiences excessive deformations as shown in Figure 4.20. Therefore, either approach 2 or 3 were used for further modelling of the roof edge when a three-plane pressure is applied against the cleat.

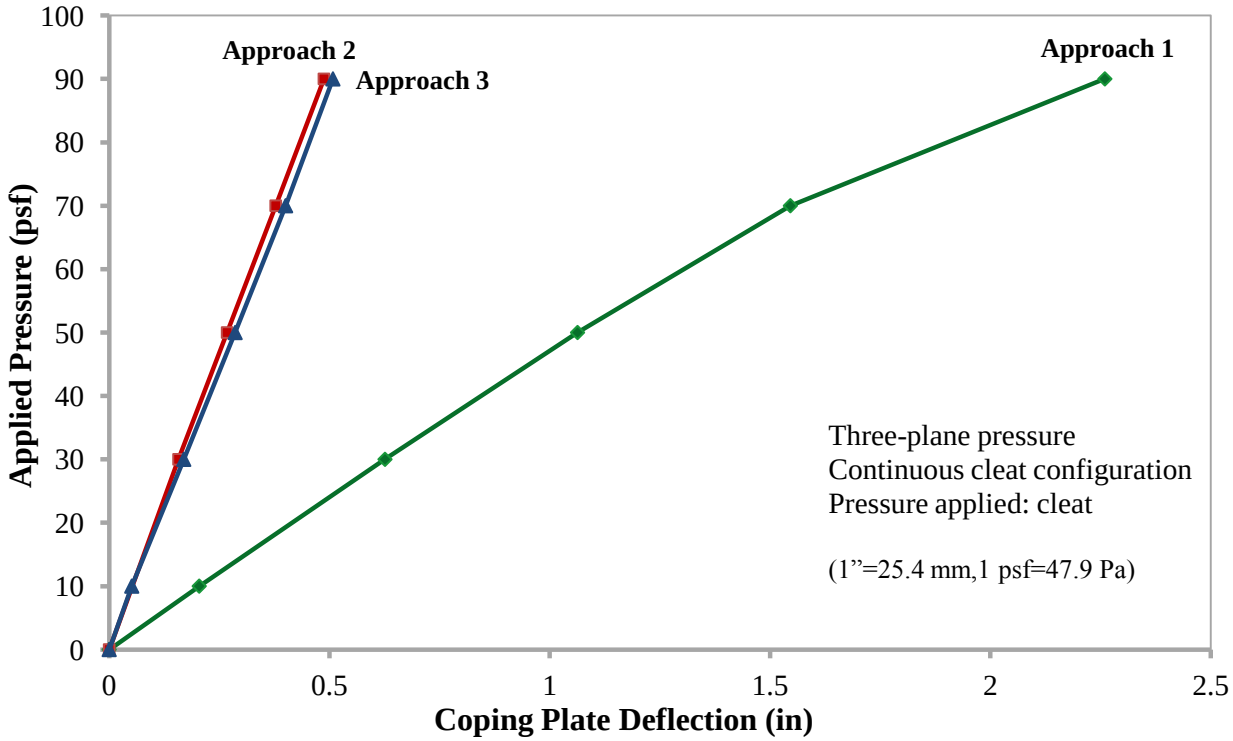

Figure 4.20 Comparison between the three modelling approaches for a three-plane pressure applied against the cleat plate for continuous cleat configuration

Verification of the finite element deflection results of the coping plate with the experimental ones shows close agreement for approach 2 as shown in Figure 4.21. This is because the system experiences a lot of instability due to connection displacement and lifting of the coping as illustrated in Figure 4.22 and approach 2 better reflects the results obtained from the experiment.

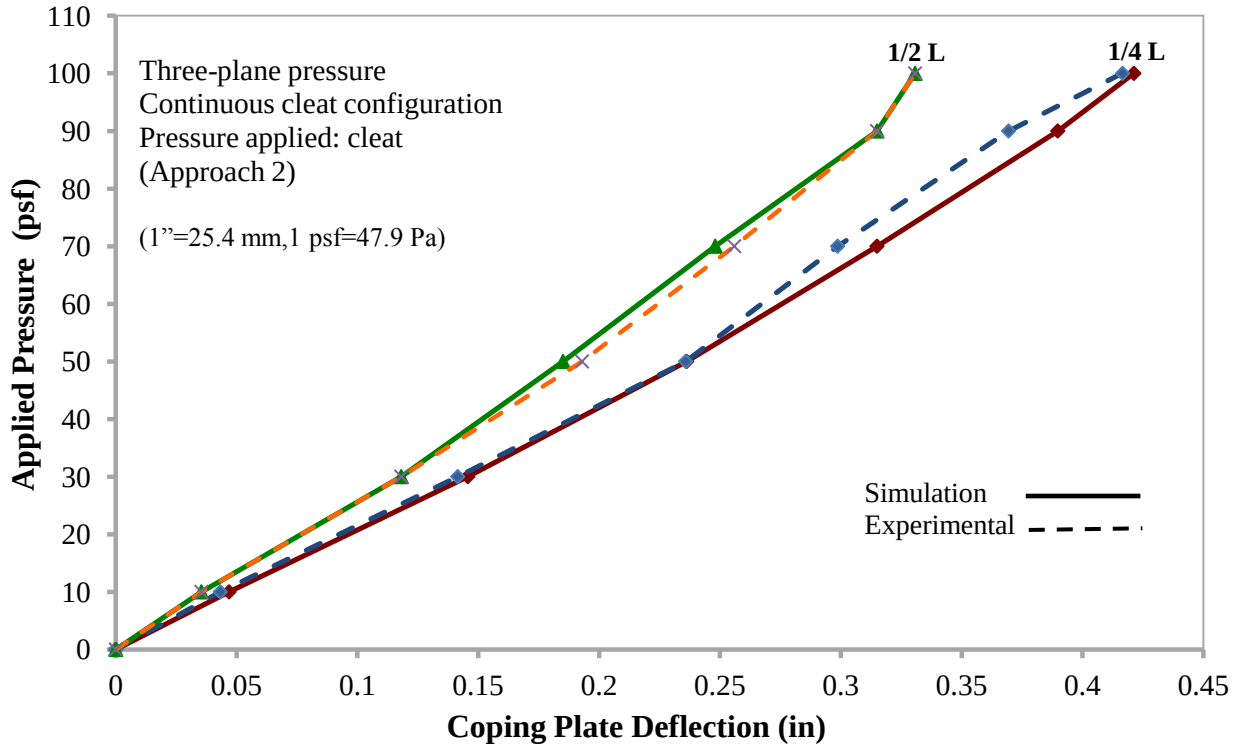

Figure 4.21 Verification of the finite element deflection results at ¼ and ½ L for a three-plane pressure applied against the cleat plate for continuous cleat configuration (approach 2)

For a three-plane pressure applied against the cleat plate for the continuous cleat configuration, the maximum coping plate deflection ocurrs at mid-depth along the front height (H_f) of the coping plate, Figure 4.22. Figure 4.22 shows that the coping /cleat connection experiences minor lifting and displacment of less than 0.1" (3 mm). This finding was similary observed and verified with the test experiments (Alassafin 2012).

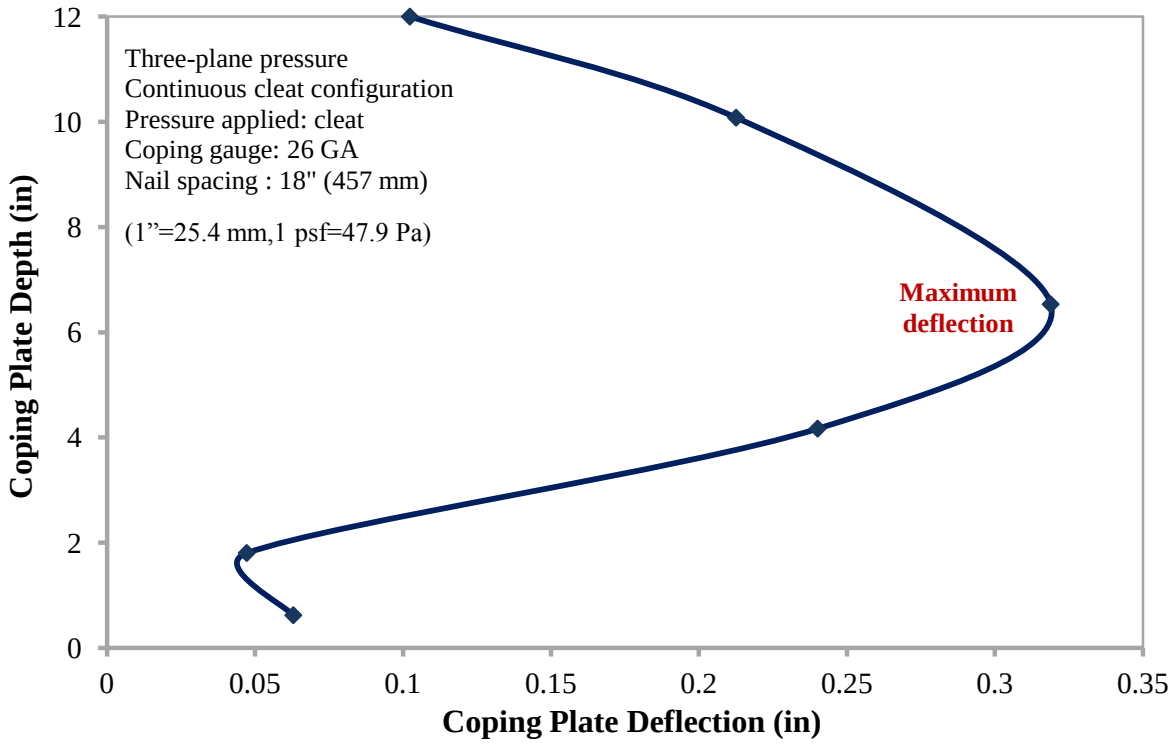

Figure 4.22 Deflection along the front height of the coping plate (H_f) for three-plane pressure against the cleat plate for continuous cleat configuration (approach 2)

Figure 4.23 shows a comparison between linear and non-linear analyses for three-plane pressure applied against the cleat plate. From the figure it is observed that the non-linear analysis better represents the results obtained from the experiments. This is because the system undergoes large deformations and rotations leading to geometrical nonlinearities. The boundary conditions also change due to the contact interaction between the cleat and coping plates; however, this phenomenon is accounted for in the contact property definition in ABAQUS.

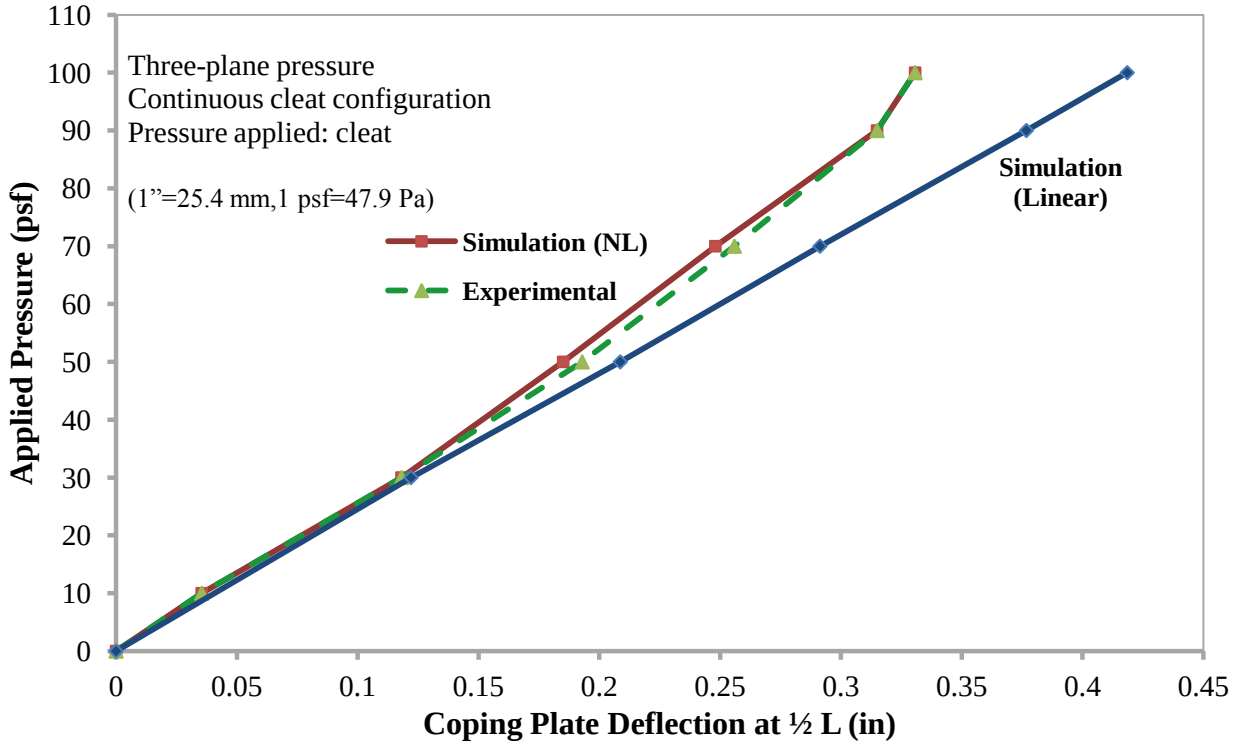

Figure 4.23 Comparison between linear and nonlinear analysis for three-pressure plane applied against the cleat plate for the continuous cleat cnfiguration (approach 2)

For a three-plane pressure applied against the cleat plate, the nail reaction increases as the applied pressure increases. As illustrated in Figure 4.24, at 90 psf (4,309 Pa), the nail reaction is approximately 60 lbf (267 N) which is almost the same value obtained at the same pressure of 90 psf (4,309 Pa) for a one-plane pressure applied against the cleat plate (Figure 4.16).

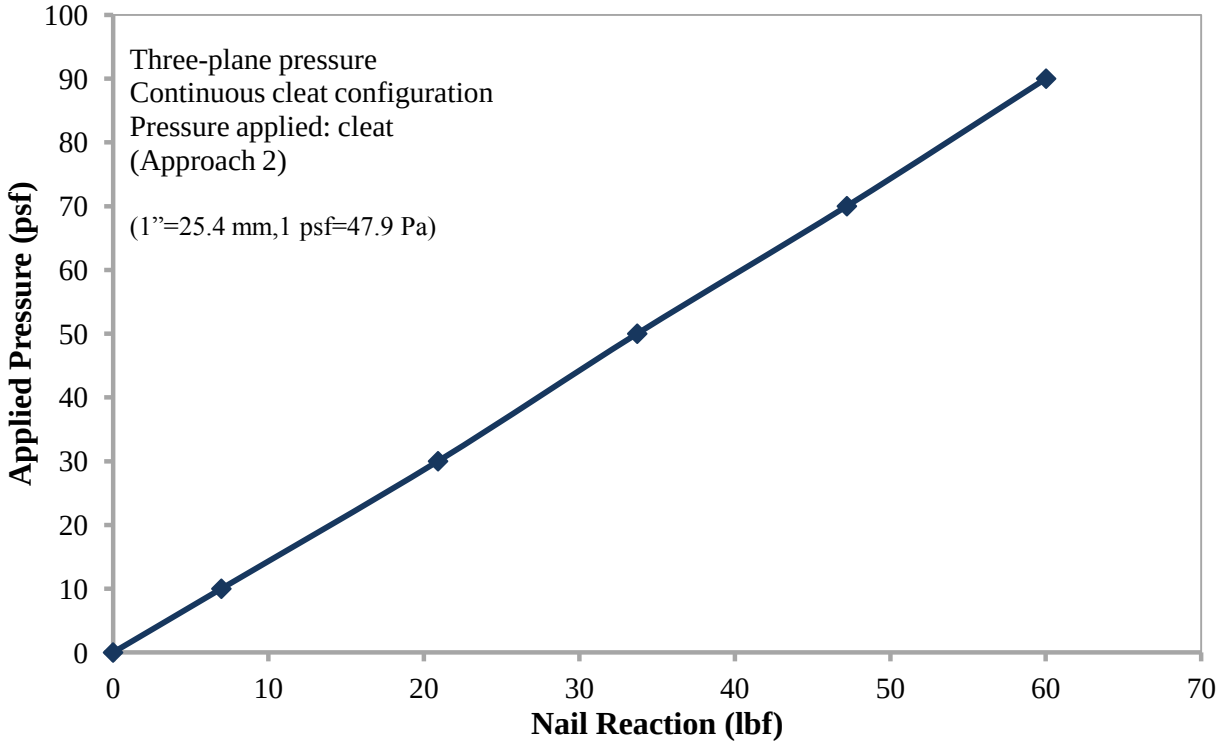

Figure 4.24 Nail reaction for a three-plane pressure for continuous cleat configuration (approach 2)

4.3.3 Concluding Remarks

For both one-plane and three-plane pressure cases, it was established that both modelling approaches 2 and 3 led to deflection results that are in a good agreement with the experimental deflection results, as opposed to approach 1. Therefore, all the remaining analyses were conducted using either approach 2 or 3.

4.3.4 One-Plane Pressure Applied Against Coping Plate

A uniform static pressure was applied against the front height (H_f) of the coping plate. Deflection of the coping plate was analyzed and verified with the deflection results obtained from the test experiments. In addition, nail reactions were calculated at five pressure points at an increment of 20 psf (958 Pa) from 10 to 90 psf (479 to 4,309 Pa). Figure 4.25 and Figure 4.26 show the contours of von Mises stresses at 90 psf (4,309 Pa) from which the following findings are observed:

- Moderate stress concentration and deflection of the cleat plate around nail area, Figure 4.25; and,
- Severe stress concentration and deflection of the coping plate at mid-depth of the coping front height (H_f), Figure 4.26.

It is evident that the coping plate transfer pressure to the cleat plate at the drip-edge connection as the coping plate deforms in shape under the effect of the applied pressure. This leads to build-up of stress concentration at the bottom height of the cleat plate and localized stress concentration around the nail area. If the drip-edge connection is omitted as in approach 1, deformations of system will be limited to the coping plate and cleat plate will remain intact. Hence, approach 1 is discarded.

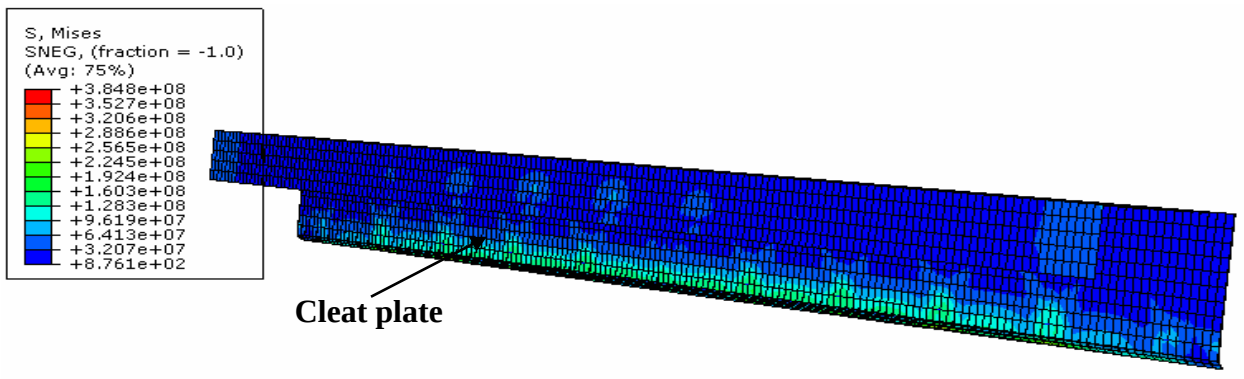

Figure 4.25 Stress contour (Pa) on the cleat plate at 90 psf (4,309 Pa)

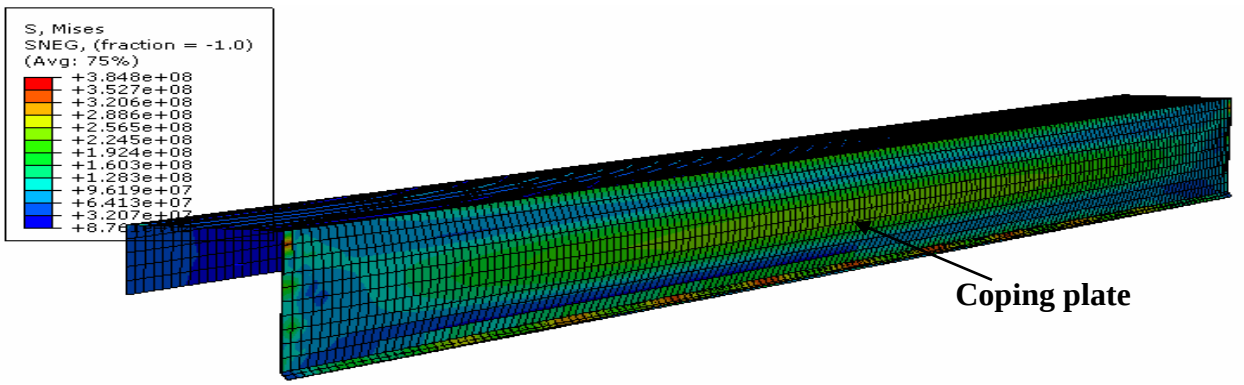

Figure 4.26 Stress contour (Pa) on the coping plate at 90 psf (4,309 Pa)

Figure 4.27 and Figure 4.28 compares the finite element deflection results of the coping plate at ¼ and ½ L respectively, with those obtained from the test experiments. Good agreement is noted between both sets. The maximum deflection of the coping plate occurs at mid-depth of the front height as illustrated in Figure 4.29.

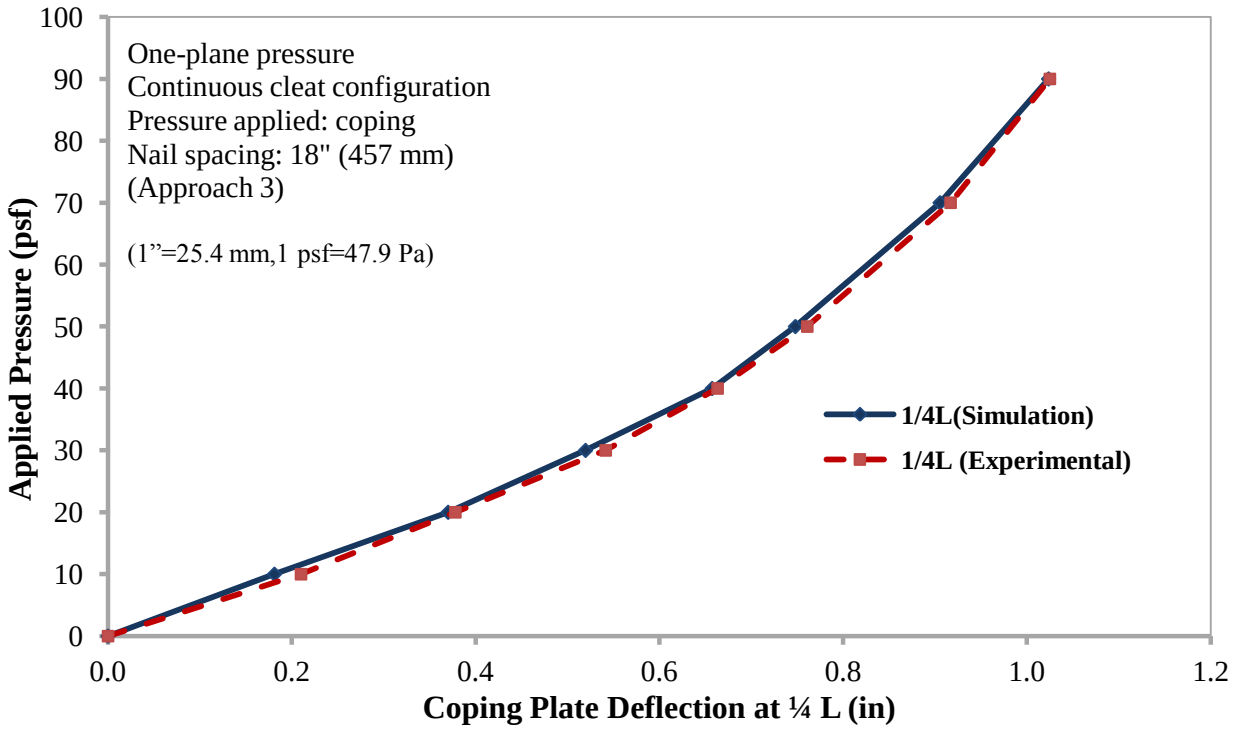

Figure 4.27 Comparion between simulation and experimental deflection results for approach 3 for a one-plane pressure applied against the coping at ¼ L

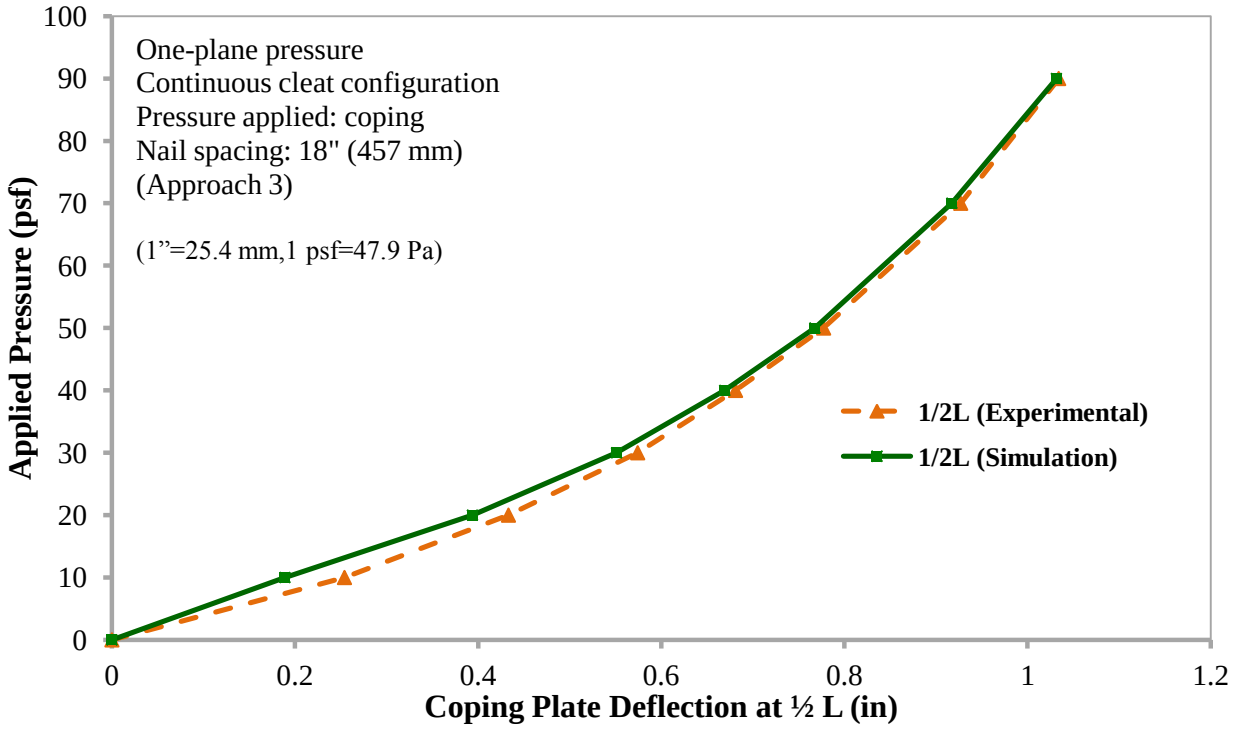

Figure 4.28 Comparion between the experimental and simulation deflection results for a one-plane pressure applied against the coping at ½ L

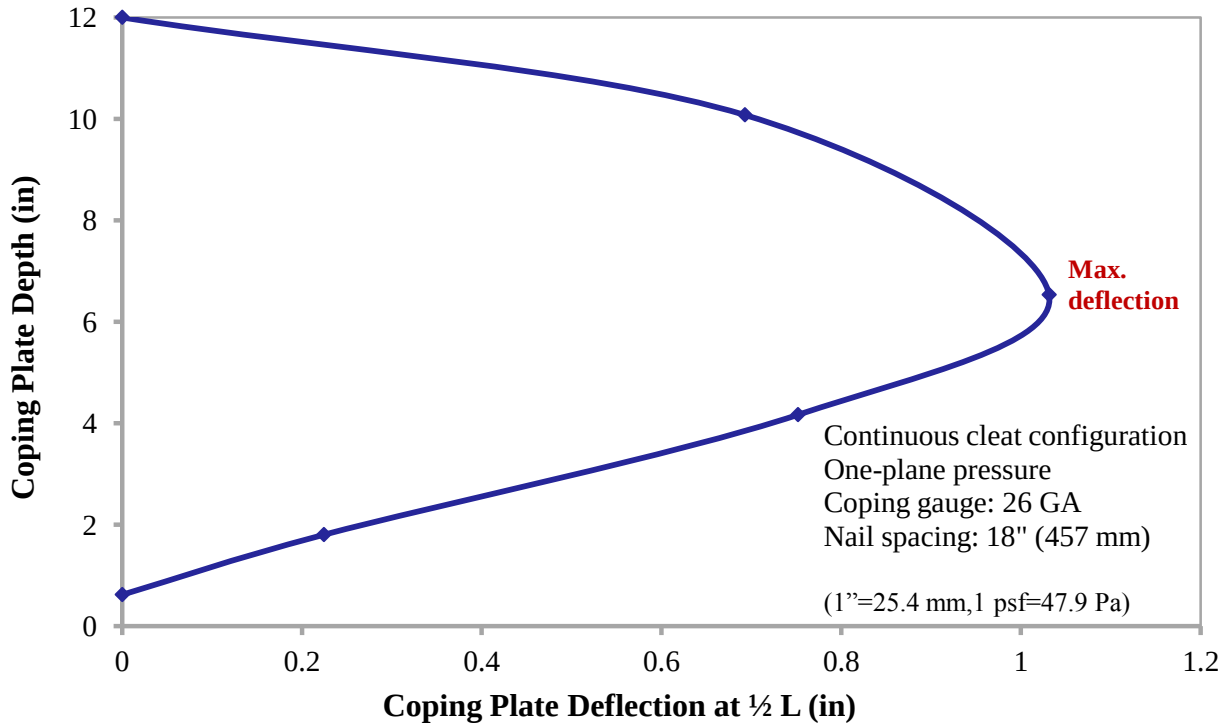

Figure 4.29 Deflection along the coping long leg (H_f)

For a one-plane pressure applied against the coping plate, the nail reaction increases as the applied pressure is increased as illustrated in Figure 4.30. It is noted that this relationship is linear up to 70 psf (3,351 Pa).

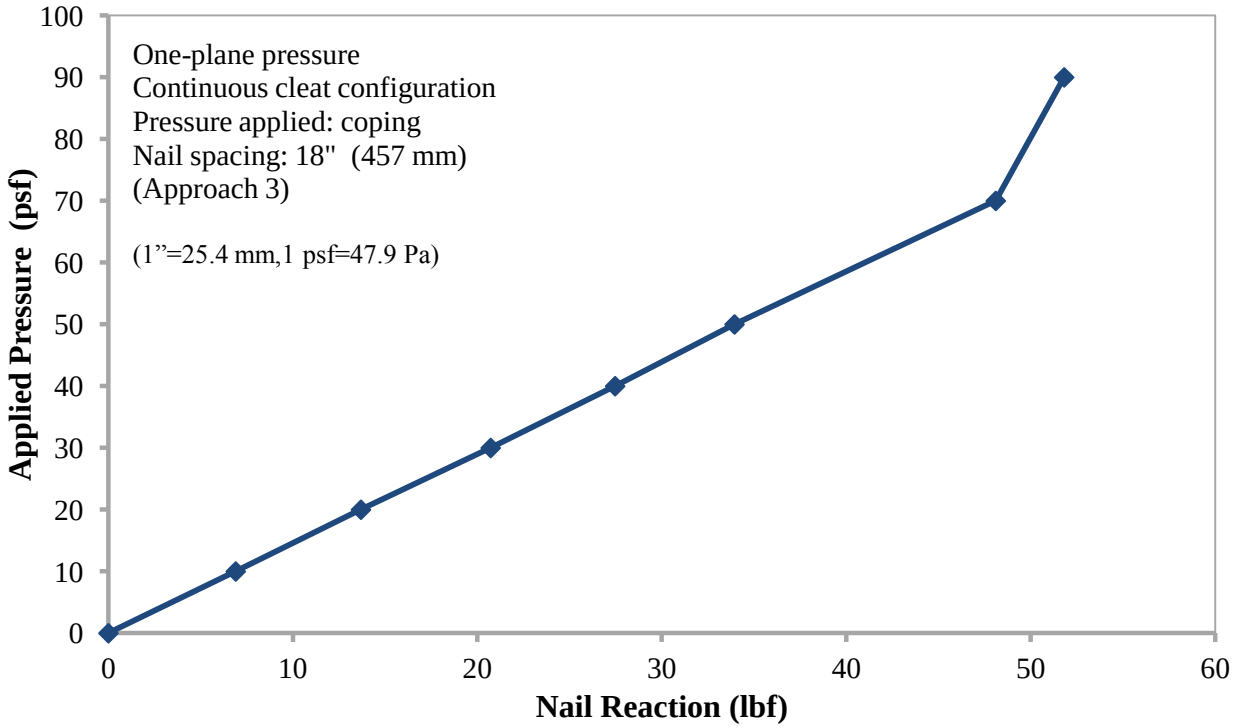

Figure 4.30 Nail reaction at various point pressure for a one-plane presssure applied against the coping

4.4 Discontinuous Cleat Configuration – Set A

The results of the finite element analyses for the discontinuous cleat configuration with cross section details Set A are presented here and compared to the experimental tests conducted at NRC. A discontinuous cleat configuration is comprised of a 40" (1 m) cleat nailed to the parapet with a group of single row of nails at 12" (305 mm) spacing o.c. Modelling approaches 2 and 3 were used for the roof edge analyses. The wind-induced pressure was applied statically on one plane against the coping plate in one case and against the cleat plate on another one.

4.4.1 One-Plane Pressure Applied Against Coping Plate

This section presents the finite element results of the discontinuous cleat configuration Set A subjected to a uniform one-plane pressure against the coping plate. The coping plate defection and nail reactions were analyzed at five pressure levels, with an increment of 20 psf (958 Pa) from 10 to 90 psf (479 to 4,309 Pa).

Figure 4.31 and Figure 4.33 illustrate the contours of the von Mises stresses resulting from the applied load value when modelling approach 3 was used. It is noted from these figures that:

- Stress concentrations and deflection of the coping plate around the 40" (1 m)-cleat segment, Figure 4.31,
- Severe stress concentration on the drip-edge connection between the coping / cleat plates, Figure 4.31,
- Moderate stress concentrations on the cleat plate around the nail area, Figure 4.32; and,
- Lifting and displacement of the drip edge connection as illustrated in Figure 4.33.

At a pressure of 60 psf (2,873 Pa) the coping plate undergoes large deformation of approximately 1 inch around the cleat plate. The drip-edge connection is displaced approximately ¼" (6 mm) and lifted 1/8" (3 mm). More importantly, the coping plate undergoes local yielding at the drip-edge connection due to stress concentrations indicating failure.

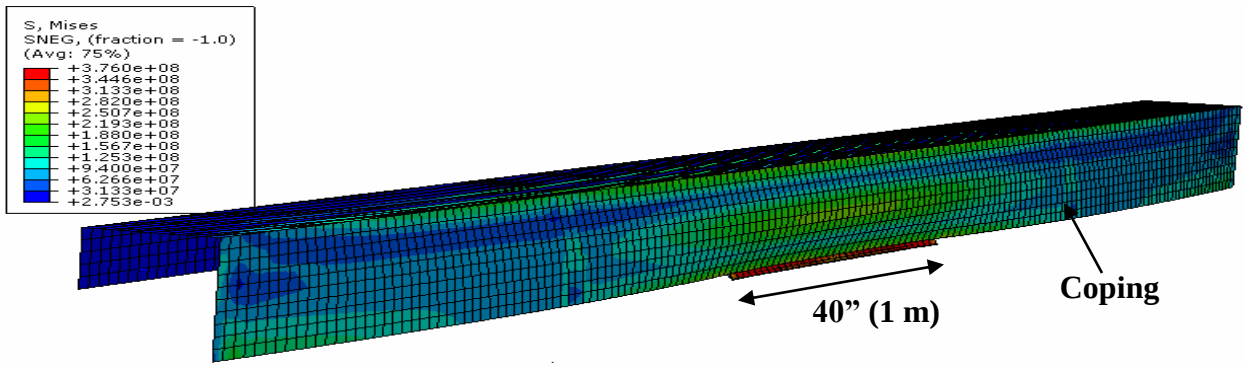

Figure 4.31 von Mises stress contours (Pa) along the coping plate at 90 psf (4,309 Pa)

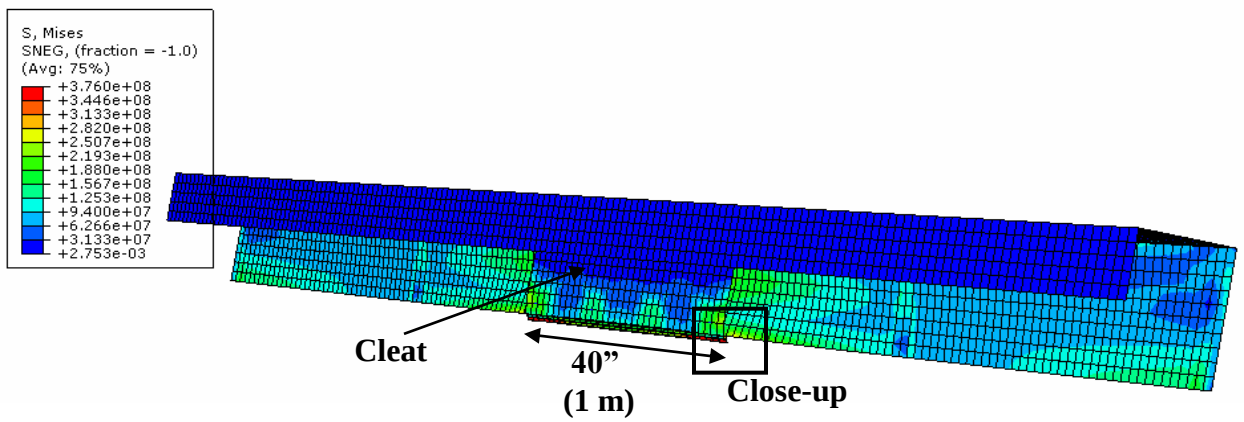

Figure 4.32 von Mises stress (Pa) contours on the cleat plate at 90 psf (4,309 Pa)

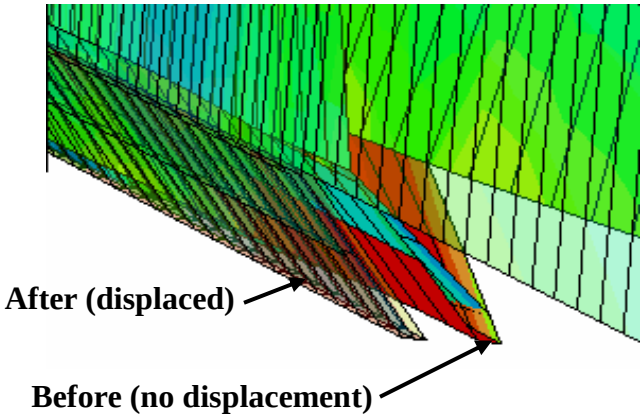

Figure 4.33 Close-up of the before / after displacement of the drip-edge connection in Figure 4.32

The results of the experimental model show severe deformation of the coping plate around the 40” (1 m) cleat plate segment as illustrated in Figure 4.34. In the experiment, failure of the roof edge was governed by disengagement of the coping / cleat drip-edge connection along the middle coping segment. In the finite element model; however, the drip-edge connection experienced minor lifting and displacement without disengagement.

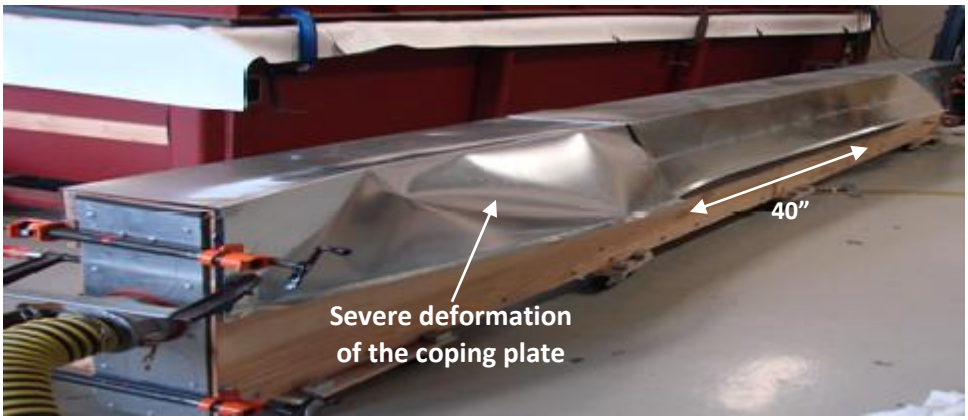

Figure 4.34 Severe deformation of the coping around the 40” (1 m) cleat segment and disengagement of the coping/cleat drip-edge connection along the coping length (Alassafin 2012)

A comparison of the deflection results at ¼ and ½ L of the coping plate between approach 2 and 3 for a one-plane pressure applied against coping plate shows agreement for both approaches as shown in Figure 4.35 illustrates deflection results at ¼ L. The resulting nail reaction is similar for both approaches for a pressure load of up to 60 psf (2,873 Pa) as illustrated in Figure 4.36. Modelling approach 3 transfers more load from the coping to the cleat, resulting in slightly higher nail reaction forces.

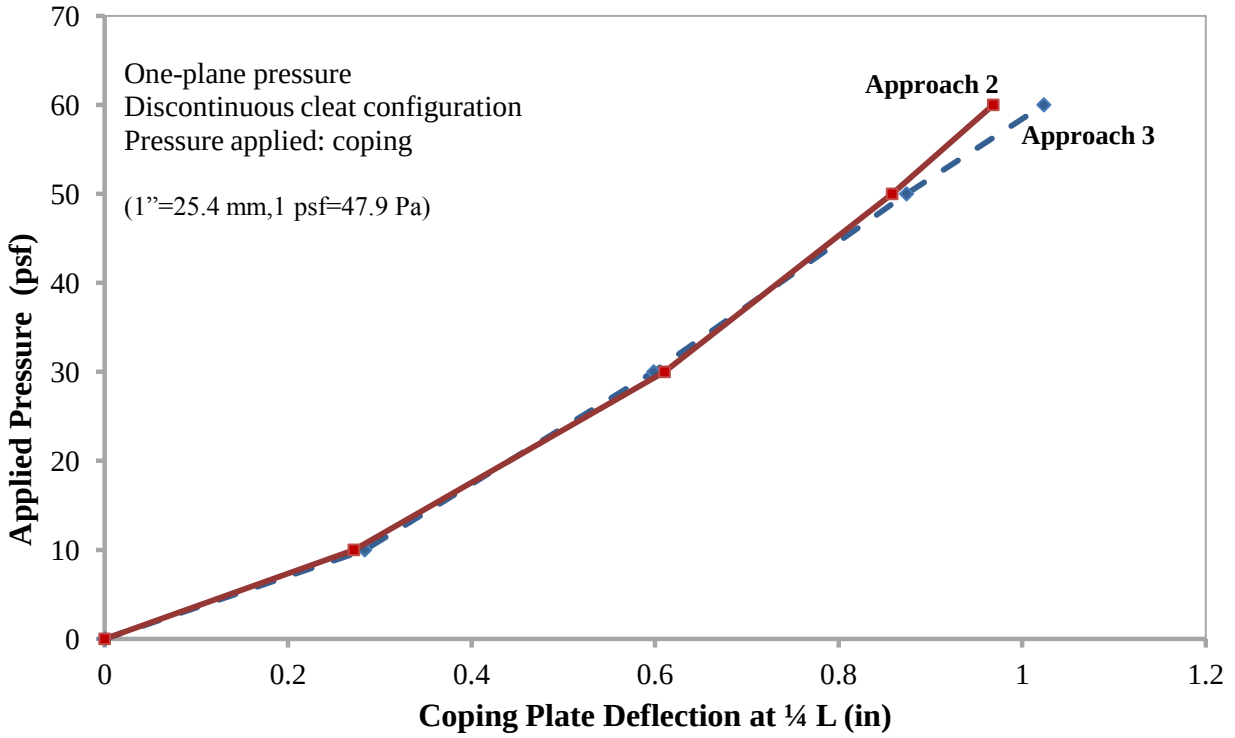

Figure 4.35 Comparison between approaches 2 and 3 for a one-plane pressure applied against the coping plate for discontinuous cleat configuration

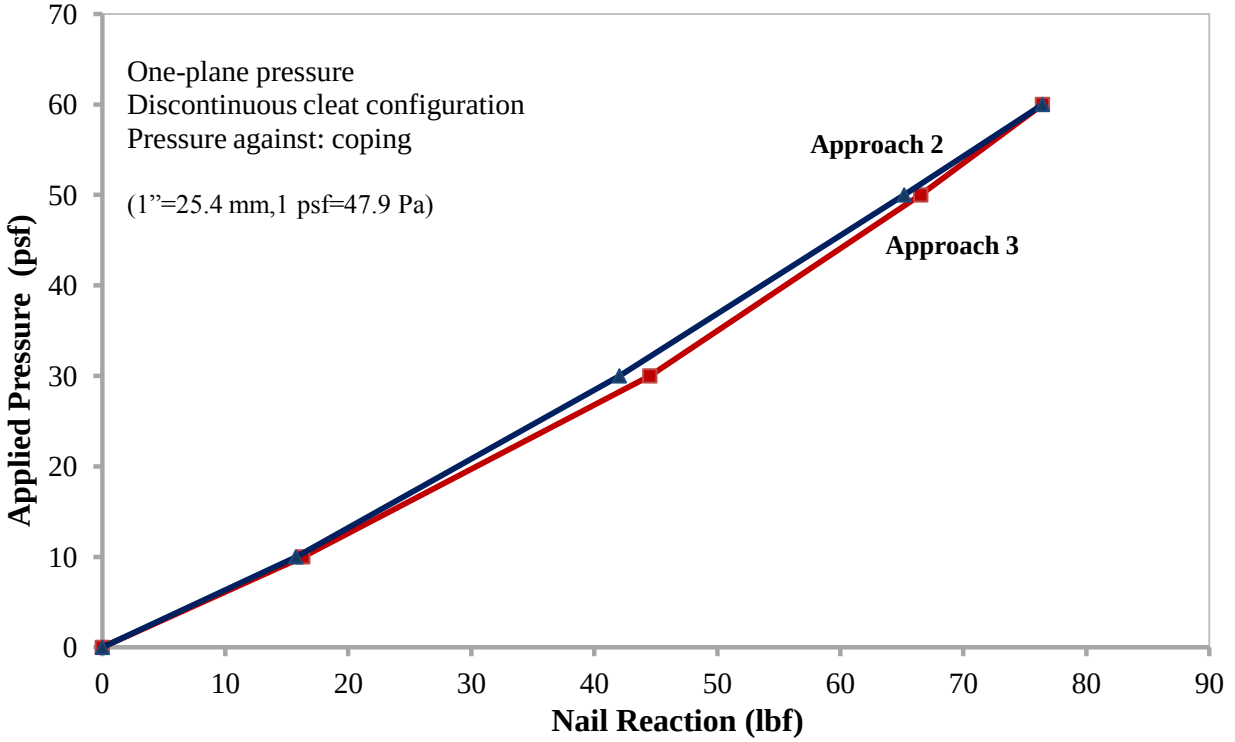

Figure 4.36 Comparison in nail reaction between approaches 2 and 3 for a one-plane pressure applied against the coping plate for the discontinuous cleat configuration

A comparison between the finite element deflection results of the coping plate with the experimental ones shows close agreement for deflection points taken at ¼ L as shown in Figure 4.37. However, the finite element model results at ½ L are 15% higher than the experimental deflection results. In the experiment, the 40" (1 m) cleat segment was assembled with a double row of nails attached to the parapet to allow for the installation of the membrane transferring the applied pressure. The additional nails stiffened the roof edge at ½ L and rendered connection disengagement the only possible failure mode. This was not modelled in the finite element model, resulting in a softer response at ½ length of the coping plate.

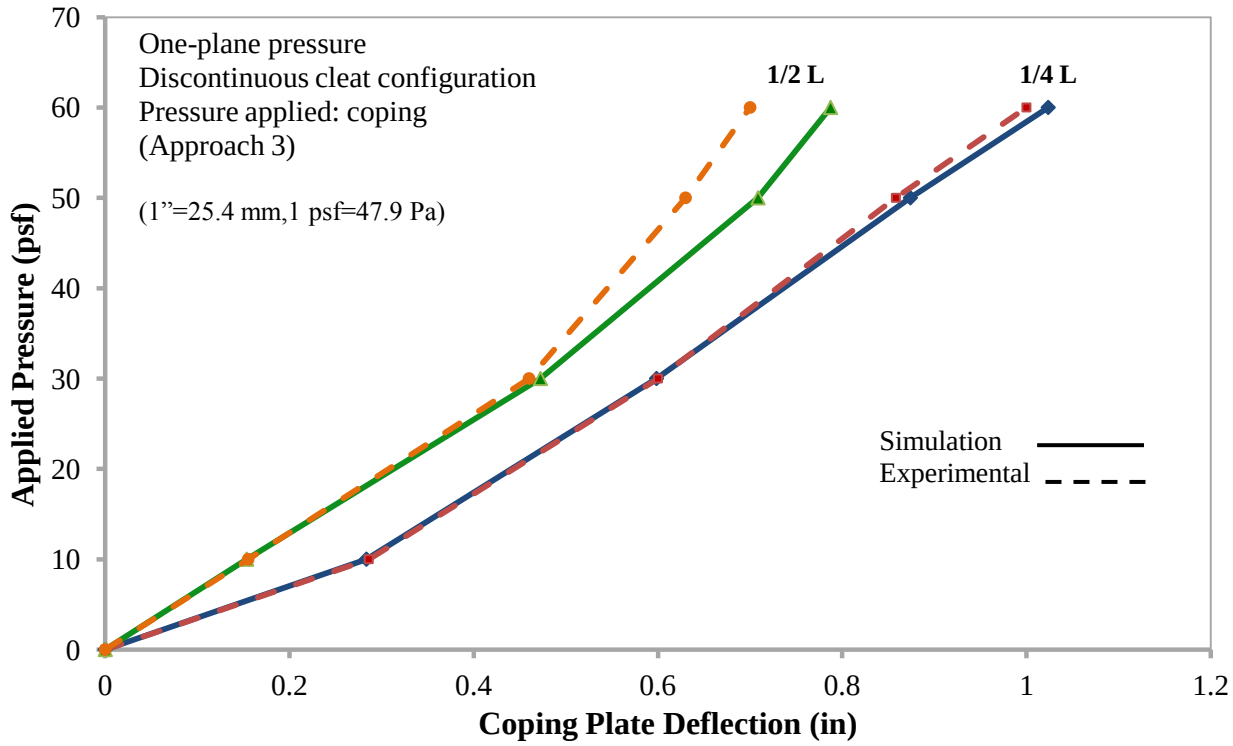

Figure 4.37 Comparion between coping plate deflection point for a one-plane pressure applied against the coping for the discontinuous cleat configuration

4.4.2 One-Plane Pressure Applied Against Cleat Plate

Finite element analysis was also conducted for the discontinuous cleat configuration when a static uniform pressure is applied against the cleat plate. The model was analyzed at five pressure

points at an increment of 20 psf (958 Pa) from 10 to 90 psf (479 to 4,309 Pa), Figure 4.38. Modelling approach 3 was used in this analysis to model the cleat / coping connection. From the contours of Mises stresses at 90 psf (4,309 Pa) pressure the following observation are made:

- Severe deflection of the coping plate around the 40" (1 m) cleat segment, Figure 4.39,
- Severe stress concentration of the drip-edge connection between the coping / cleat plates, Figure 4.39,
- Stress concentrations of the cleat plate around the nail area as illustrated in Figure 4.40; and,
- Maximum displacement of ¼" (6 mm) and minor lifting of the drip edge connection, Figure 4.41.

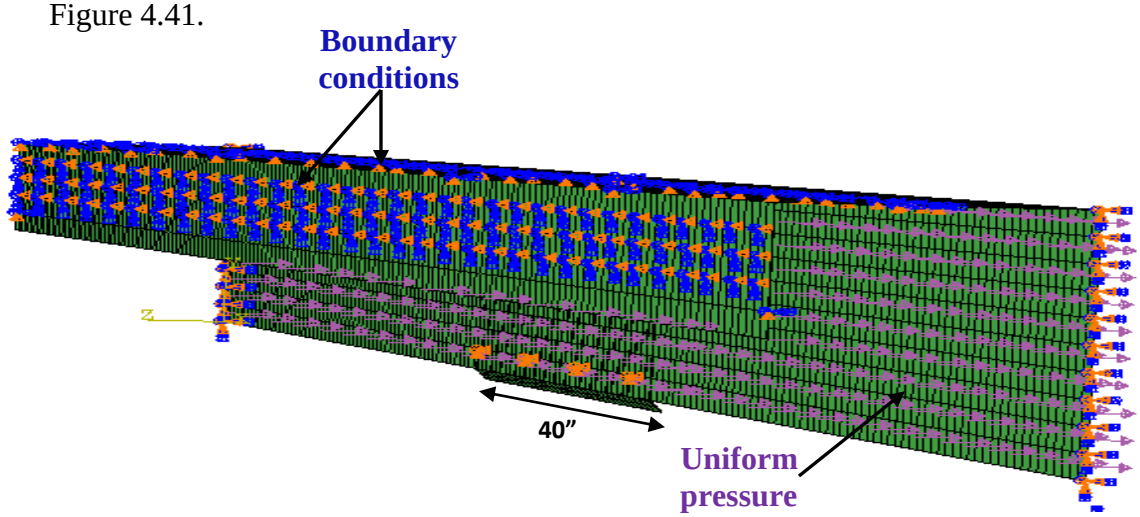

Figure 4.38 One-plane pressure applied against cleat (approach 3)

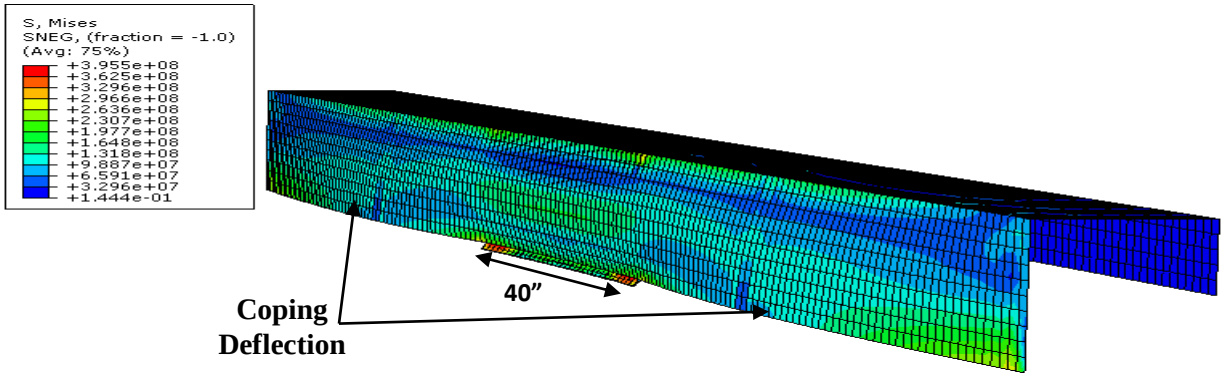

Figure 4.39 Stress contour (Pa) on the coping at 90 psf (4,309 Pa)

The finite element model behaviour showed behaviour similar to that of the experimental test in which the coping plate on the sides of the cleat experiences excessive deformation as shown in Figure 4.42.

Figure 4.43 illustrates the comparison in the coping deflection at ¼ L when both modelling approaches 2 and 3 were used. The results indicate a stiffer response of approach 2, as expected.

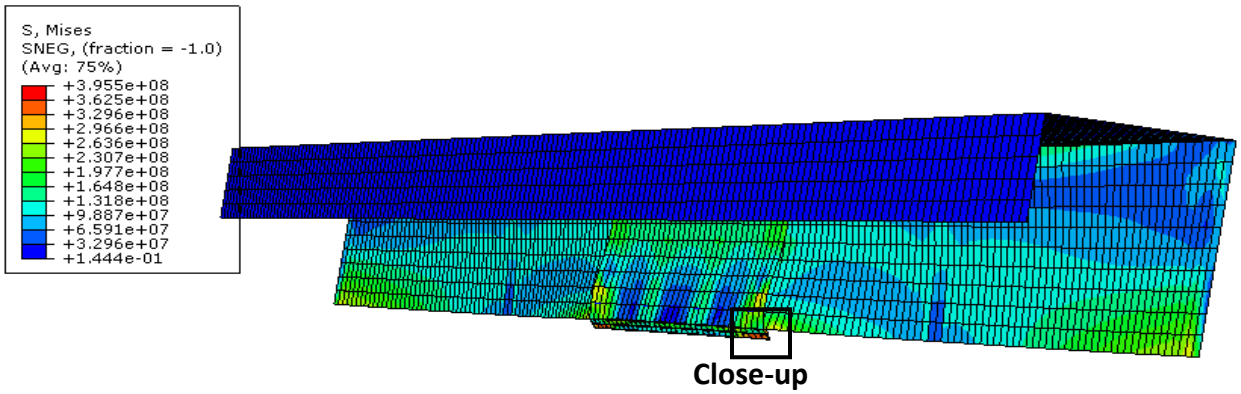

Figure 4.40 Stress contour (Pa) on the cleat at 90 psf (4,309 Pa)

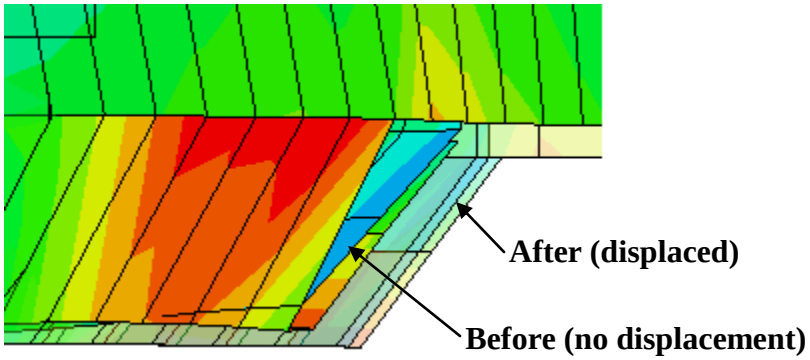

Figure 4.41 Close-up of the before / after displacement of the drip-edge connection in Figure 4.40

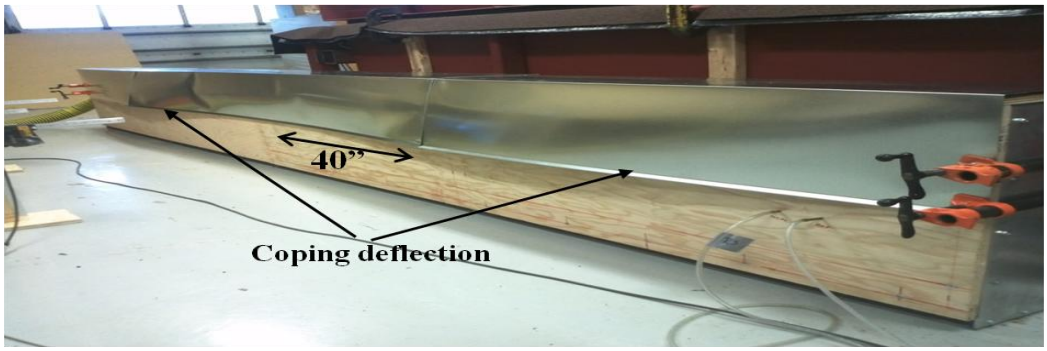

Figure 4.42 Severe deformation of the coping plate outside the 40” (1 m) cleat plate segment (Alassafin 2012)

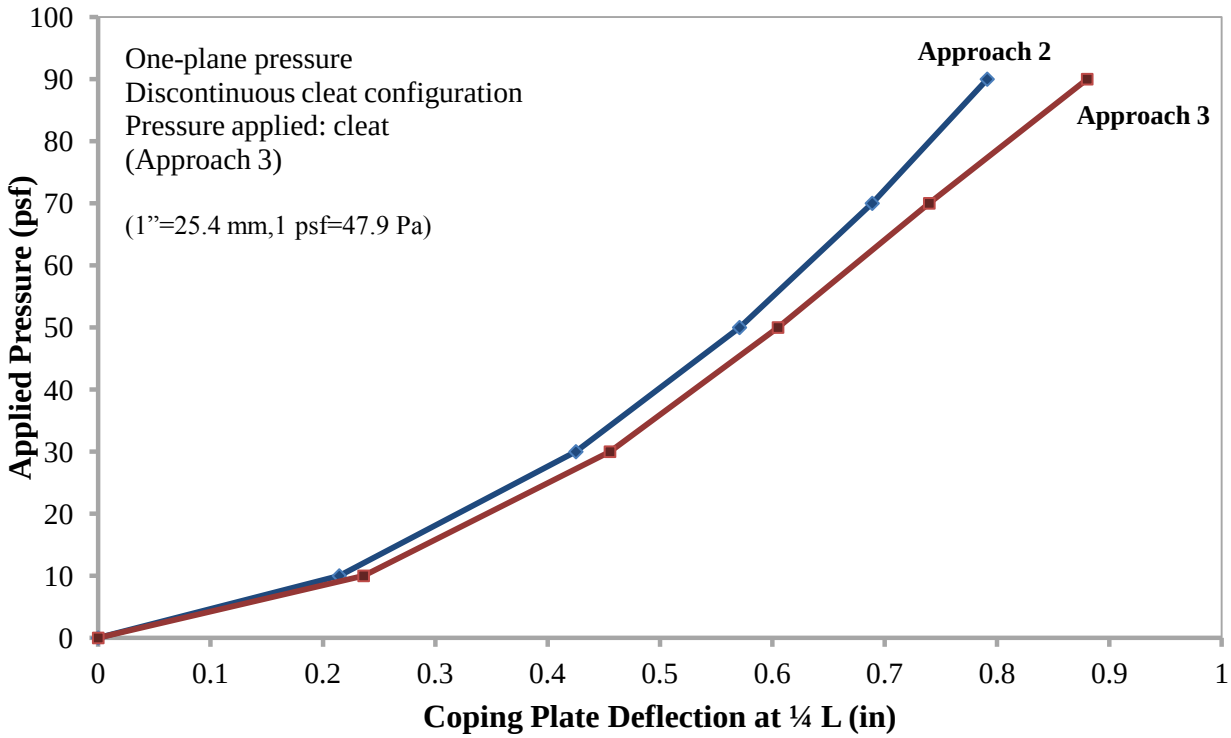

Figure 4.43 Comparison between approach 2 and 3 for a one-plane pressure applied against the cleat plate for discontinuous cleat configuratin

For the discontinuous cleat configuration, the roof edge experienced large deformations and rotations. In addition, the onset of localized material yielding was observed at the corners of the drip-edge connection. Consequently, linear analysis is not sufficient or acceptable to predict the roof edge behiavour. On the other hand, nonlinear analysis yielded a reasonable structural behiavour that shows a failure mode similar to the experimental one. As shown in Figure 4.44, the nail reaction increases almost linearly as the applied pressure increases. For this case at 90 psf (4,309 Pa), the nail reaction is 91 lbf (405 N), which is 23% higher than the one obtained when the pressure was applied against the coping.

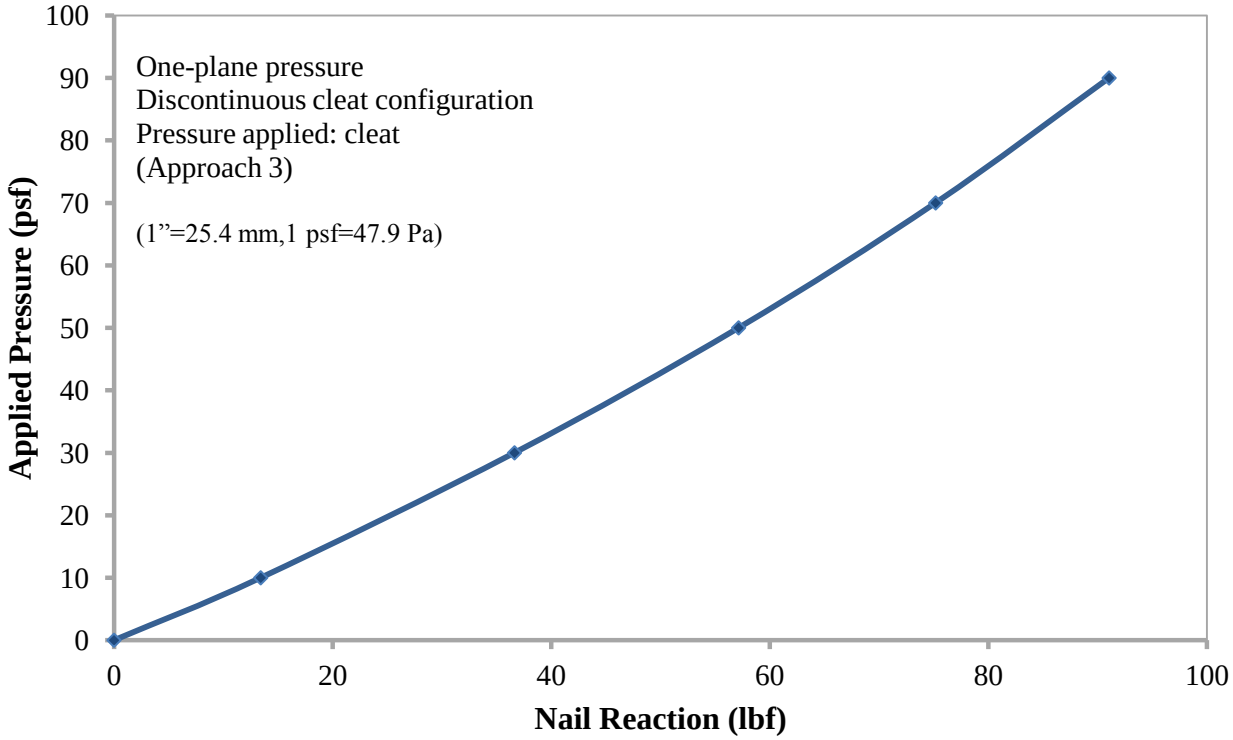

Figure 4.44 Nail reaction as a function of the applied pressure

4.5 Continuous Cleat Configuration - Set B

The results of the finite element analyses for the continuous cleat configuration with cross section details Set B are presented here and compared to the experimental tests conducted at NRC (Alassafin 2012). The wind-induced pressure was applied statically on one plane against the coping plate. The pressure was applied at an increment of 20 psf (958 Pa) from 10 to 90 psf (479 to 4309 Pa). The deflection of the coping plate is analyzed and verified with the experimental results. In addition, nail reactions were calculated and monitored for failure. From the previous finite element analyses, it was established that modelling approaches 2 and 3 are a good representation of the roof edge. Approach 2 is a stiffer model that is suited for a system that experiences large deformations or rotations. Therefore, either approach can be used. In the case of continuous cleat configuration Set B, approach 3 was used to predict the roof edge structural behaviour. Furthermore, for Set B under the effect of a one-plane pressure applied against the

coping plate, the roof edge experiences very small deformations, the material response of the system is linear, and the geometrical shape is constant. Therefore, a linear analysis is adequate to predict the system structural performance. From the contours of the von Mises stresses resulting from the applied load, the following is observed:

- Minor stress concentrations of the cleat and coping plates at mid-depth, Figure 4.45; and,
- Stress concentrations on the cleat plate around the nail area, Figure 4.46.

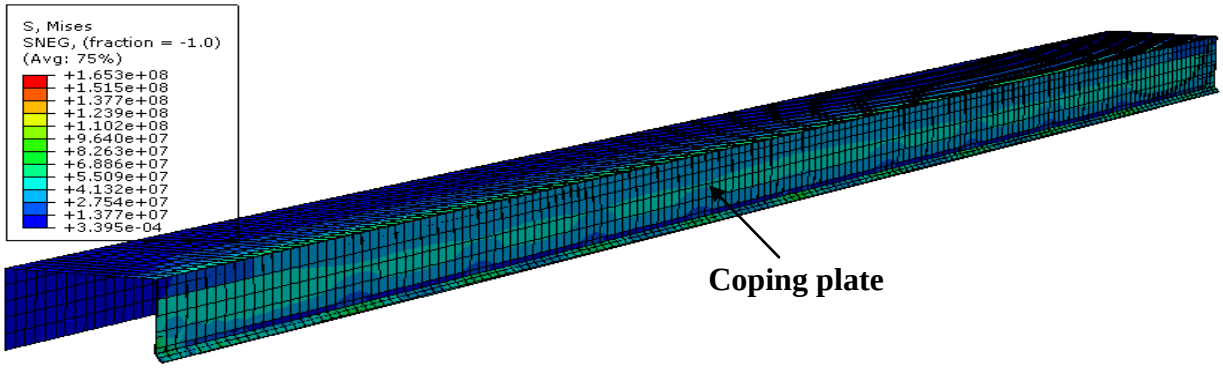

Figure 4.45 Stress contour (Pa) on the coping plate at mid-depth at 90 psf (4,309 Pa)

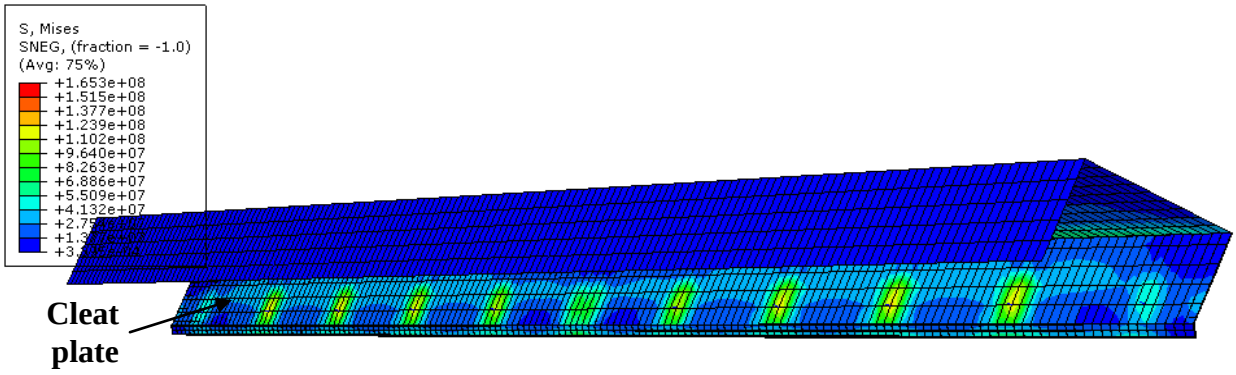

Figure 4.46 Stress contour (Pa) on the cleat plate around the nail area at 90 psf (4,309 Pa)

Figure 4.47 illustrates the comparison of the finite element deflection results of the coping plate at ¼ and ½ of its length to the experimental ones. The figure shows very close agreement between the two sets of results; there is an agreement within 95% at a pressure of 70 psf (3,352 Pa) and 98% at the other pressure points. Figure 4.48 shows the values of the reaction forces at

different pressure points. The nail reactions increase linearly as the applied pressure against the system increases. At an applied pressure of 90 psf (4,309 Pa), the maximum nail reaction is 29 lbf (129 N), in comparison to 52 lbf (231 N) for on the continuous cleat configuration Set A, Figure 4.29. Reducing the coping / cleat plate depth from 12" to 6" (305 mm to 152 mm) decreases the nail reactions by a minimum of 44%.

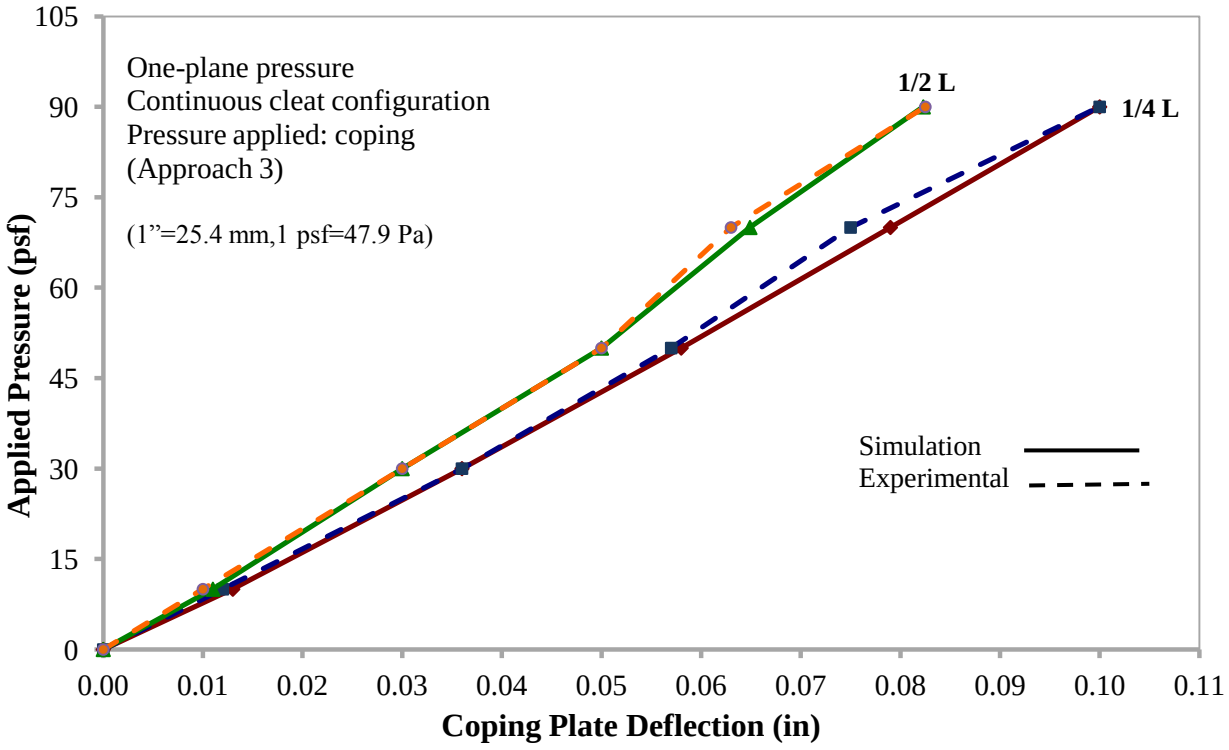

Figure 4.47 Comparison between deflection results of the finite element analysis to experimental results for a one-plane pressure applied against the coping plate for continuous cleat configuration

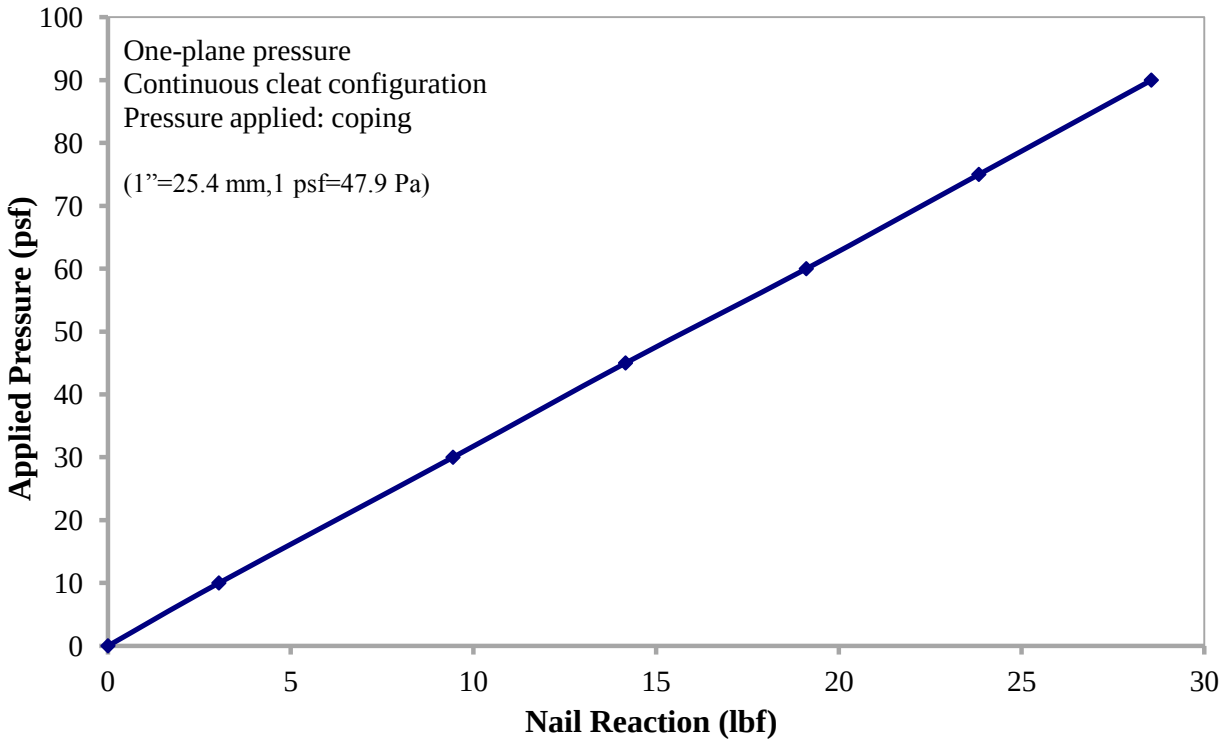

Figure 4.48 Nail reaction as a function of the applied pressure

4.6 Summary

Deflection results of the coping plate at ¼ and ½ L for both the continuous and discontinuous cleat configurations obtained from the finite element analysis were validated with those obtained from the experimental tests conducted at the NRC (Alassafin 2012). Validation of the system using approach 3 and linear and non-linear analysis concluded with a good agreement between the deflection results. Consequently, the following findings are observed:

- Set A experiences significant deflection of the coping at 90 psf (4,309 Pa) for continuous cleat configuration subjected to a one-plane pressure against the coping,
- Set B experiences minor deflection of the coping at 90 psf (4,309 Pa) for continuous cleat configuration subjected to a one-plane pressure against the coping,

- The discontinuous cleat configuration yields at 60 psf (2,873 Pa) and experiences significant deflection when subjected to a one-plane pressure against the coping,
- Displacement of the drip-edge connection occurs for the discontinuous cleat configuration when subjected to a one-plane pressure against the coping,
- Maximum deflection of the coping plate for continuous cleat configuration occurs at mid-depth of the front height (H_f) of the coping,
- Nail reaction increases as the applied pressure is increased; and,
- Local stress concentration develops around the nail areas.

Chapter 5 **Parametric Analysis**

5.1 Introduction

A parametric analysis was conducted to better understand the structural behaviour of the roof edge under the effect of wind-induced wind pressure. More importantly, the parametric analysis was used to establish design curves to be used as a guideline for the roofing industry in the design and manufacture of roof edge system. The roof edge system was analyzed by varying different parameters which include coping gauge, nail spacing, coping plate depth and length and load application as shown in Figure 5.1. The results were compared in terms of the deflection at mid-height of the front face of the coping plate, and the nail reaction and drip-edge connection are monitored and analyzed.

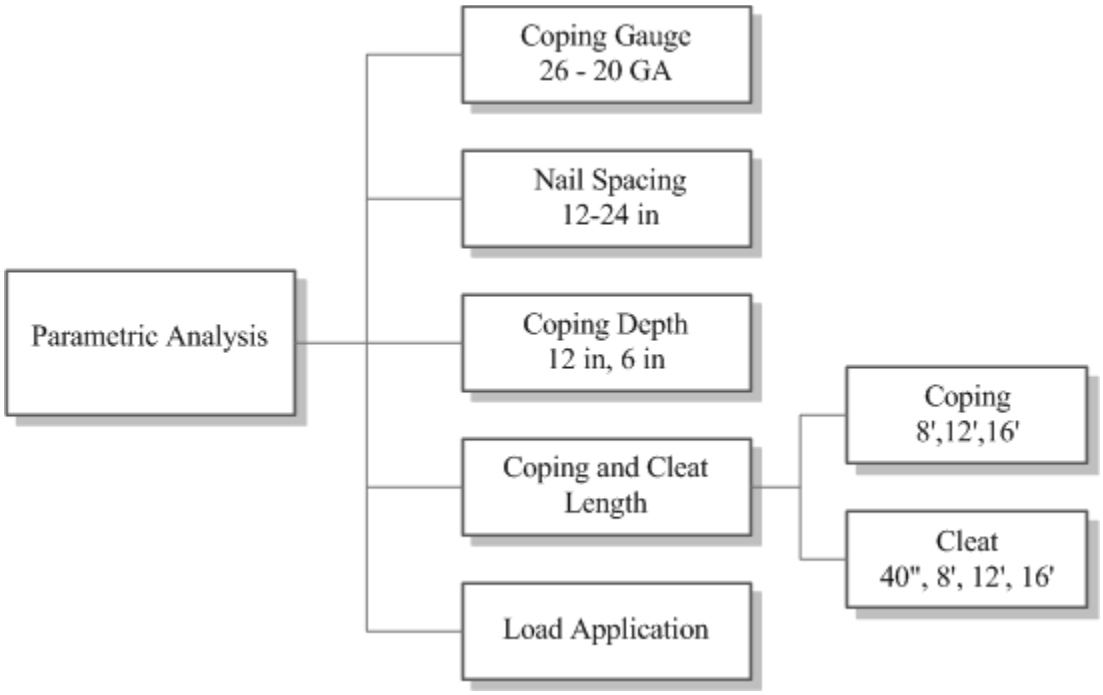

Figure 5.1 Parameters investigated in the parametric analysis to be investigated

For the parametric analysis both continuous and discontinuous cleat configurations were used; their performances for the different parameters are compared. The analyses were conducted on a system that is subjected to a uniform one-plane pressure against the coping plate for both configurations; hence, any variation in the load application was examined as specified in Figure 5.1. For both system configurations, modelling approach 3 as explained in chapter 3 was implemented except for the three-plane pressure applied against the cleat plate for the continuous cleat configuration, for which approach 2 was used to model the roof edge.

5.2 Coping Gauge

A complete analysis in which the coping gauge was increased from 26 GA (0.55 mm) to 20 GA (1 mm) was conducted to determine the roof edge response under the effect of coping gauge variations and to establish the maximum pressure the system could resist at each coping gauge without exceeding the deformation limit. Although the coping gauge was varied from 26 GA to 20 GA, the cleat plate was kept at a constant gauge of 24 GA (0.27 mm). A static uniform pressure was applied at 20 psf (958 Pa) increments from 10 to 90 psf (479 to 4,309 Pa) in one-plane pressure against the coping plate. Subsequently, coping plate deflection is determined at ¼ and ½ L of the coping plate middle segment for both configurations. In addition, the nail reaction of the cleat was calculated, and the values of the nail reactions were examined under the effect of coping gauge variations.

Figure 5.2 illustrates the coping plate deflection at ¼ of the length against the applied pressure for both continuous and discontinuous cleat configurations at constant nail spacing of 12” (305 mm). From the figure it is observed that the coping plate deflection increases as the coping gauge increases from 20 GA to 26 GA. For example, at 90 psf (4,309 Pa) a coping plate of 26 GA in the continuous cleat configuration experiences 1.2” (31 mm) deflection, while at 20 GA the

deformations are reduced by ⅔. This results from the fact that with the decrease of the coping gauge (increase in plate thickness), the system is stiffer and stronger in resisting the applied pressure. Hence, decreasing the coping gauge from 26 GA to 20 GA improves the system behaviour by reducing the coping plate deflection. The results also illustrate that the discontinuous cleat configuration experiences more deflections at the same pressure compared to the continuous cleat configuration. For instance, at 60 psf (2,873 Pa), the deflection for a 26 GA coping plate for both the discontinuous and continuous cleat configurations are 0.82" (21 mm) and 1" (25 mm), respectively. This is explained by the fact that the continuous cleat configuration is comprised of a continuous cleat plate that provides more support for the coping plate to resist the applied pressure.

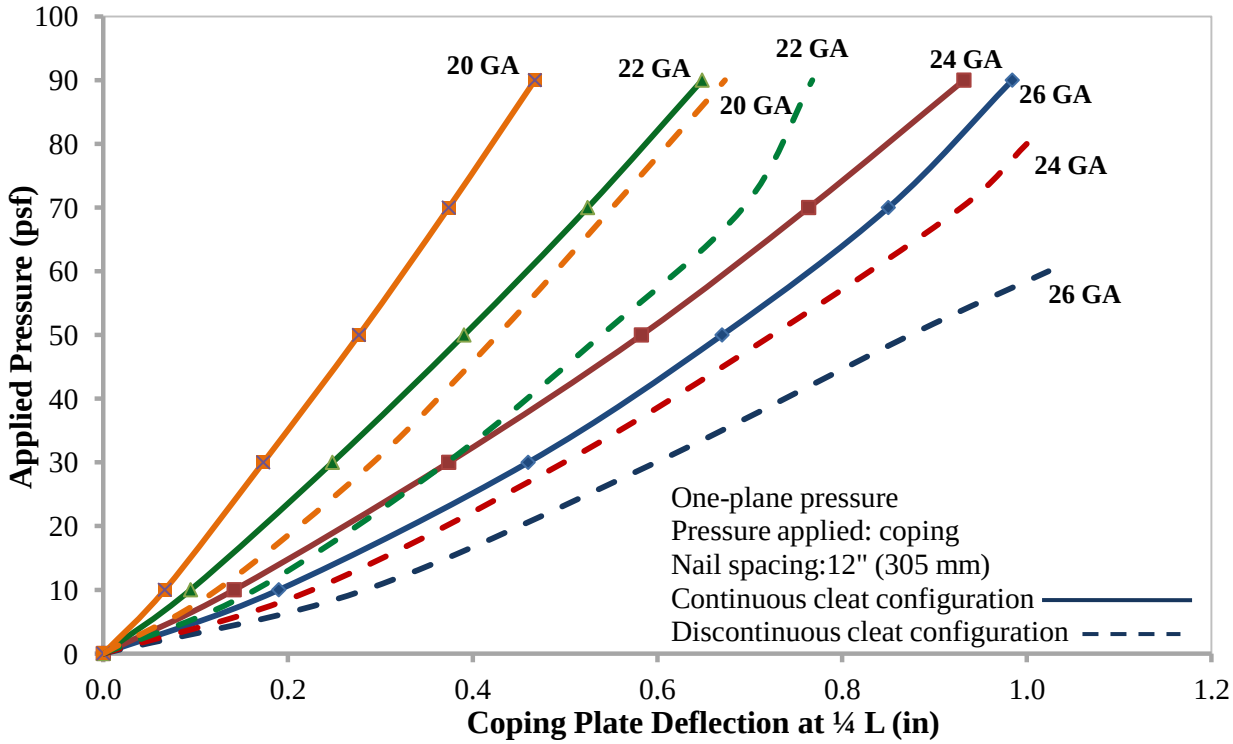

Figure 5.2 Comparison between deflections of the coping plate at ¼ L at different coping gauge for one-plane pressure applied against the coping for continuous and discontinuous cleat configurations

Similarly, for both continuous and discontinuous cleat configuration, the results of nail reactions are examined at variable coping gauges, Figure 5.3. It is observed that nail reaction does not significantly increase with the increase of the coping gauge.

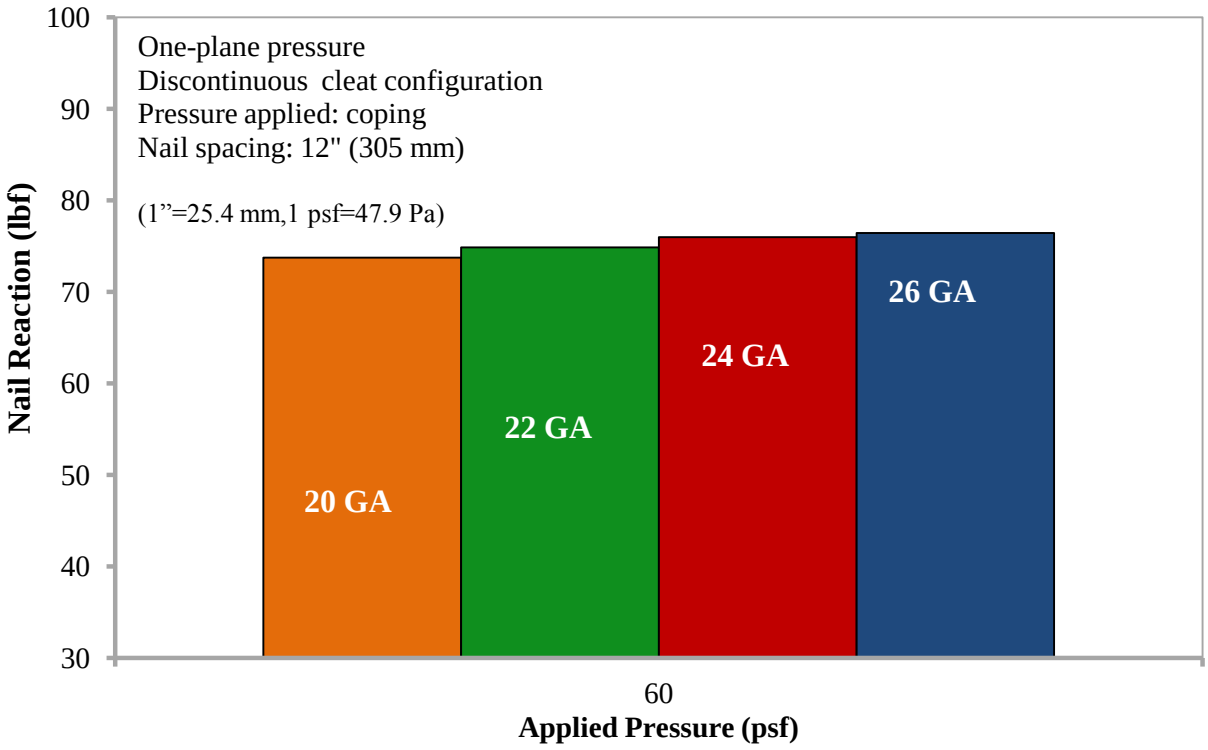

Figure 5.3 Comparison between nail reaction at different coping gauges for one-plane pressure applied against the coping plate for the discontinuous cleat configuration

5.3 Nail Spacing

The effect of nail spacing, which was set to 12” (305 mm), 18” (457 mm) and 24” (610 mm) was invistegated for both continuous and discontinuous cleat confgurations for one-plane pressure applied against a coping plate of 26 GA, Figure 5.4. Both the deflection of the coping plate at ¼ of the length and the nail reactions were calculated from the finite element analyses.

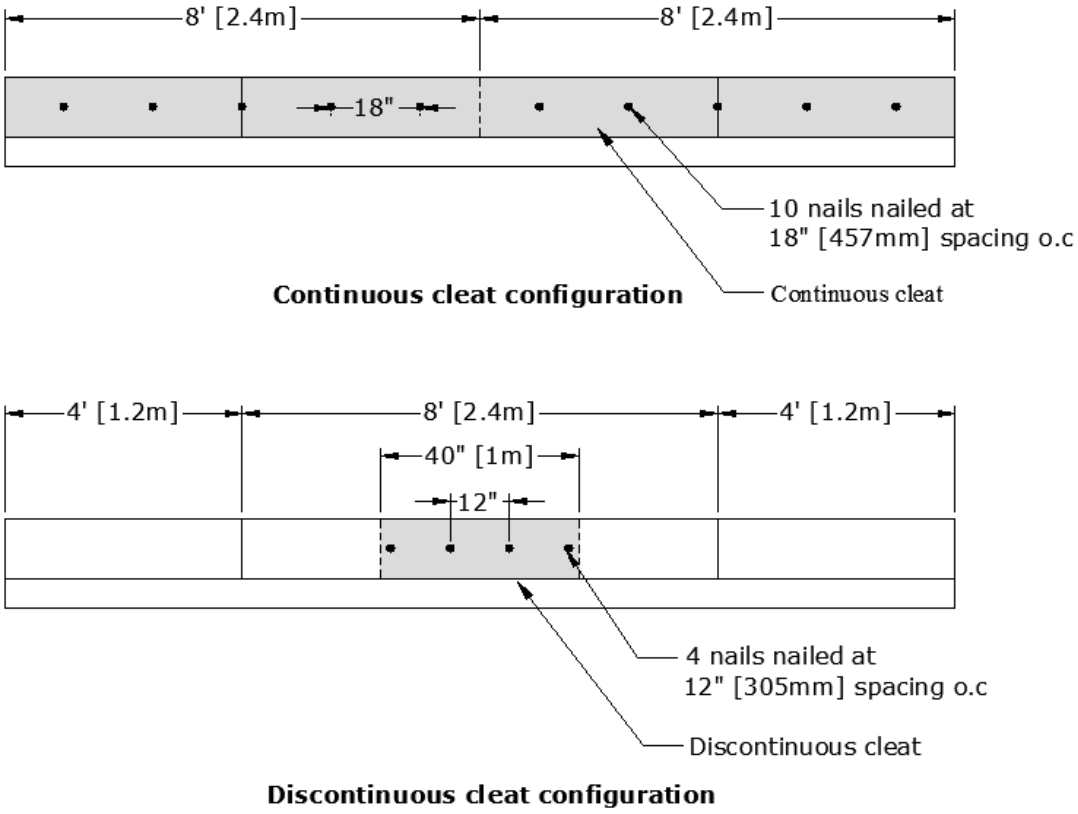

Figure 5.4 Nail spacing for both continuous and discontinous cleat configurations

Figure 5.5 illustrates the coping plate deflection at ¼ of the coping length against the applied pressure for various nail spacings and both roof edge configurations. From the figure it is observed that for both continuous and discontinuous cleat configurations the deflection of the coping plate is increased as the nail spacing is increased from 12” to 24” (305 to 610 mm). However, a comparison between the deflection of both configurations shows that the discontinuous cleat configuration experiences higher deflections than the continuous cleat

configuration. As the nail spacing is increased the number of nails available to resist the applied pressure decrease. Hence, a roof edge with fewer nails is more susceptible to excessive deformations especially for the system with discontinuous cleat. Furthermore, these available nails will have to withstand more pressure. Hence, the nails reactions are increased, Figure 5.6 and Figure 5.7. For example, for the discontinuous configuration subjected to 60 psf (2,873 Pa), the nail reaction increases from 76.4 lbf to 210 lbf (340 to 934 N) when the nail spacing increases from 12" to 24" (305 to 610 mm) respectively, Figure 5.7. The continuous cleat configuration is nailed and assembled with double amount of nails in comparison to the discontinuous system; hence, the applied pressure is distributed among more nails and each resists lower reaction force, Figure 5.8.

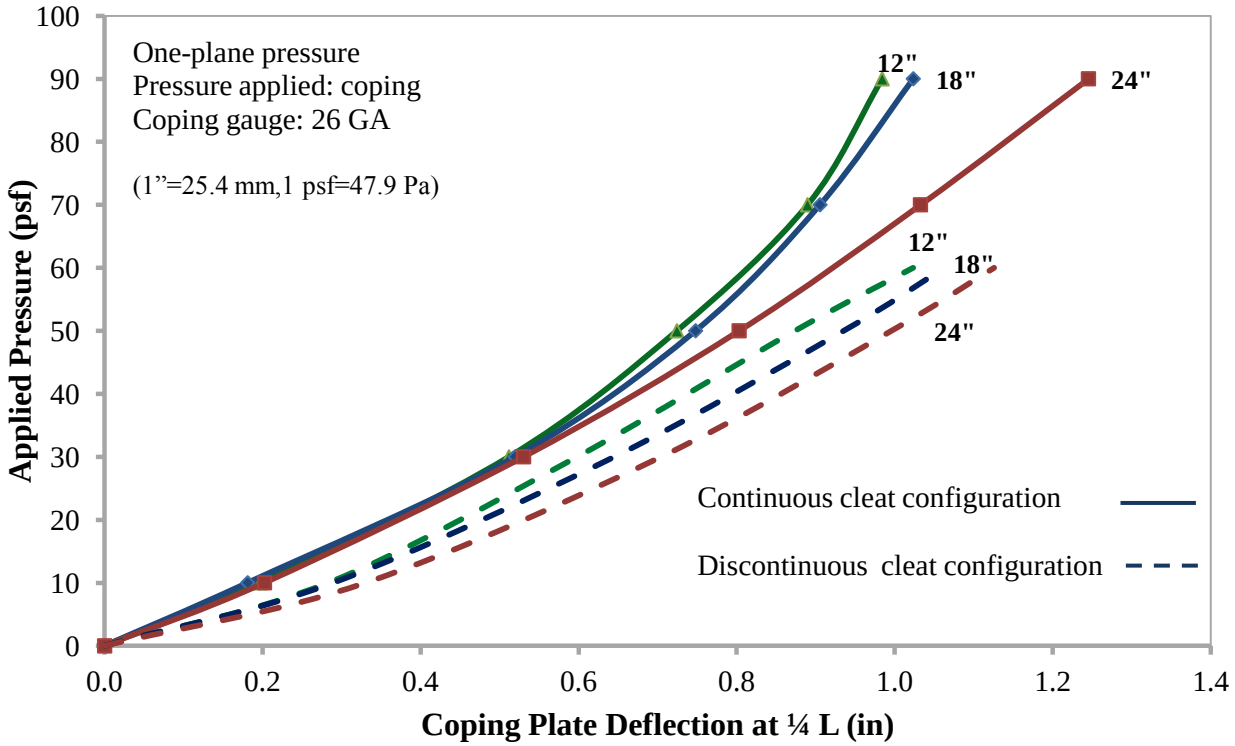

Figure 5.5 Comparison between coping deflections at different nail spacing for one-plane pressure applied against the coping plate for the continuous and discontinuous cleat configurations

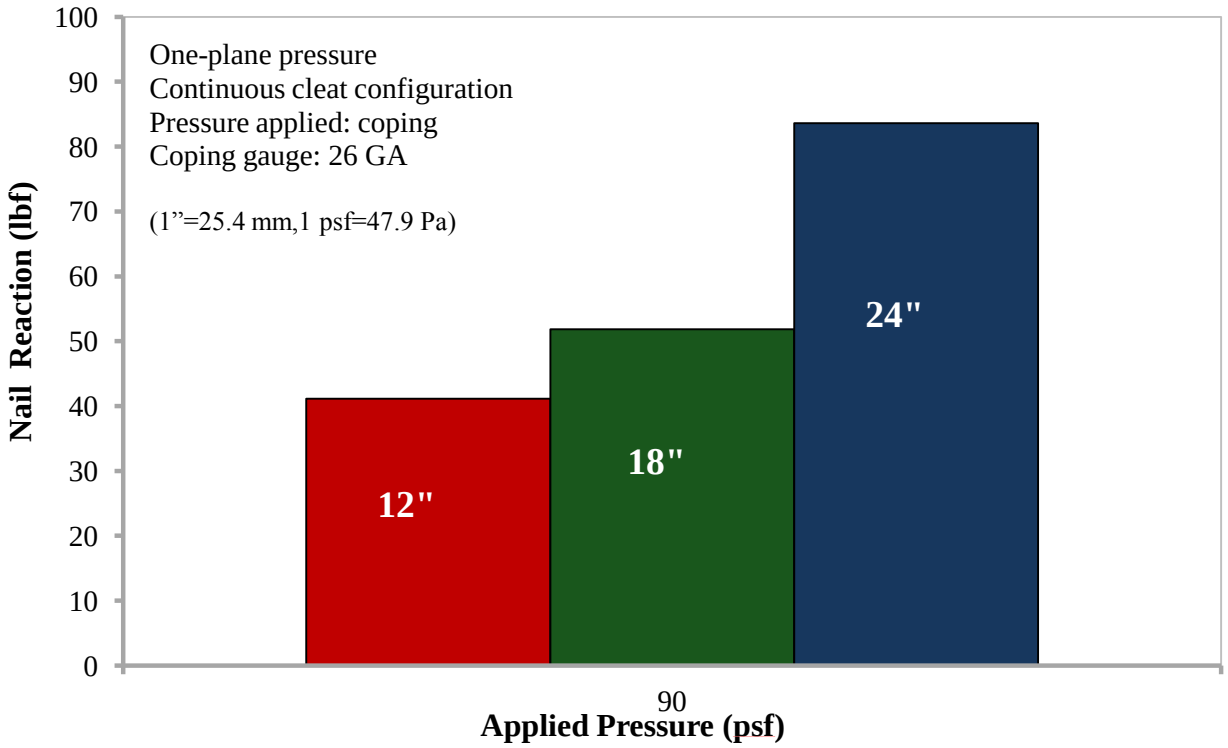

Figure 5.6 Comparison between nail reaction at different nail spacing for one-plane pressure applied against the coping plate for the continuous cleat configuration

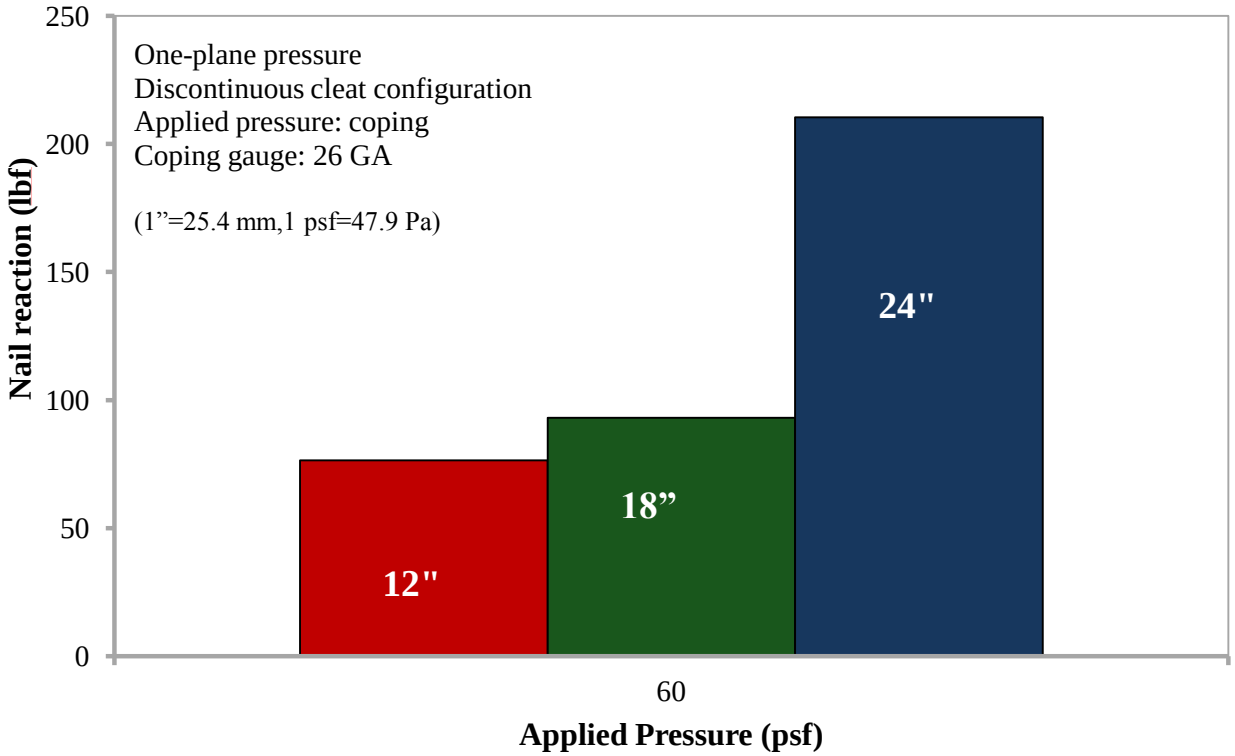

Figure 5.7 Comparison between nail reaction at different nail spacing for one-plane pressure applied against coping plate for the discontinuous cleat configuration

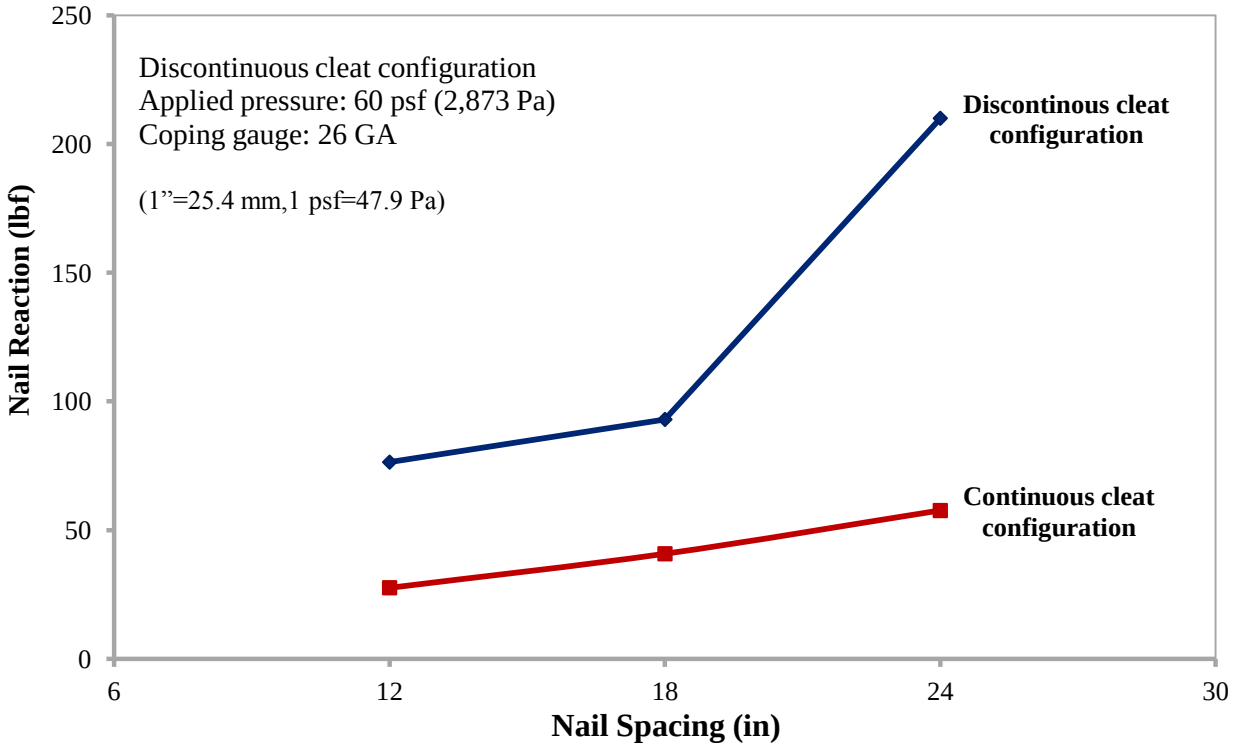

Figure 5.8 Comparison between nail reaction at 60 psf (2,873 Pa) for one-plane pressure applied against the coping for the discontinuous and continuous cleat configurations.

5.4 Coping Plate Depth

Plate depth from 12" (305 mm) to 6" (152 mm) is investigated for the effect of reducing the depth of the coping for continuous cleat configuration subjected to a one-plane pressure applied against coping plate. The geometry of the two sections analyzed is shown in Figure 5.9. The section with a coping depth of 12" (305 mm) is referred to as Set A, while the section with a coping plate of 6" (152 mm) is referred to as Set B.

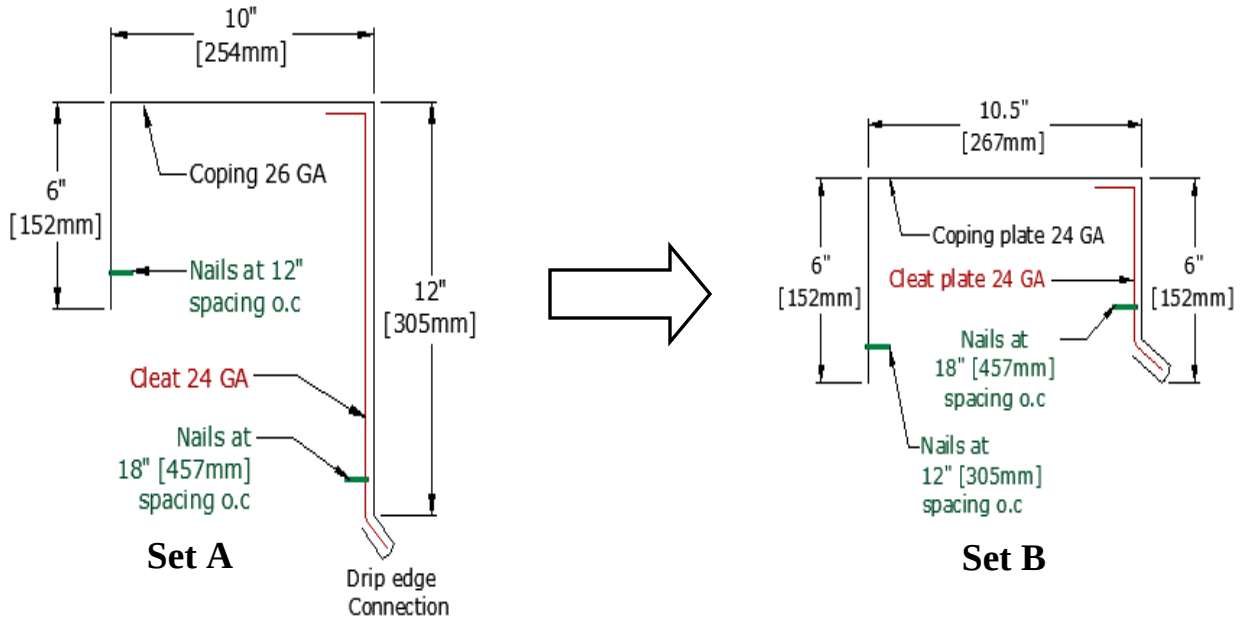

Figure 5.9 Geometry of Set A and Set B

Figure 5.10 shows the resulting coping plate deflection at ¼ and ½ L for both sets when subjected to 90 psf (4,309 Pa). A comparison between the deflection results of the two sets shows that the coping plate deflection for Set A is significantly higher than that of Set B by approximately 90%. This is because Set A (H_f=12") is slender than Set B (H_f=6"). By comparing corresponding nail reactions for both sets as shown in Figure 5.11, it is evident that the nail reaction for Set A is 74% higher than nail reaction for Set B. Although nail reaction for Set A is significantly higher in comparison to Set B, the reaction forces for the continuous cleat configuration are relatively low in comparison with Set A for the discontinuous cleat configuration.

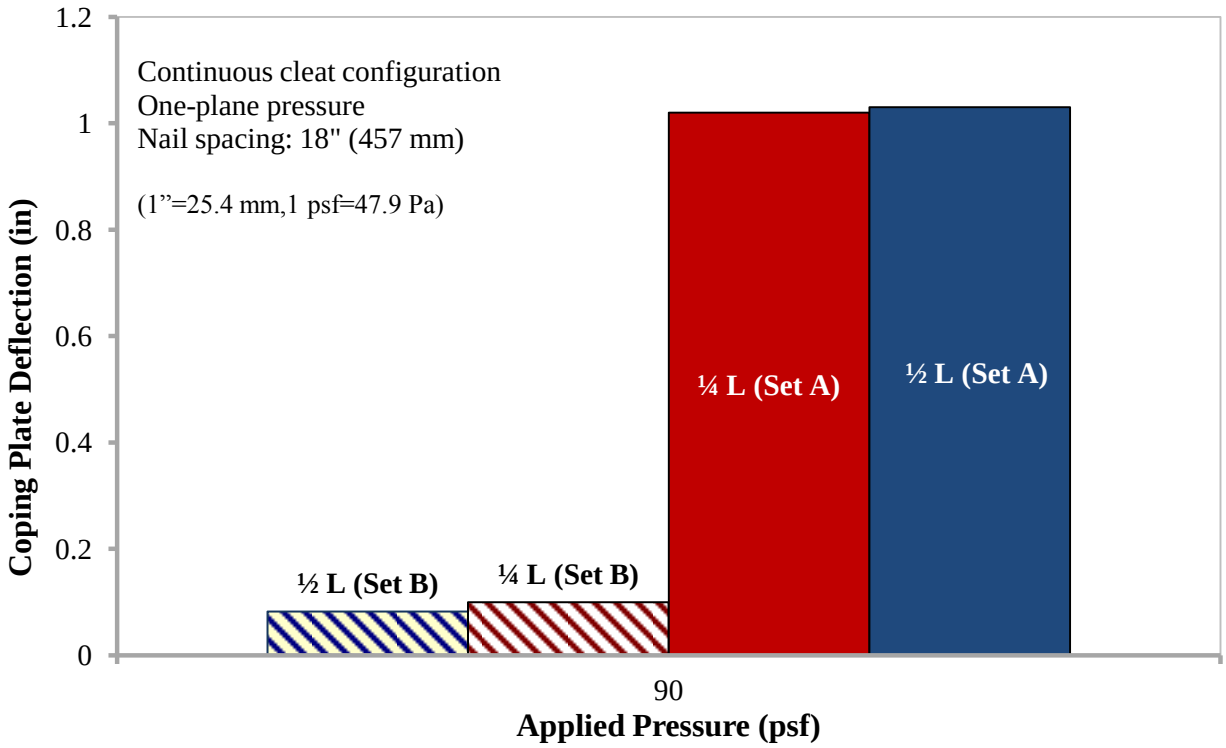

Figure 5.10 Comparison between the coping plate deflections of the continuous cleat configuration Set A and Set B for one-plane pressure applied against the coping plate

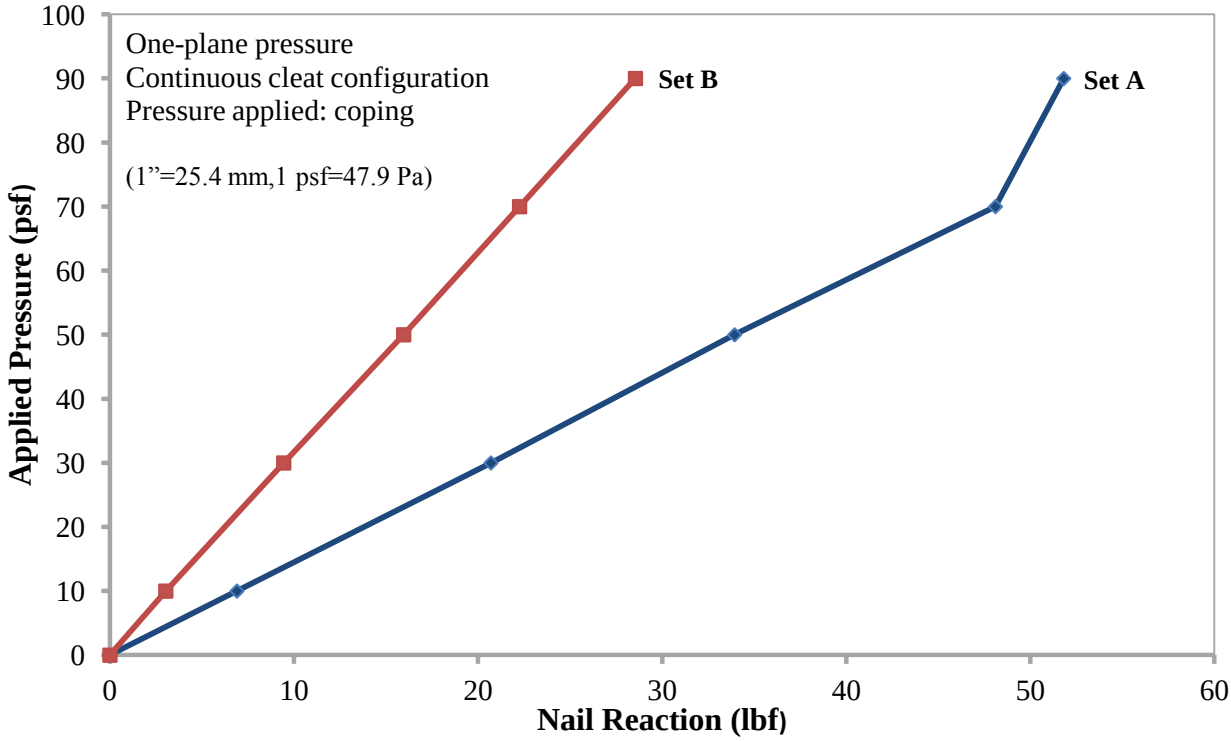

Figure 5.11 Comparison between nail reaction of Set A and B for continuous cleat configuration for one-plane pressure applied against the coping plate

5.5 Plate Length

The effects of coping and cleat lengths on the roof edge response are investigated by varying the length of the coping plate from 8 ft to 16 ft (2.4 to 4.86 m), and by varying the length of the cleat plate from 40" (1 m) to 16 ft (4.86 m). In theses analyses a one-plane pressure was applied against the coping plate for both the continuous and discontinuous cleat configurations with a constant coping gauge of 26 GA and a constant nail spacing of 18" (457 mm).

5.5.1 Coping Plate Length

The effect of the coping plate length was studied by analyzing two additional cases with coping plate lengths of 8' (2.4 m) and 12' (3.7 m) as shown in Figure 5.12, and by comparing the results with previous analyses performed at a coping plate length of 16' (4.86 m), Figure 5.13 to Figure 5.15 shows the contours of von Mises stresses that result when the length of the coping plate is changed. These results are obtained from a roof edge system with a 40" (1 m) discontinuous cleat. They show high concentration of stresses in the middle segment of the coping plate, where the coping plate is restrained at the bottom edge by the cleat / coping connection. For the 12' (3.7 m) and 16' (4.86 m) coping lengths, the two 4' segments of the coping plate on each side of the cleat have low Mises stresses and undergo large plate deflections that increase as the plate length increase.

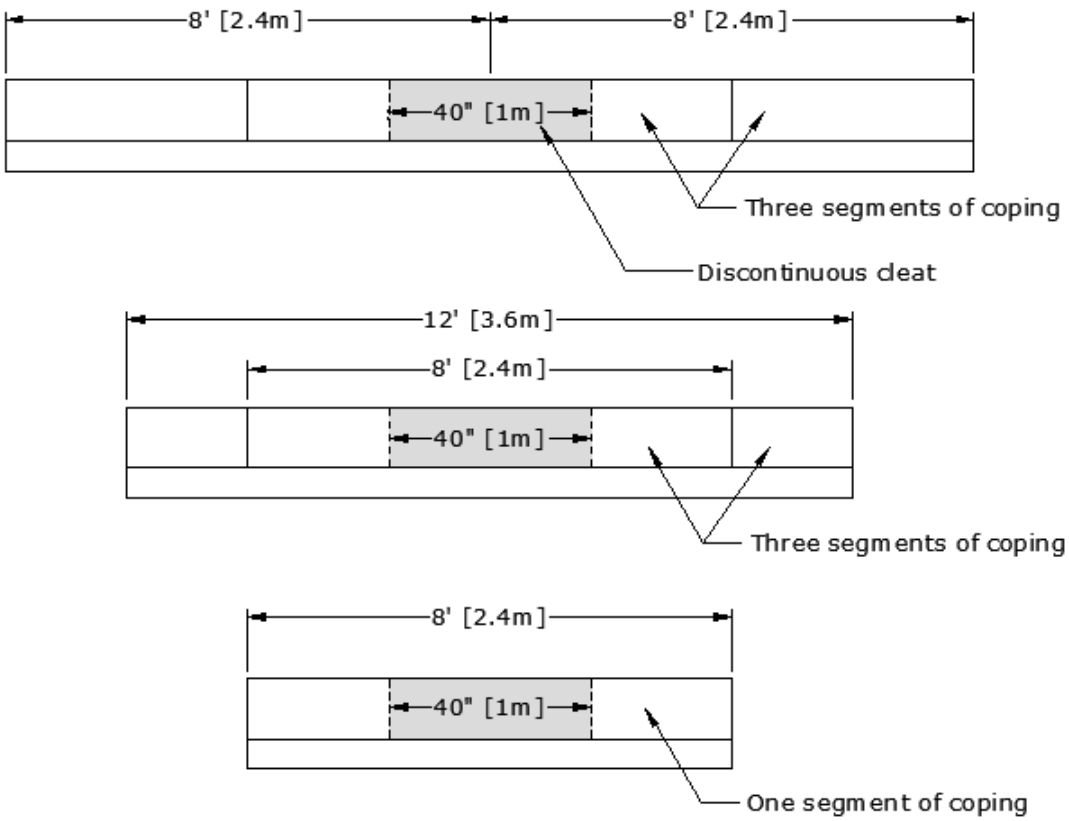

Figure 5.12 Variation of the coping length.

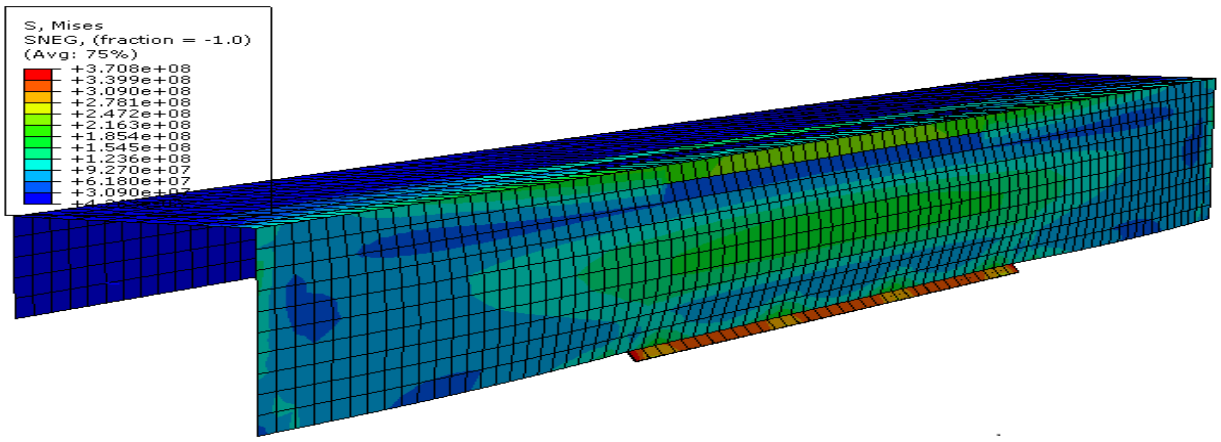

Figure 5.13 von Mises stress contours (Pa) for roof edge with coping length of 8’ (2.4 m) subjected to a one-plane pressure at 90 psf (4,309 Pa)

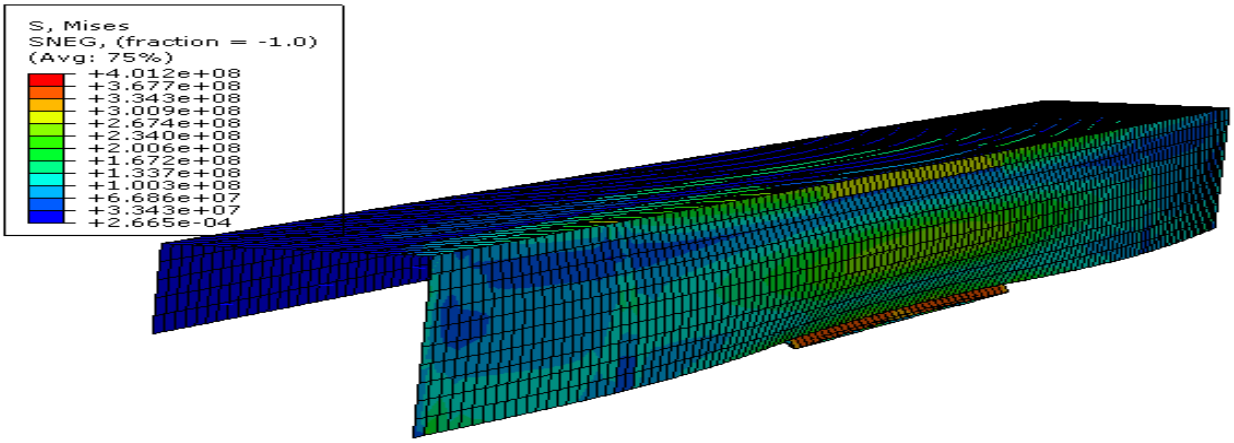

Figure 5.14 von Mises stress contours (Pa) for roof edge with coping length of 12’ (2.4 m) subjected to a one-plane pressure at 90 psf (4,309 Pa)

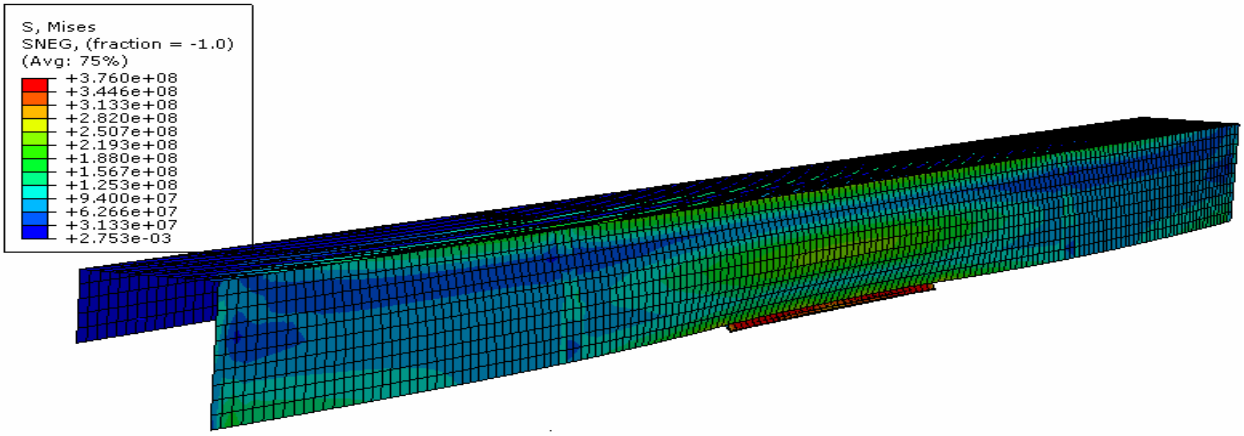

Figure 5.15 von Mises stress contours (Pa) for roof edge with coping length of 16’ (4.86 m) subjected to a one-plane pressure at 90 psf (4,309 Pa)

A comparison of coping plate deflections at ¼ L for each case with different length Figure 5.16 shows that the deflection increases as the coping length increases from 8’ (2.4 m) to 16’ (4.86 m). For a coping plate of 8’ (2.4 m) length, the maximum plate deflection occurs at ½ L point contrary to a coping plate of 12’ (3.7 m) and 16’ (4.86 m) length, where the maximum deflection occurs at ¼ L point, as shown in Figure 5.16. Likewise, the nail reaction forces increase as the coping plate length increases as illustrated in Figure 5.17. Note that the cleat plate is 40” (1 m) for all cases, and as the coping plate length is increased, the same amounts of nails holding the cleat are subjected to a higher net force.

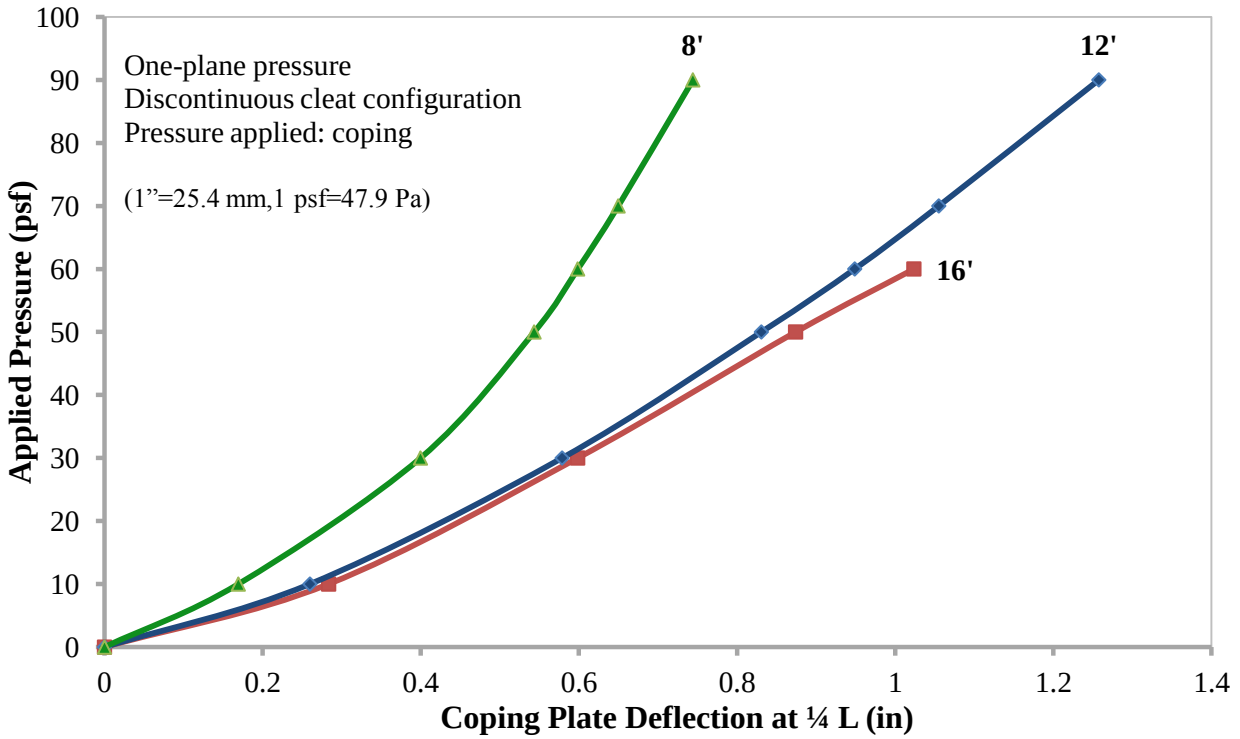

Figure 5.16 Comparison between deflection results at ¼ L at coping plate lengths of 8' (2.4 m), 12' (3.7 m), and 16' (4.86 m) for a one-plane pressure applied against the coping plate

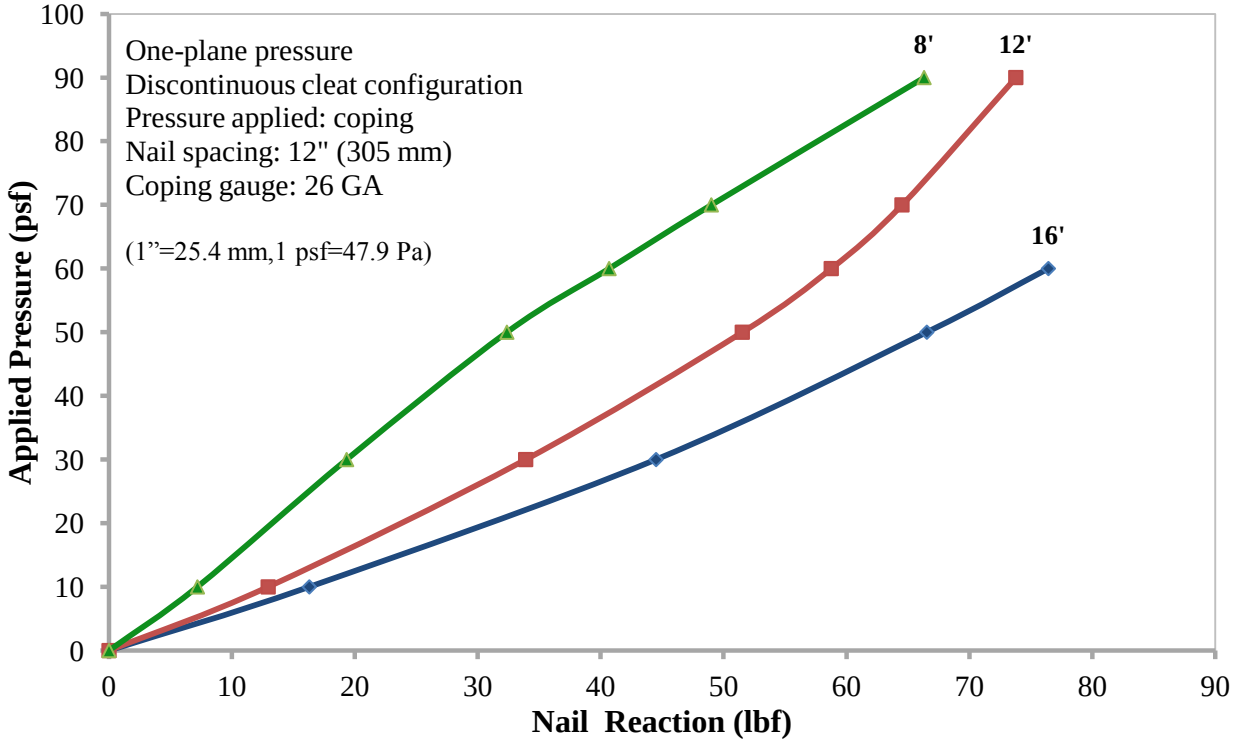

Figure 5.17 Comparison between nail reaction at various coping plate lengths for a one plane pressure applied against the coping plate for the discontinuous cleat configuration

5.5.2 Cleat Plate Length

To account for the effect of the cleat plate length, which was changed from 40” (1 m) (discontinuous cleat configuration) to 8’ (2.4 m) and 12’ (3.7 m), the coping plate was fixed at 16’ (4.86 m) as shown in Figure 5.18.

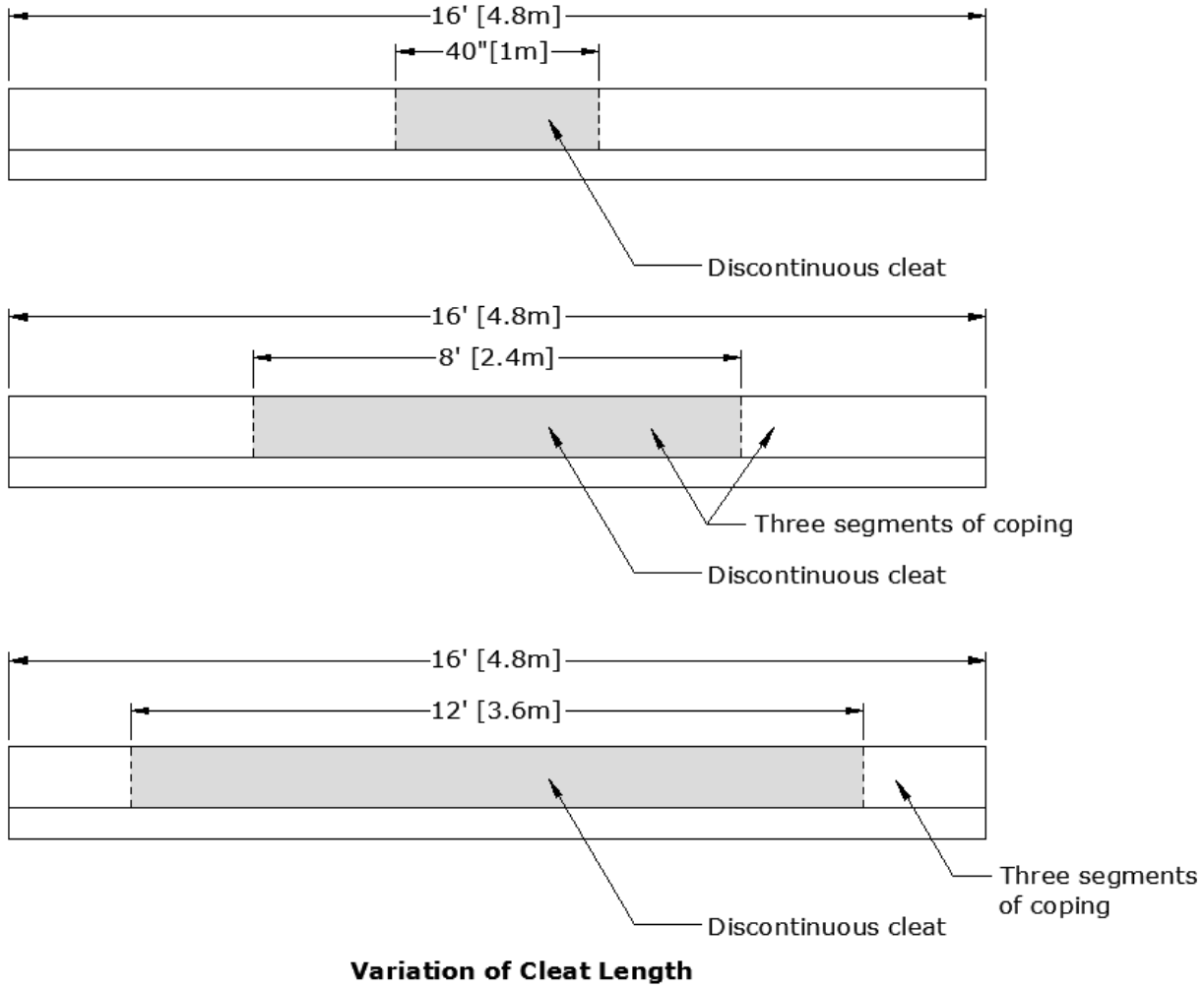

Figure 5.18 Variation of the coping plate length

Figure 5.19 illustrates the coping plate deflection at ¼ L versus the applied pressure. From the figure it is observed that the deflection of the coping plate increases as the cleat plate decreases in length. Hence, the deflection of the coping plate at ¼ is more critical for a discontinuous and

short cleat configuration than for the continuous cleat configuration with continuous cleat underneath the coping plate. In addition, the nail reaction increases as the cleat plate length decreases as shown in Figure 5.20. As the length of the cleat decreases, the number of available nails to resist the applied pressure is decreased. Hence, the pressure uptake by each nail is increased as it is evident in Figure 5.20.

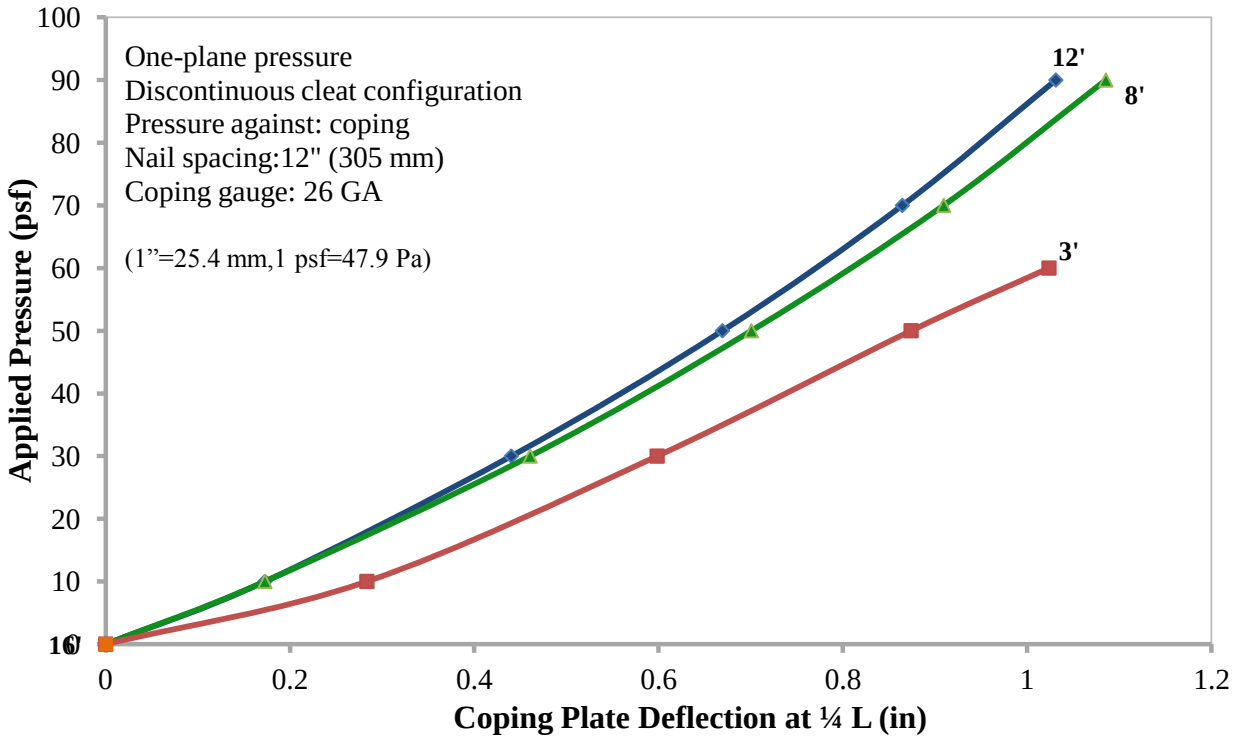

Figure 5.19 Comparison between deflections of the coping plate at various cleat plate lengths for the one-plane pressure applied against the coping

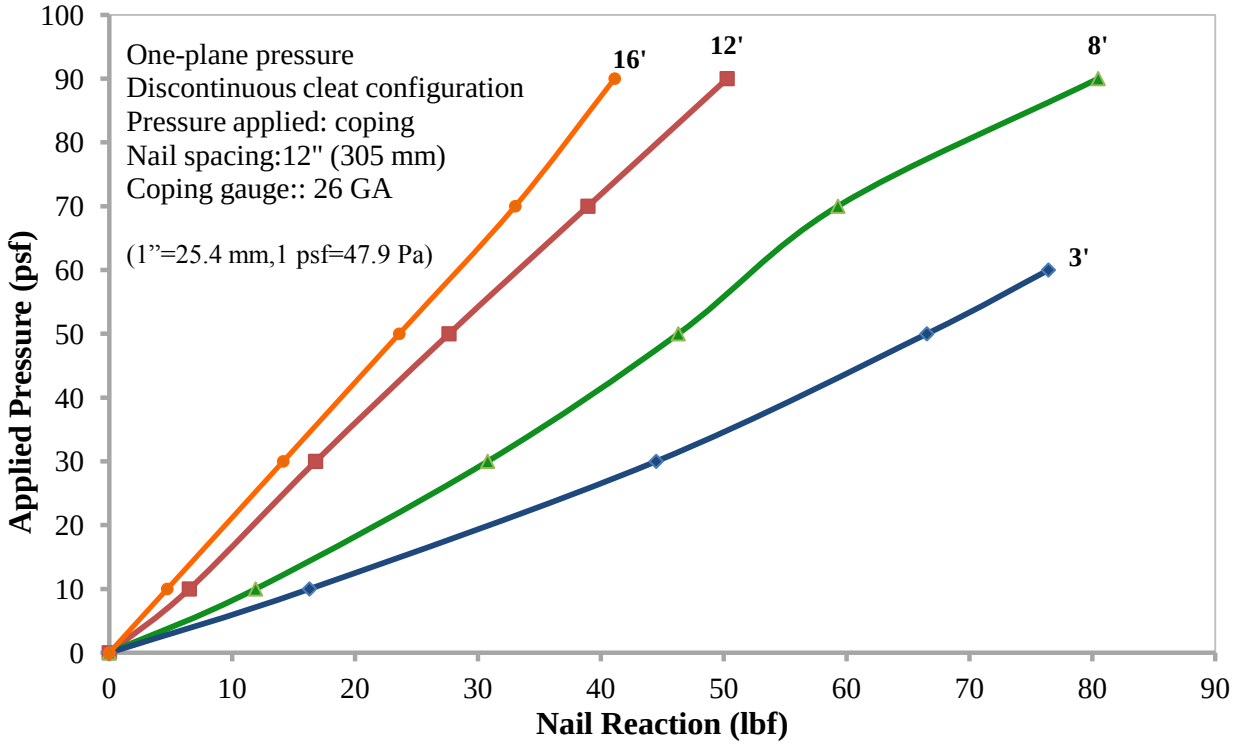

Figure 5.20 Comparison between nail reaction at various cleat plate lengths for one-plane pressure applied against the coping

5.6 Load Application

Load application is varied by first, applying a uniform one-plane pressure against either the coping or the cleat plate. Second, a uniform static pressure is applied against the coping in wither one-plane or three-plane pressure.

5.6.1 Pressure is Applied against the Face of the Cleat or Coping

The effect of applying the pressure against the face of the cleat or the face of the coping is investigated here as shown in Figure 5.21.

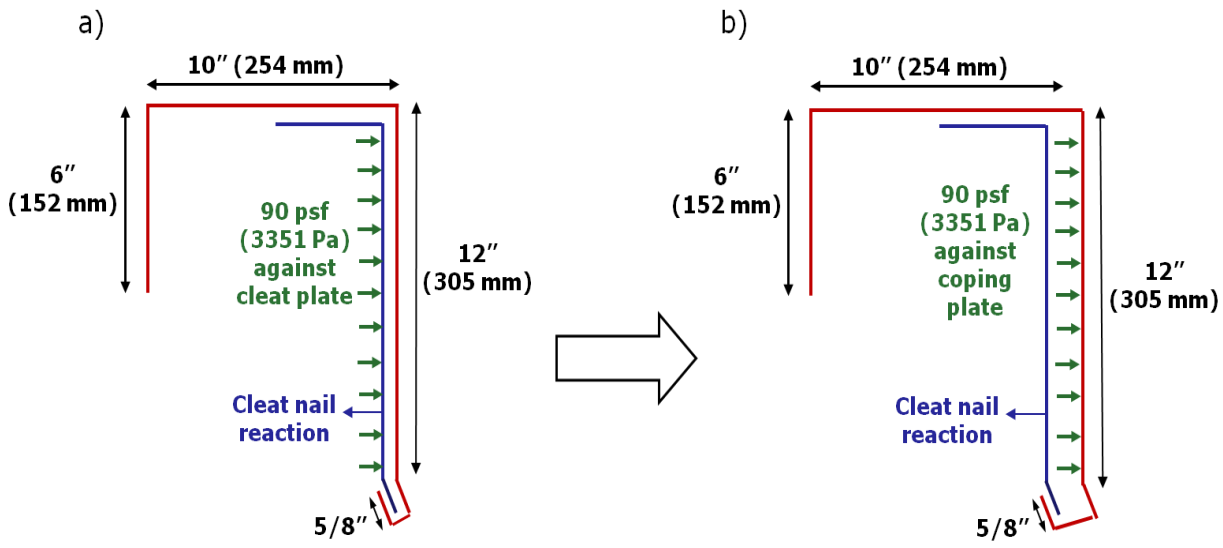

Figure 5.21 Pressure applied against a) cleat plate or b) coping plate

Figure 5.22 shows the coping plate deflections taken at ¼ and ½ L when the pressure is applied against either the coping or cleat plates at a constant nail spacing of 18” (457 mm) and constant coping gauge of 26 GA for continuous cleat configuration. The results in the figure indicate a significant increase in the deflection results when the pressure is applied against the coping plate. This is because the cleat plate (24 GA) is stiffer than the coping plate (26 GA); hence, the cleat plate deforms less in resisting the applied pressure before it is transferred to the coping plate by contact. At a pressure of 90 psf (4,309 Pa), the nail reaction is approxematly 52 lbf (231 N) in comparion to 62 lbf (276 N) when the load is applied against the cleat plate. Therefore, there is a 19% increase in the nail reaction when the presure is applied against the cleat. However, for pressure lower than 70 psf (3,352 Pa) the nail reaction for a one-plane pressure against either the coping or the cleat is very close in value as illustrated inFigure 5.23.

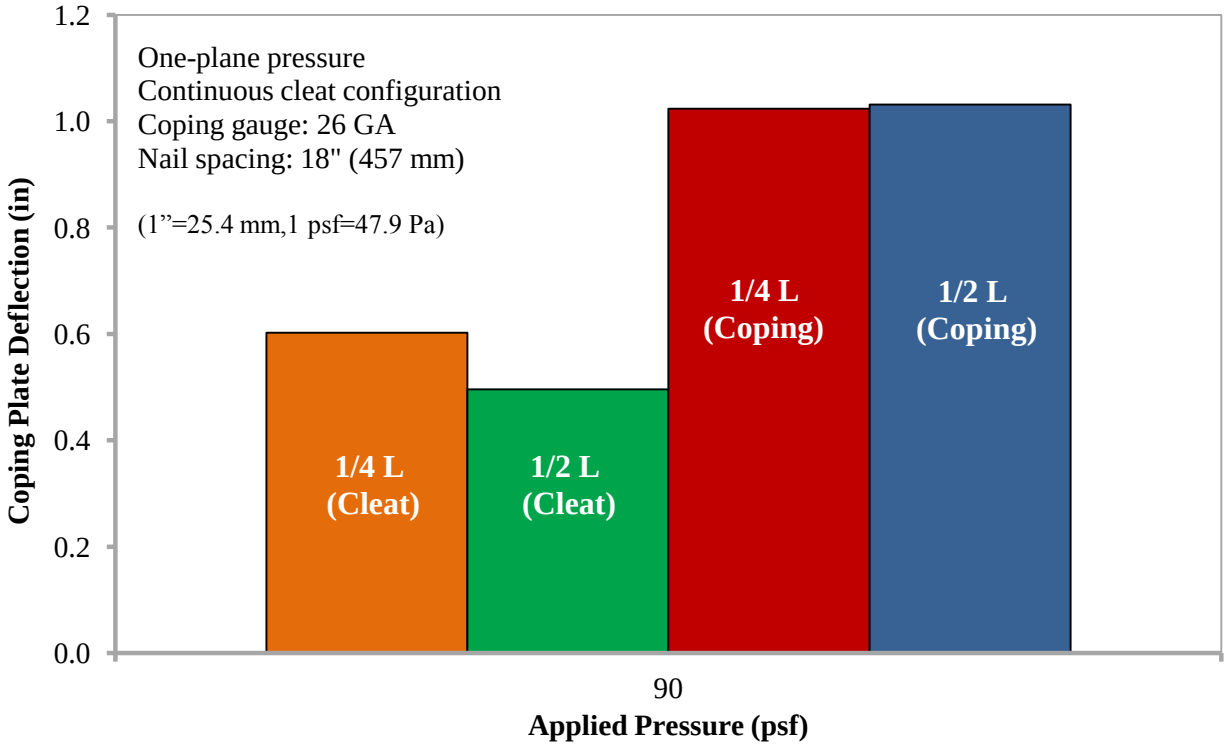

Figure 5.22 Comparison between deflection results at ¼ and ½ L for a one-plane pressure applied against the coping and cleat plates for the continuous cleat configuration

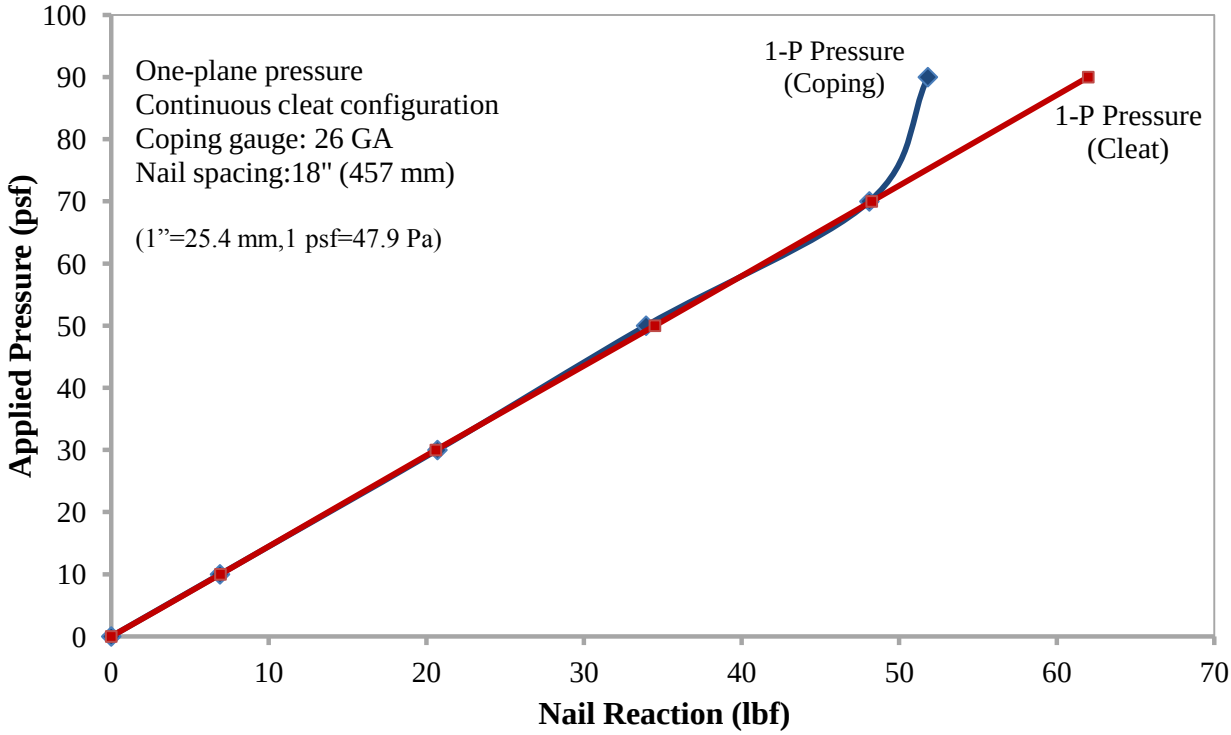

Figure 5.23 Comparison between nail reaction of one-plane pressure applied against the coping and cleat plates for the continuous cleat configuration

The coping deflections for the continuous cleat configuration subjected to a one-plane pressure applied against either the coping or the cleat are also examined and compared under the effect of nail spacing variations, as illustrated in Figure 5.24. The nail spacing was varied from 18” (457 mm) to 24” (610 mm), from the figure it is evident that the deflection of the coping plate is significantly higher than that of the coping at 24” (610 mm) spacing.

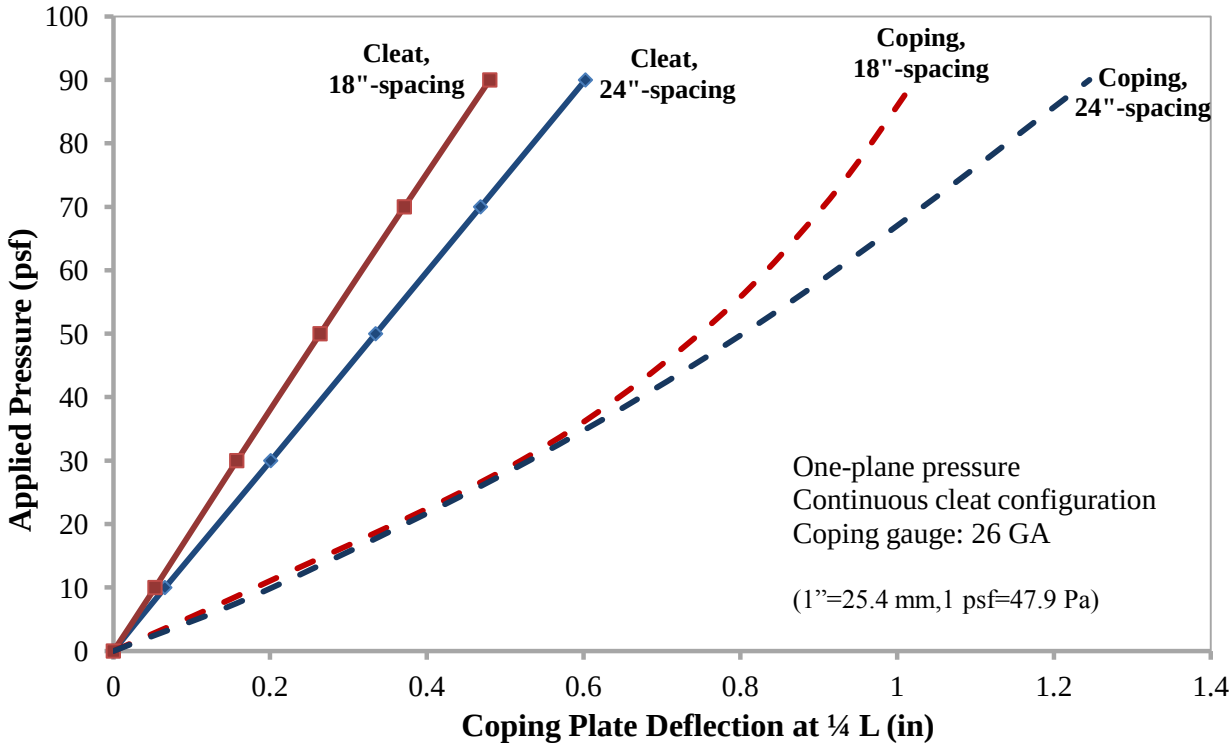

Figure 5.24 Comparison between coping plate deflection at ¼ L for a one-plane pressure against the cleat for the continuous cleat configuration

Furthermore, increasing the spacing between the cleat nails from 18” (457 mm) to 24” (610 mm) increases the reaction force resisting the applied load as shown in Figure 5.25. The reaction force for the case when the pressure is applied against the coping is lower than that when the pressure is applied against the cleat.

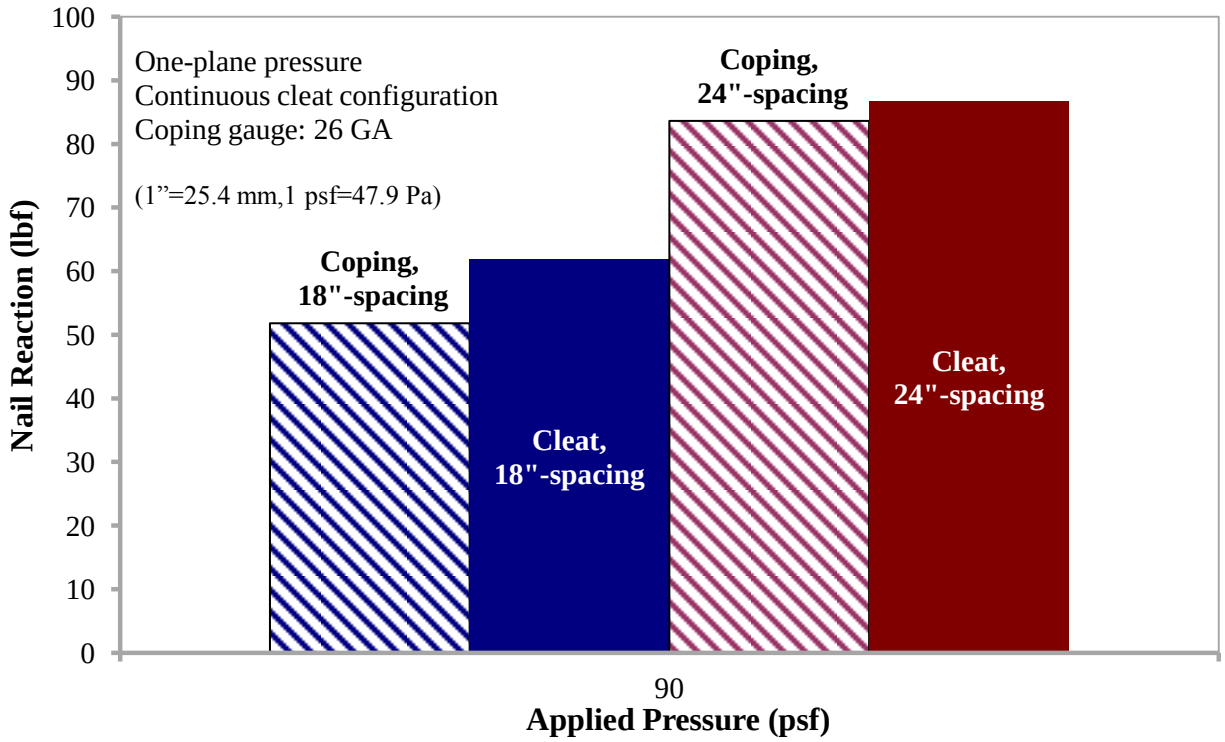

Figure 5.25 Nail reaction at 90 psf (4,309 Pa) applied against either coping or cleat and and varying nail spacing

Similar to the continuous cleat configuration, for a one-plane pressure applied against either the cleat or coping plates for the discontinuous cleat configuration, the deflection of the coping plate is higher when the pressure is applied against the coping as shown in Figure 5.26. In this figure, it is evident that the deflection of the coping plate at ¼ L is reduced by 40% as the thickness of the coping plate increases to 20 GA at a pressure of 90 psf (4,309 Pa).

For the discontinuous configuration the effect of coping gauge variations were investigated as shown in Figure 5.27. Figure 5.27 illustrates the effect of variation of the coping gauge (20, 22, 24, and 26 GA) on the deflection of the coping plate at ¼ for pressures ranging from 10 to 90 psf (479 to 4,309 Pa) when this pressure is applied against the 40" cleat plate segment. Furthermore, for a one-plane pressure applied against the coping plate, it is observed that the deflection of the coping plate is reduced by 35% as the thickness of the coping plate increases to 20 GA from 26 GA as shown in Figure 5.27.

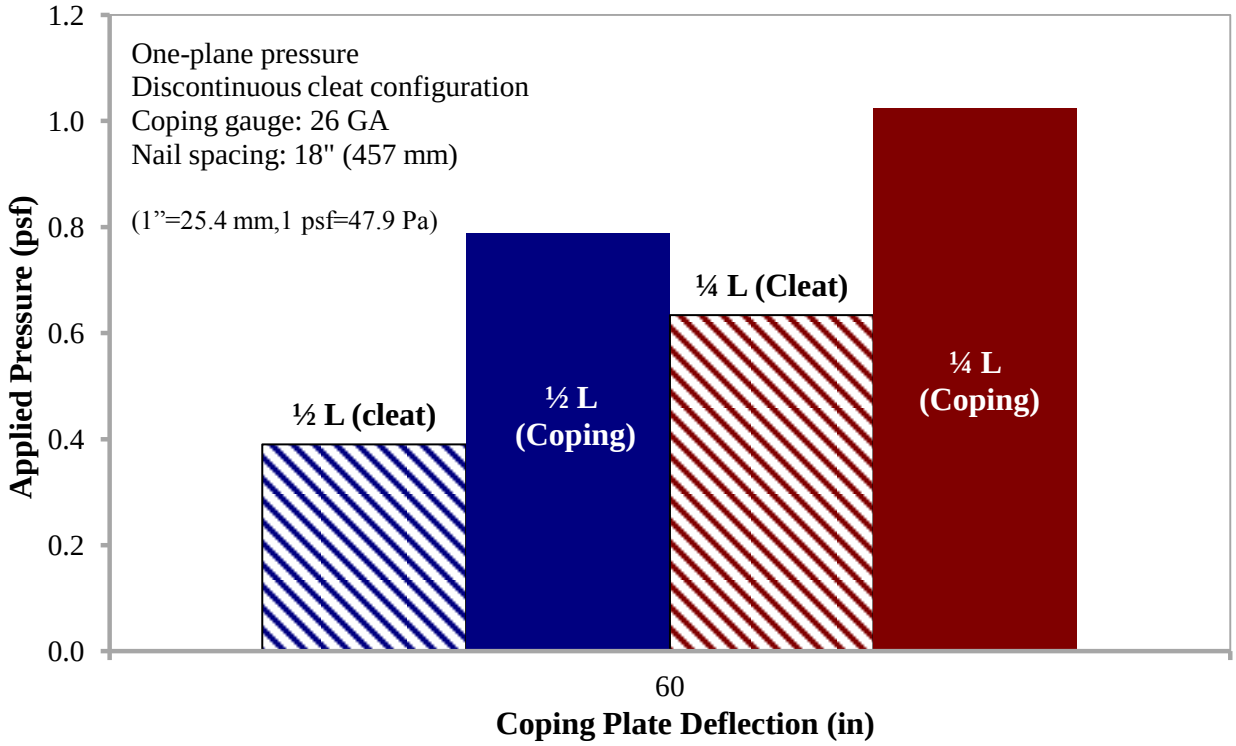

Figure 5.26 Comparison between deflections at both ¼ and ½ L for both one-plane pressure of 60 psf (2,873 Pa) applied against either cleat or coping plate for the discontinuous configuration

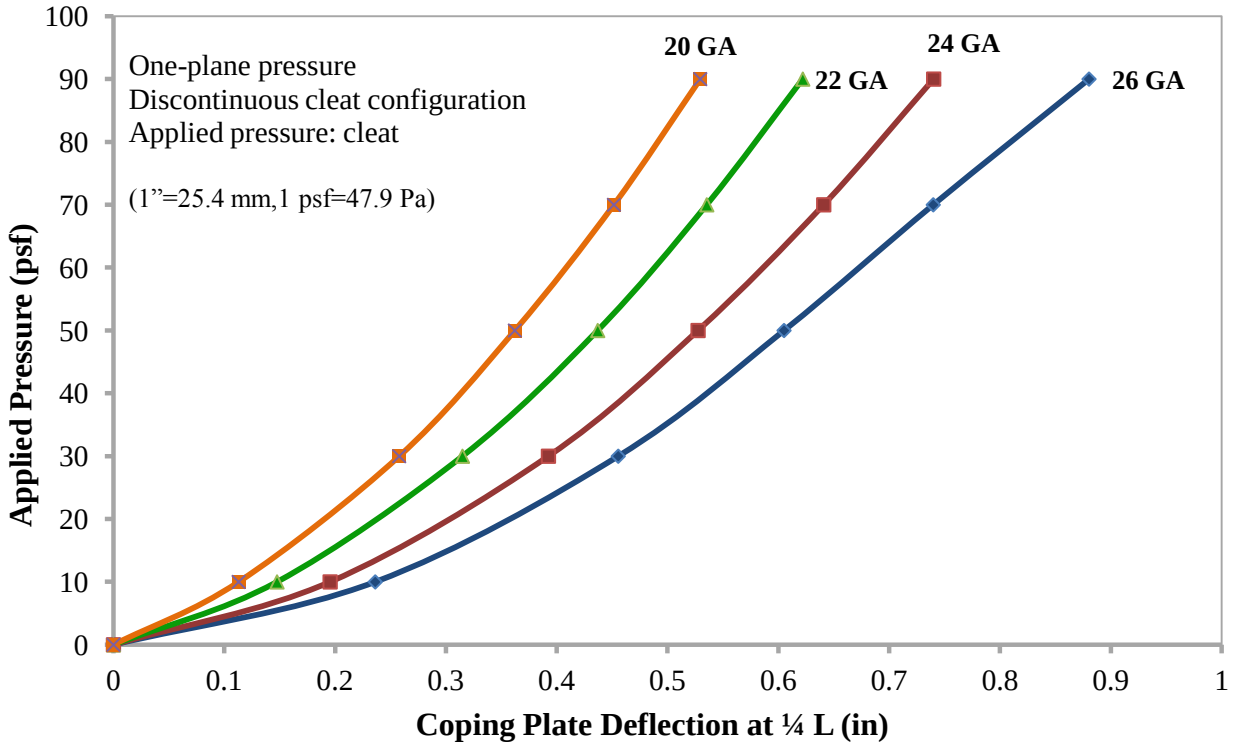

Figure 5.27 Deflection results for the one-plane pressure applied against the cleat for the discontinuous cleat configuration

For a one-plane pressure applied against the cleat plate for the discontinuous configuration, it is evident that the variation of coping gauge has no signeficant influence on the nail reaction value, as shown in Figure 5.28. Nail reaction decreases by 8% as the coping gauge decreases to 20 GA, Figure 5.28. For example at 26 GA, the Nail reaction at 90 psf (4,309 Pa) is approximately 90 lbf (400 N) while at 20 GA the nail reaction is 84 lbf (374 N). On the other hand, for one-plane pressure applied against the coping plate, the coping plate experiences excessive deformations and rotations and yields at 60 psf (2,873 Pa). And at 60 psf (2,873 Pa), the maximum nail reaction recorded was 76.5 lbf (340 N), Figure 5.29. This figure also illustrates that for discontinuous cleat configuration the nail reaction of the roof edge is higher when a one-plane pressure is applied against the coping plate. This is because the coping plate of 26 GA coping gauge resist less loads than the cleat plate of 24 GA consequently more loads are transferred to the cleat nail when a one-plane pressure is applied against the coping plate.

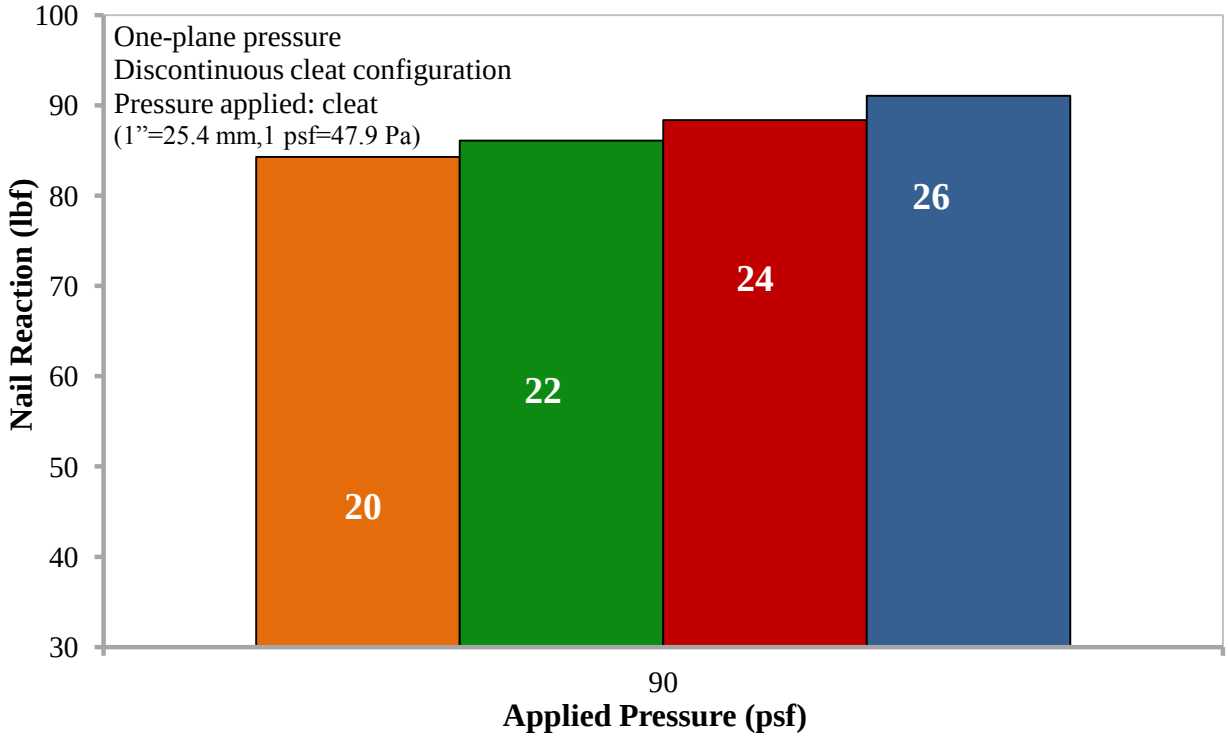

Figure 5.28 Comparison between nail reaction at different coping gauge for a one-plane pressure applied against the cleat plate for the discontinuous cleat configuration

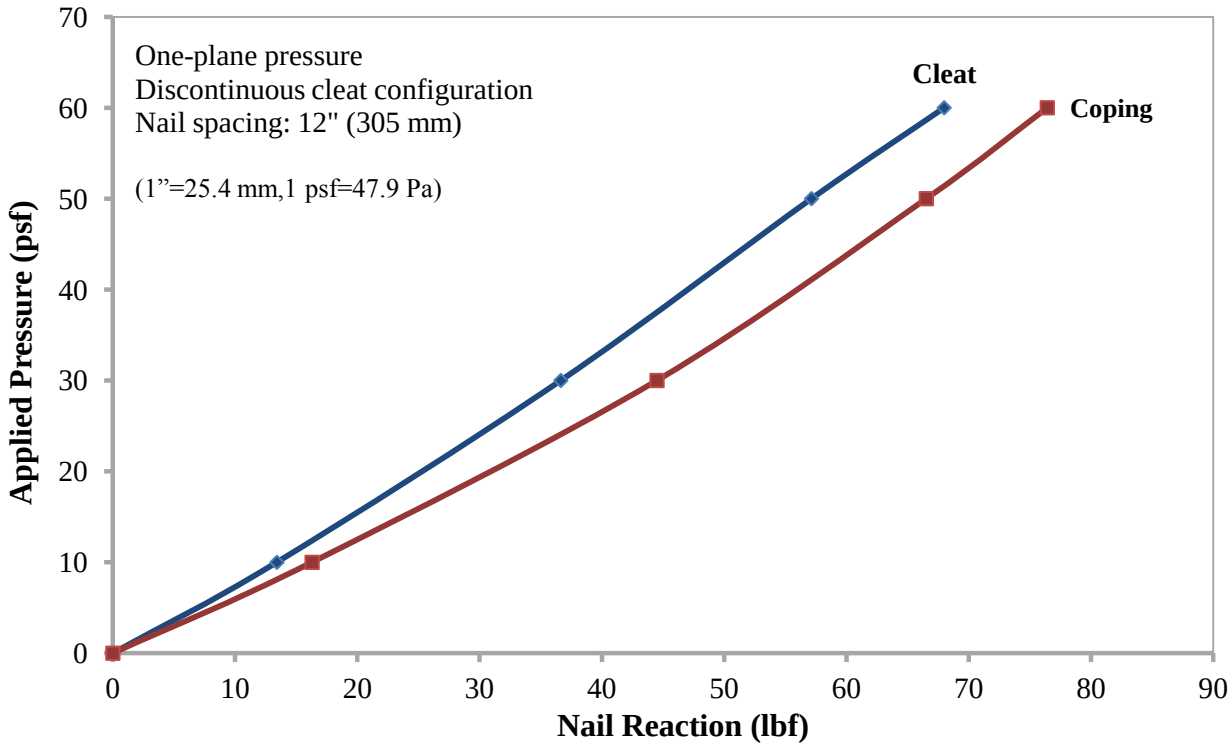

Figure 5.29 Comparison between nail reaction of one-plane pressure applied against the coping and cleat plates for the discontinuous cleat configuration

5.6.2 Pressure is Applied on One-plane or Three-Planes Against the Coping

In the experimental tests conducted at NRC (Alassafin 2012), pressure was applied in one plane along the front coping depth; an approach that accounts for only the negative pressure acting along the horizontal direction of the roof edge. However, peak negative pressure was recorded in both the horizontal and vertical directions of the roof edge, as discussed in chapter 2 and was shown in Figure 2.3. As a result, the horizontal and vertical pressure distribution was accounted for by the development of a three-plane pressure in the finite element analysis.

Boundary conditions on a system were imposed to simulate the two load conditions as illustrated in Figure 5.30. Additional boundary conditions had to be defined for one-plane pressure to resemble the restraining effects of the parapet, which is not modelled. This prevented the inward deflection of the top and back face of the coping. After boundary conditions use imposed on the system, a uniform static and distributed load was applied on one-plane pressure or three-plane pressure against the coping as shown in Figure 5.31.

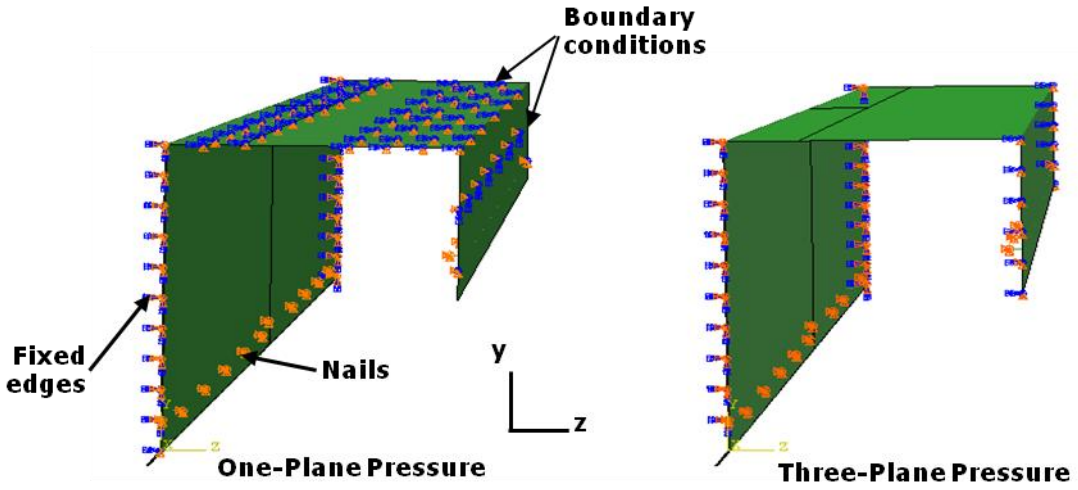

Figure 5.30 Boundary conditions

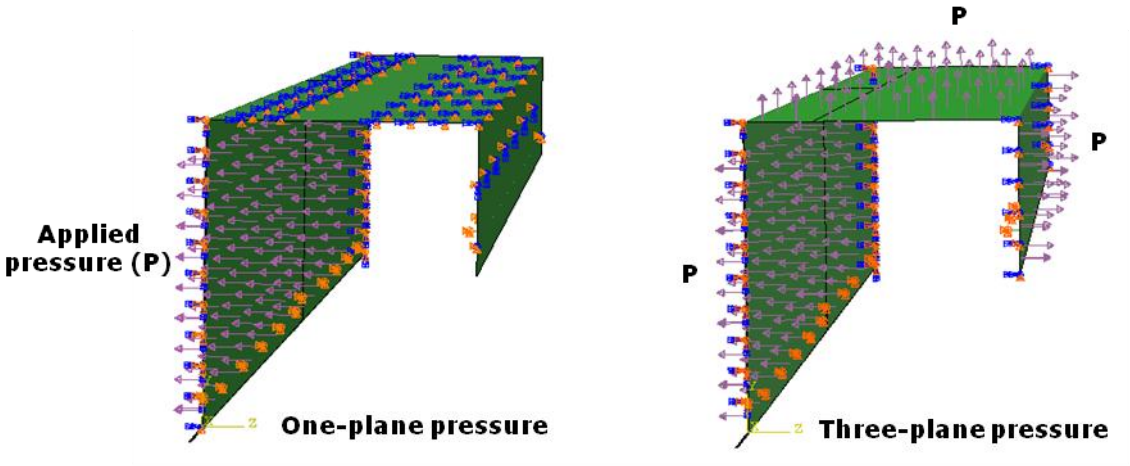

Figure 5.31 Application of a uniform pressure against the coping

Figure 5.32 shows the coping plate deflections subjected to a three-plane pressure applied against the cleat plate for the continuous cleat configuration and for different coping gauges. From the figure, it is noted that the coping plate deflection decreases by half as the coping gauge decreases from 26 GA to 20 GA when a pressure of 90 psf (4,309 Pa) is applied.

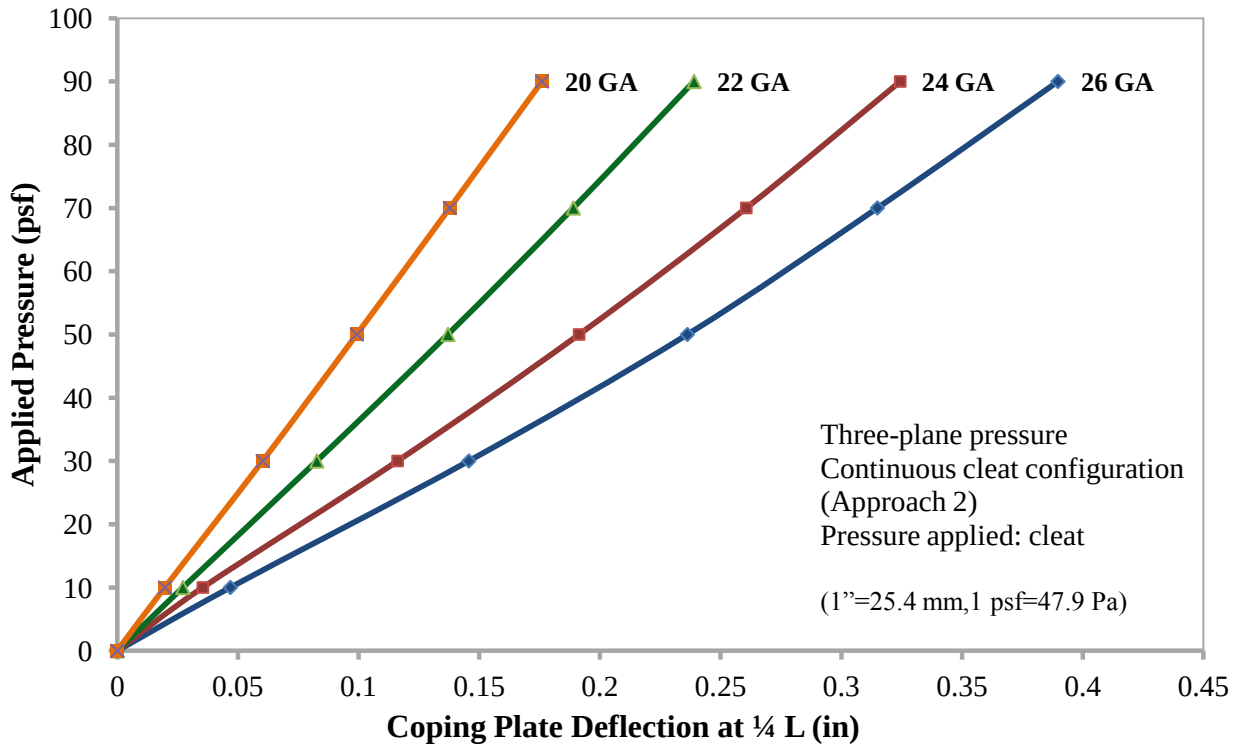

Figure 5.32 Comparison between coping plate deflection at ¼ L at different coping gauges for a three-plane pressure applied against the cleat plate for the continuous cleat configuration

The deflection of the coping plate at ¼ and ½ L where L=8' (2.4 m) (coping middle segment) was also calculated for a three-plane pressure applied against wither the cleat or the coping plate for discontinuous cleat configuration. Modelling approach 3 was used when the discontinuous configuration was subjected to a three-plane pressure applied against either the cleat or coping plate. Comparison between deflection results of the coping plate at ¼ and ½ L for three-plane pressure applied against either the coping or the cleat plate shows that deflection of the coping plate is higher. For example, when a uniform pressure of 80 psf (3,830 Pa) is applied against

coping plate the deflection results of the coping plate at ¼ L is higher by 32% as shown in Figure 5.33 and Figure 5.34. Figure 5.35 shows that the nail reaction for a three-plane pressure applied against the coping plate is higher than the nail reaction calculated for a three-plane pressure applied against the cleat plate. Likewise, the nail reactions for one-plane pressure applied against the coping is higher than those calculated against the cleat plate as shown is Figure 5.29. As a result, a parametric analysis was conducted for only the worst case scenario which is the three-plane pressure plane applied against the coping plate. From Figure 5.36 which shows deflections of the coping plate at different gauge, it is evident that for three-plane pressure applied against the coping plate, the deflection of the coping plate increases as the coping gauge increases. Similar results were obtained for the continuous cleat configuration subjected to a three-plane pressure against the cleat Figure 5.31. As the coping plate thickness decreases the deflection of the coping plate doubled for a pressure of 80 psf (3,830 Pa). On the other hand, varying the coping gauge, for discontinuous configuration, does not influence the corresponding nail reactions as shown in Figure 5.37. For example, at an applied pressure of 70 psf (3,352 Pa) the nail reaction at different coping gauges has the same value of 80 lbf (356 N). Also, similar results were concluded for a one-plane pressure applied against the coping for the discontinuous cleat configuration as shown in Figure 5.3.

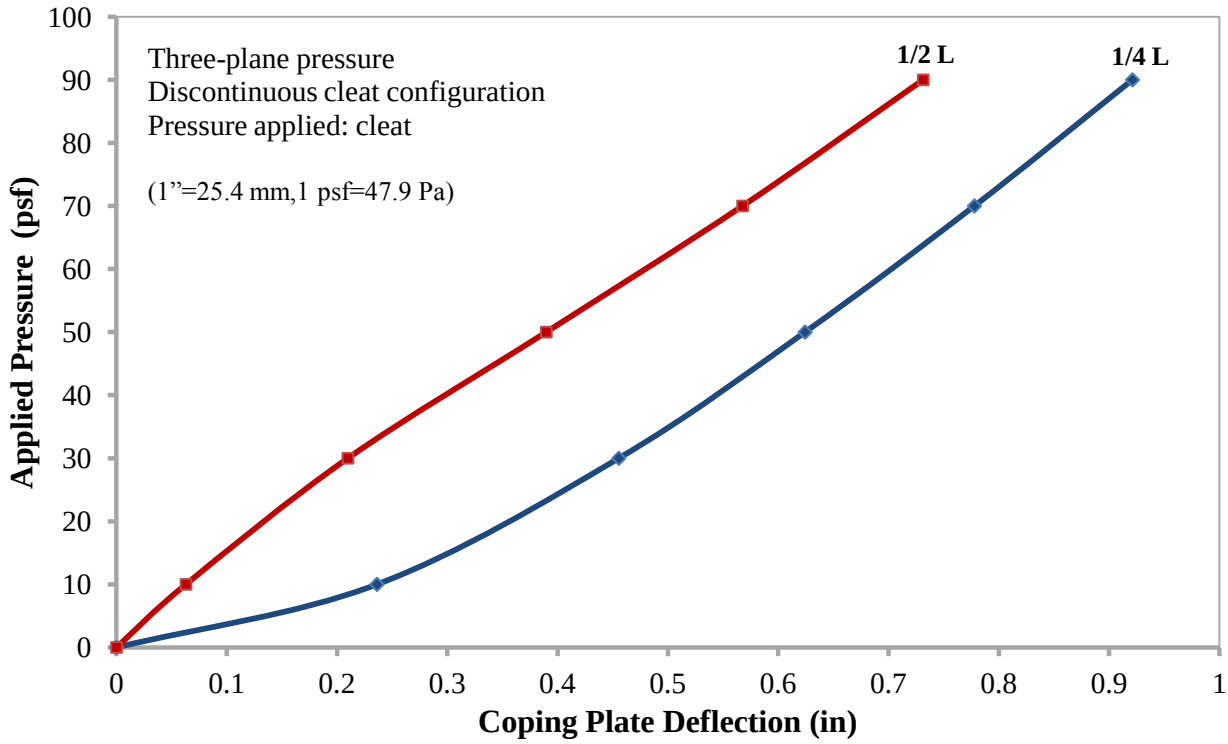

Figure 5.33 Finite element deflection results for a three-plane pressure applied against the cleat plate for the discontinuous cleat configuration

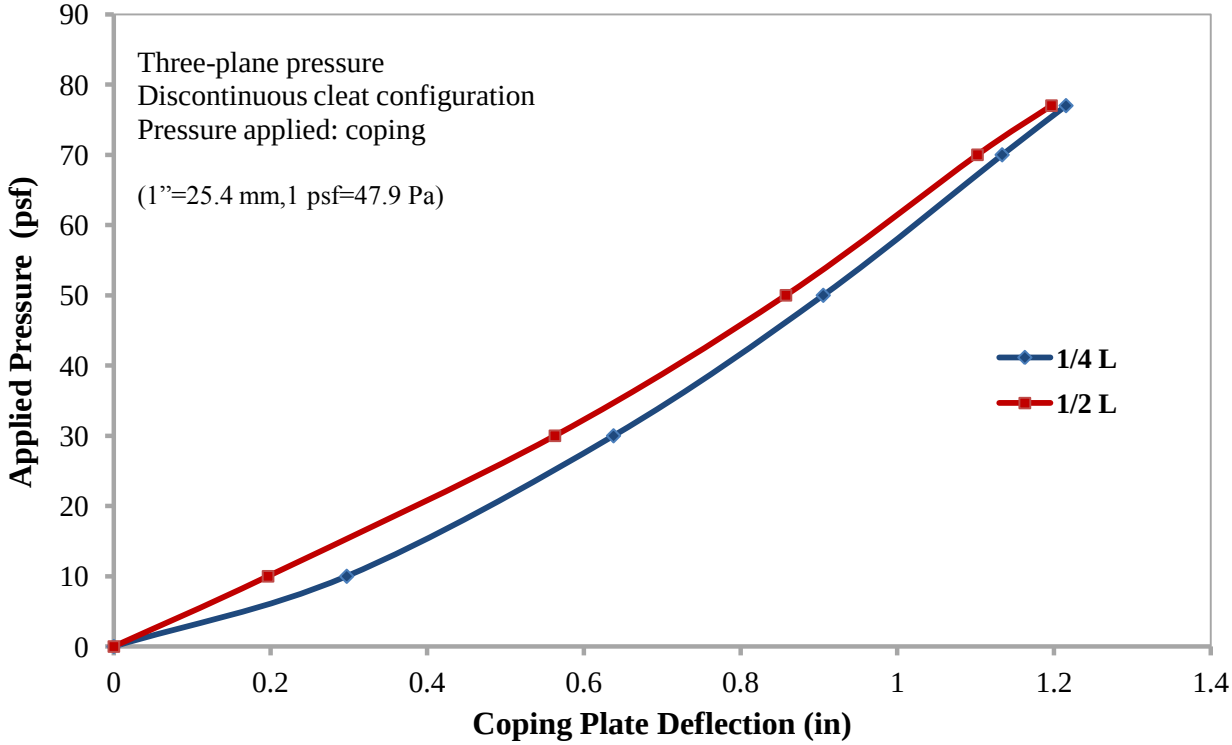

Figure 5.34 Finite element deflection results for a three-plane pressure applied against the coping plate for discontinuous cleat configuration

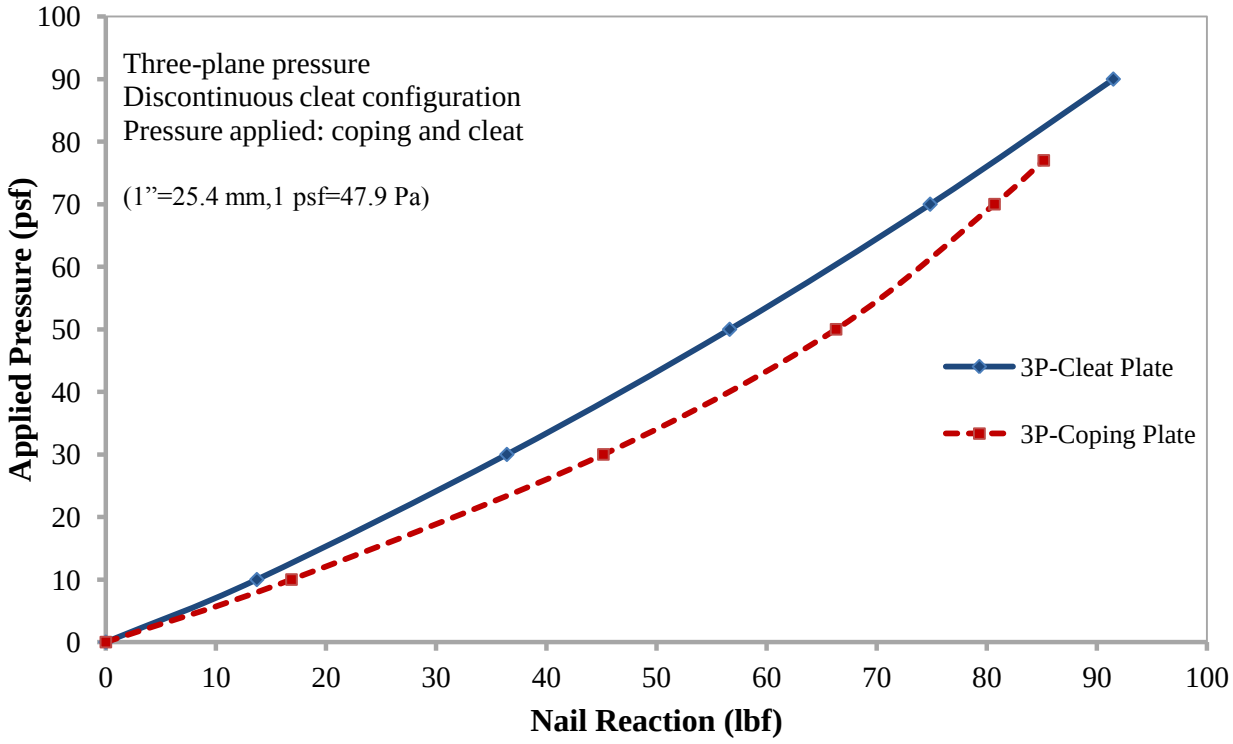

Figure 5.35 Comparison between nail reaction for a three-plane pressure applied against coping and cleat plate for the discontinuous cleat configuration

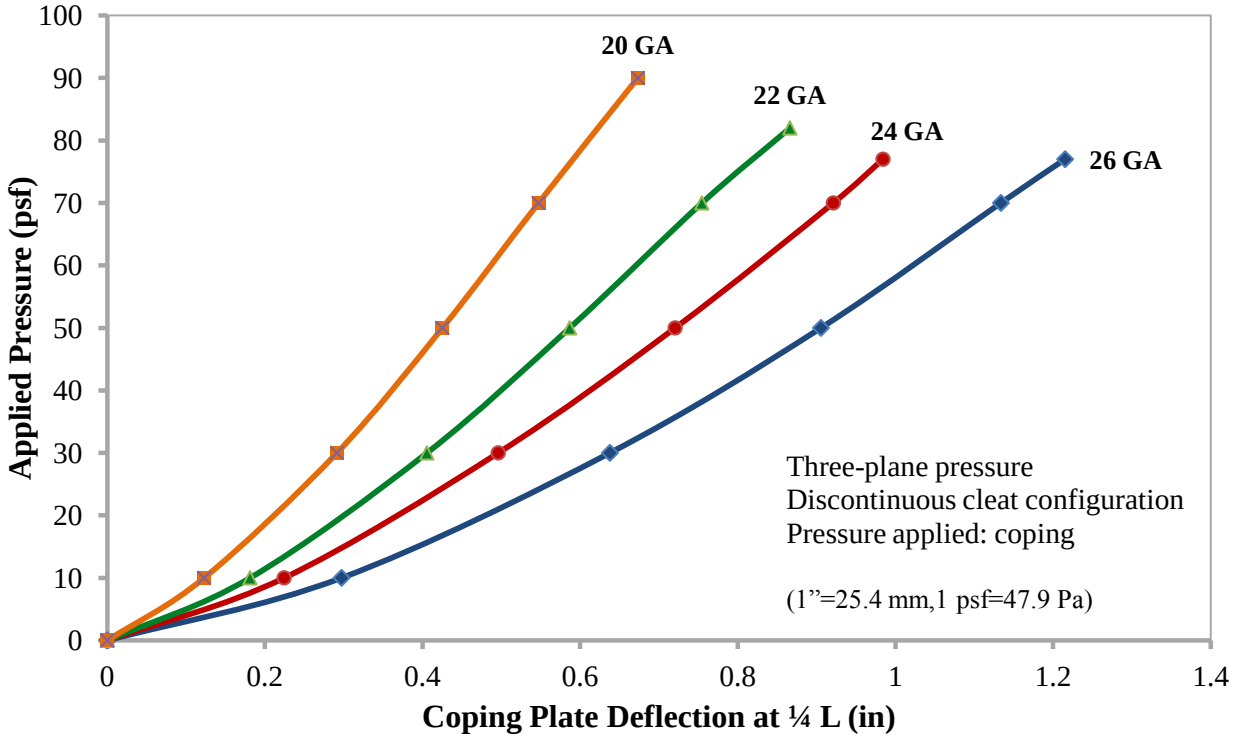

Figure 5.36 Comparison between coping plate deflection at ¼ L at different coping plate thickness for a three-plane pressure applied against the coping plate for discontinuous cleat configuration

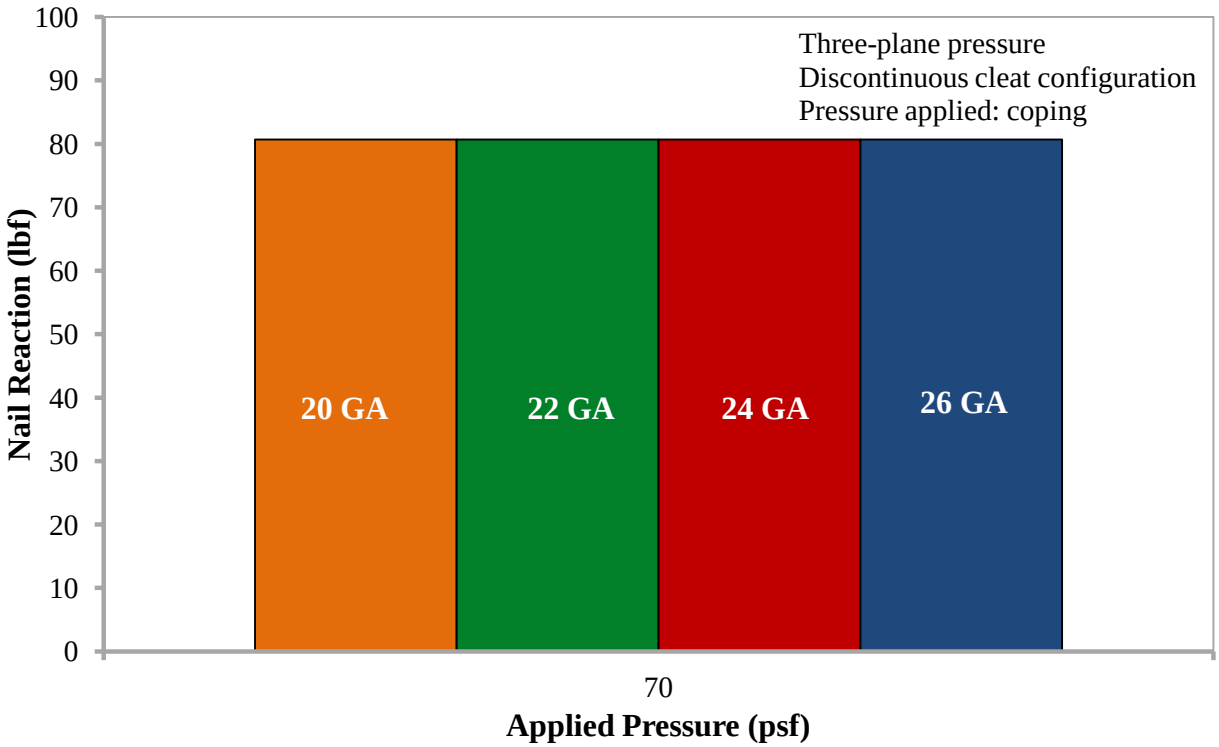

Figure 5.37 Comparison between nail reaction at different coping gauge for a three-ane pressure applied against the coping plate for discontinuous cleat configuration

Comparing the two cases, one-plane pressure and three-plane pressure against the coping, shows that the deflection of the coping for a three-plane pressure is higher than that resulting from a one-plane pressure, Figure 5.38. When the pressure is applied on a three-plane pressure the roof edge is resisting more pressure (i.e., higher loads), which results in higher deflections of the coping plate. This difference becomes greater as the applied pressure increases.

On the other hand, the nail reactions of both one- and three-plane pressure load cases are not significantly different as shown in Figure 5.39. For an applied pressure of 60 psf (2,873 Pa), the nails for the case subjected to a one-plane pressure resist 11% more load than when a three-plane pressure is applied.

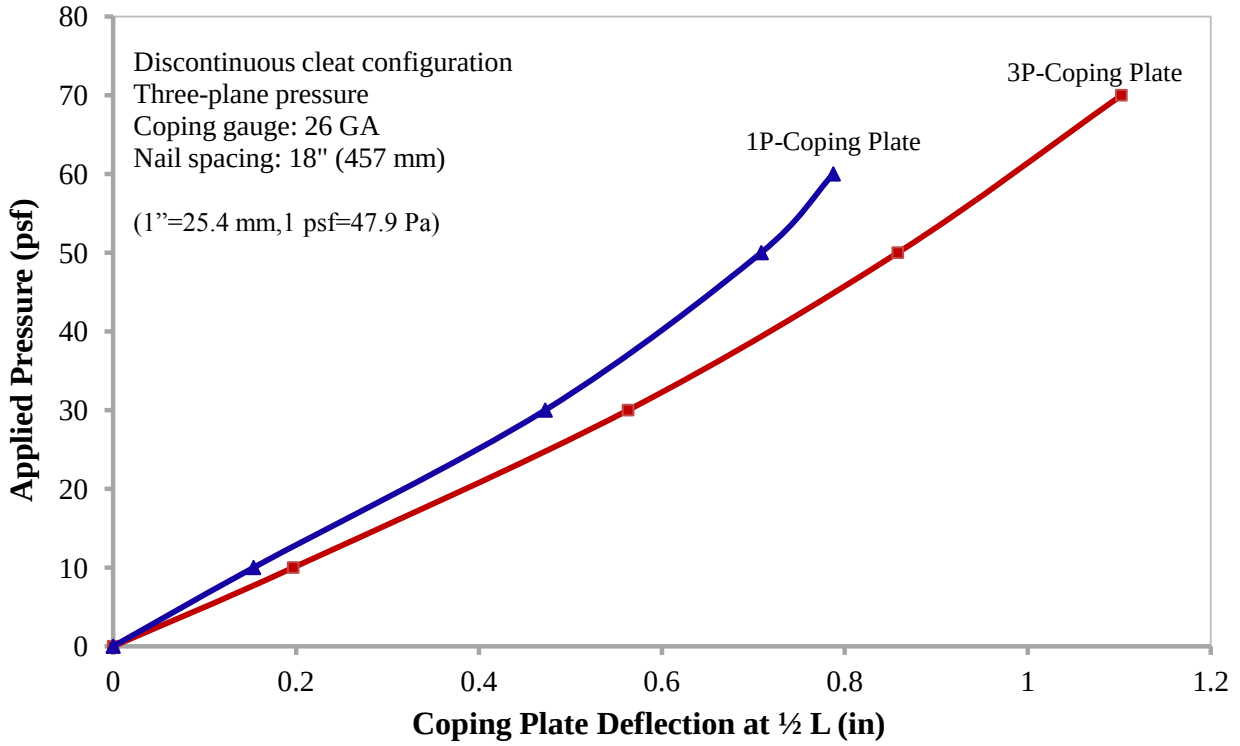

Figure 5.38 Comparison between coping deflections at ½ L for one- and three-plane pressure for discontinuous cleat configuration

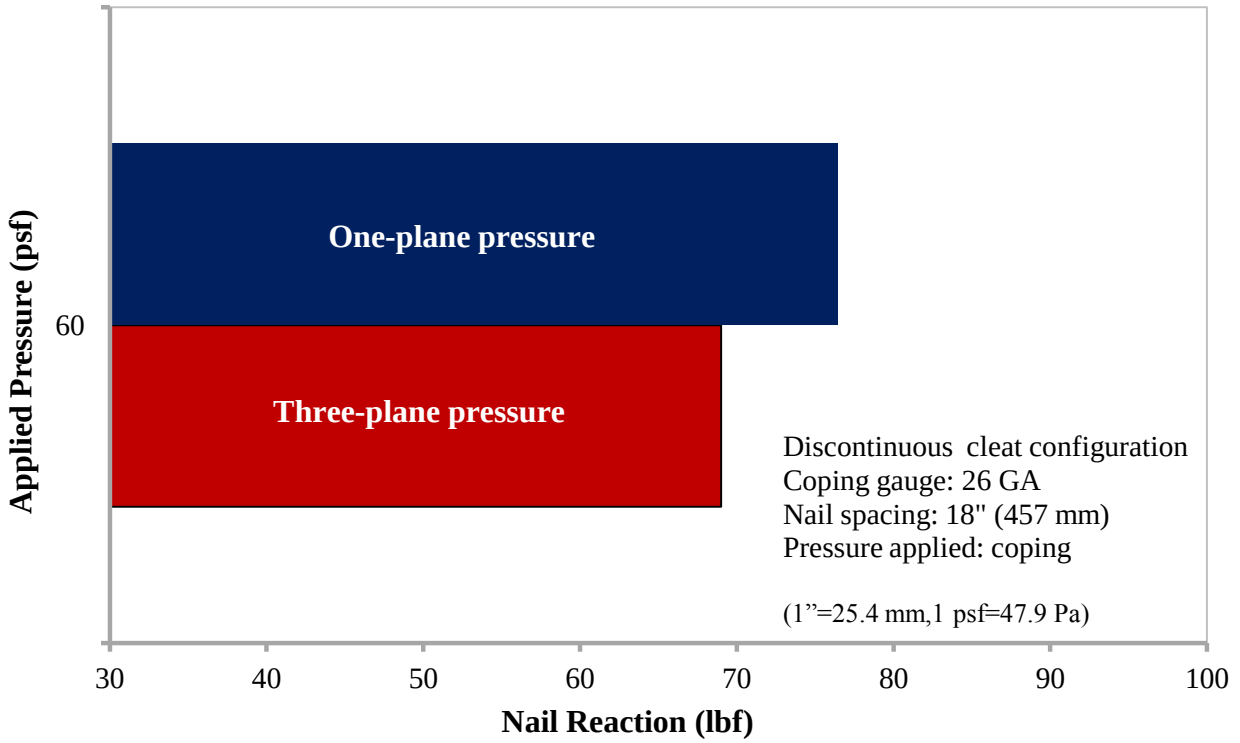

Figure 5.39 Nail reaction results for one- and three-plane pressure applied against coping plate for discontinuous cleat configuration

5.7 Concluding Remarks

The parametric analysis of the roof edge under the effect of varying parameters, coping gauge, nail spacing, coping depth, plate length and load applications, was used to predict the roof edge behaviour subject to wind-induced loads. From this parametric analysis, several findings are concluded including the followings:

- Deflections of the coping plate increase as the coping gauge is increased,
- Deflections of the coping plate and nail reactions increase as the nail spacing is increased,
- Deflections of the coping and nail reactions increase as the coping plate depth is increased,
- Deflections of the coping plate for discontinues cleat configuration decreases as the coping length decreases,
- Deflections of the coping plate increase as the cleat plate is decreased from continuous to discontinuous cleat configurations,
- Nail reaction of the system increases as the cleat length is decreased from continuous to discontinuous cleat,
- Deflections of the coping plate are higher for both one- and three-plane pressure applied against the coping plate,
- Coping gauge variations does not influence nail reaction of the roof edge,
- For both the continuous and discontinuous cleat configurations the deflection of the coping is more critical when the system is subjected to a one-plane pressure against the coping comparing to a one-plane pressure against the cleat,

5.8 Thermal Analysis

The effect of temperature fluctuations and variations from season to season has also been investigated on the roof edge performance. A thermal analysis was conducted to understand the structural response of the system under temperature variations. In the finite element model of the roof edge, the system was initially subjected only to a temperature change, $\Delta T = 80°C$, without the application of wind pressure. This value of $\Delta T = 80°C$ was selected to reflect the worst case scenario to which a system might be subjected. Figure 5.40 shows the contours of the longitudinal displacement (expansion) of the roof edge due to that increase in pressure. From Figure 5.40 and Figure 5.41, it is evident that a system exposed to a temperature change of 80°C results in maximum deflection concentrations at mid-span and depth of the front height of the coping plate. This is because the system is restrained at the boundary from simple expansion along the long axis. As a result the coping plate deflects outwardly at mid-span and mid depth of the front height of the coping plate as illustrated in Figure 5.42. On the other hand, Figure 5.42 illustrates that deflection for the continuous cleat configuration results due to temperature effects are about 25% of those obtained from a system that is subjected to a uniform one-plane pressure. Furthermore, it was observed that an increase of 15°C to the initial change of temperature of 80°C to 95°C results in an 11% increase of the deflection results. Consequently, in the design of a roof edge system that is subjected to extreme temperature fluctuations around the year, it is important to take into account temperature effects on the system along with the wind-induced pressure.

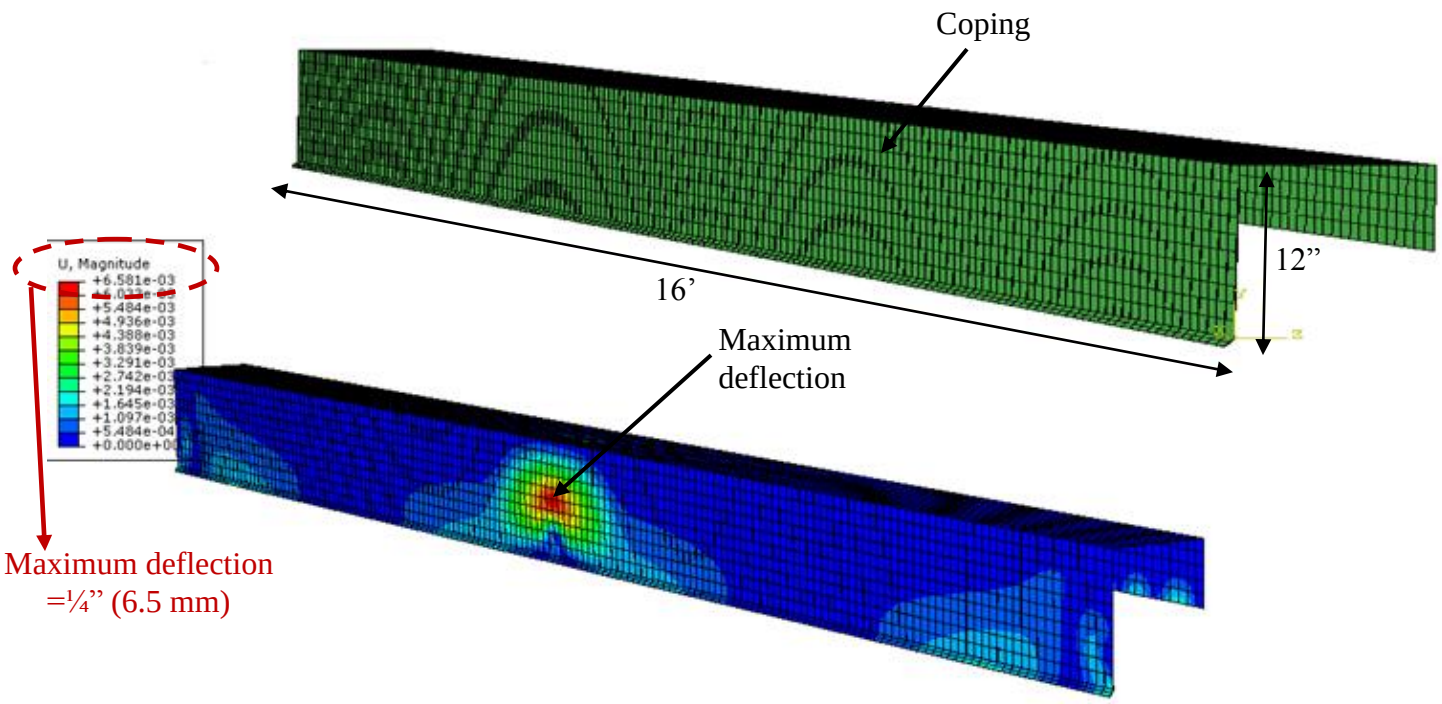

Figure 5.40 Displacement contour on the roof edge due to temperature variations at the mid-span section of the coping plate

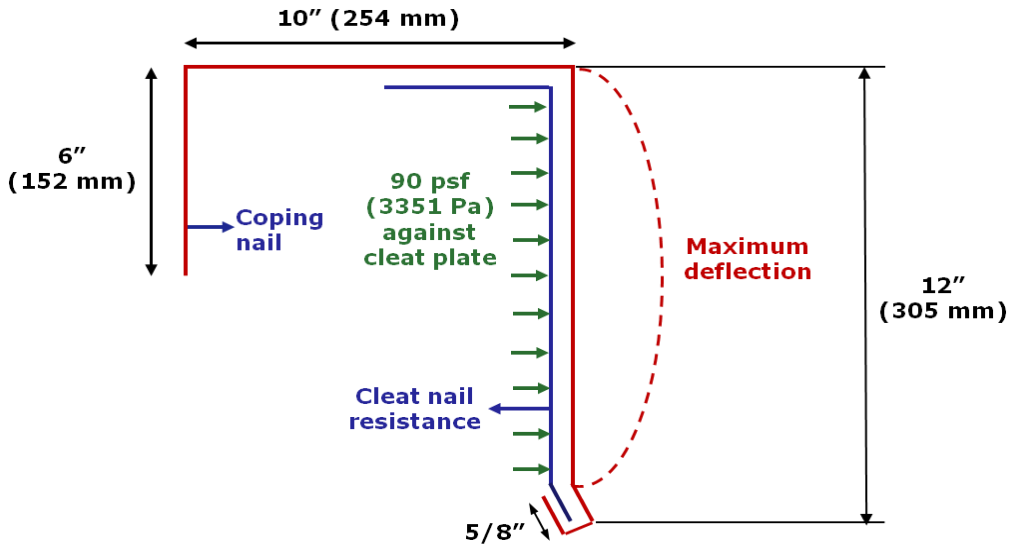

Figure 5.41 Maximum deflection of the coping plate at mid-span and depth of the front height of the coping plate for continuous cleat configuration

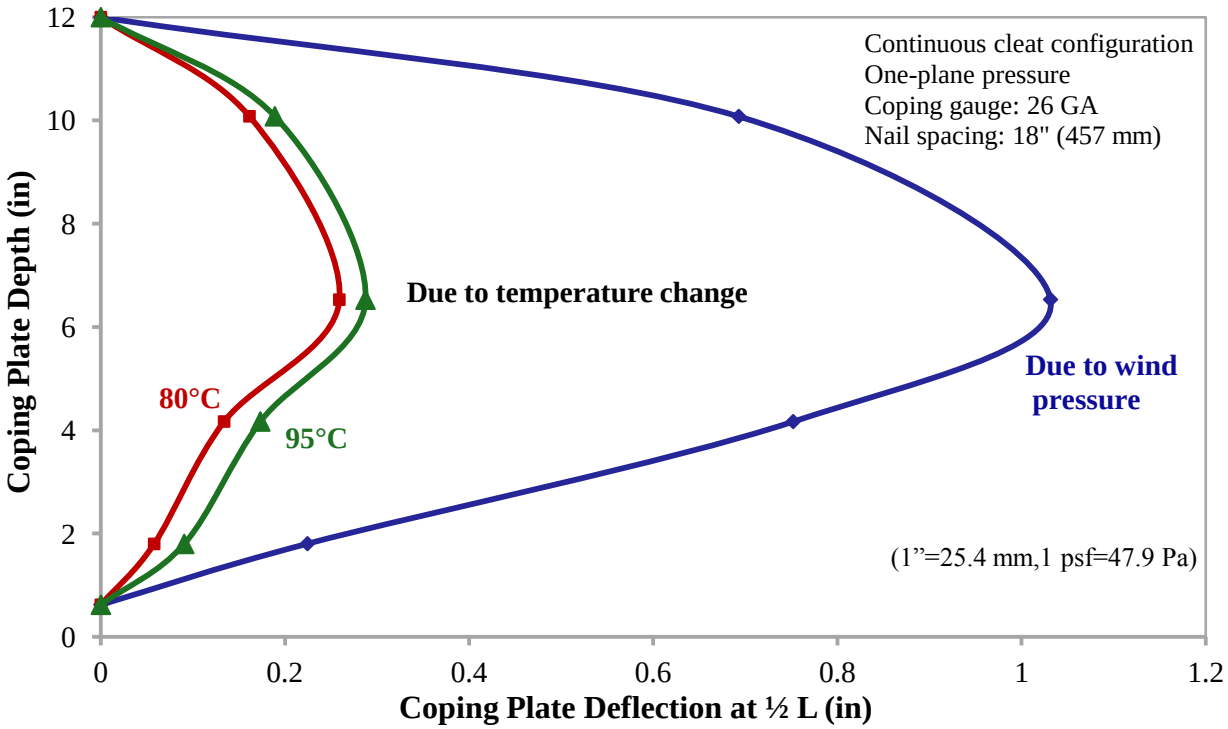

Figure 5.42 Comparison between maximum coping deflections at mid-span and height for a system subjected to temperature variations and for a one-plane pressure applied against the coping for the continuous cleat configuration

5.9 Preliminarily Development of Design Curves for Roof Edges

Design curves can be used as guidelines to aid in the design of roof edge systems. In this study, preliminarily design curves are developed for a designer to determine the maximum applied pressure a system could resist without exceeding a deflection limit. For roof edge system, it is established that a deflection limit of 5% of the coping depth is the maximum limit not to be exceeded in roofing design. This is a value that has been recommended by practitioners in the roofing industry. Based on the parametric analysis presented in this chapter and this deflection limit, three different design curves were developed one for the continuous cleat configuration and two for discontinuous cleat configuration. For a one-plane pressure applied against the coping plate for continuous cleat configuration, a relationship between nail spacing and coping gauge was developed based on the 5% deflection limit as illustrated in Figure 5.43. From Figure 5.43, it is evident that the maximum applied pressure that a system could resist without exceeding the limit deflection increases as the coping gauge decrease; for example, at 26 GA and 20 GA the maximum pressures are 50 psf (2,394 Pa) and 100 psf (4,788 Pa), respectively. However, the same figure illustrates that the nail spacing does not influence the pressure results of the system at different gauges. For instance, at a particular coping gauge the maximum pressure does not decrease as the nail spacing increases (as expected based on the parametric analysis). This is because the continuous cleat configuration is a system that is assembled with a continuous cleat and installed with a group of multiple nails along its length, whose spacing does not influence the maximum pressure that the system can resist.

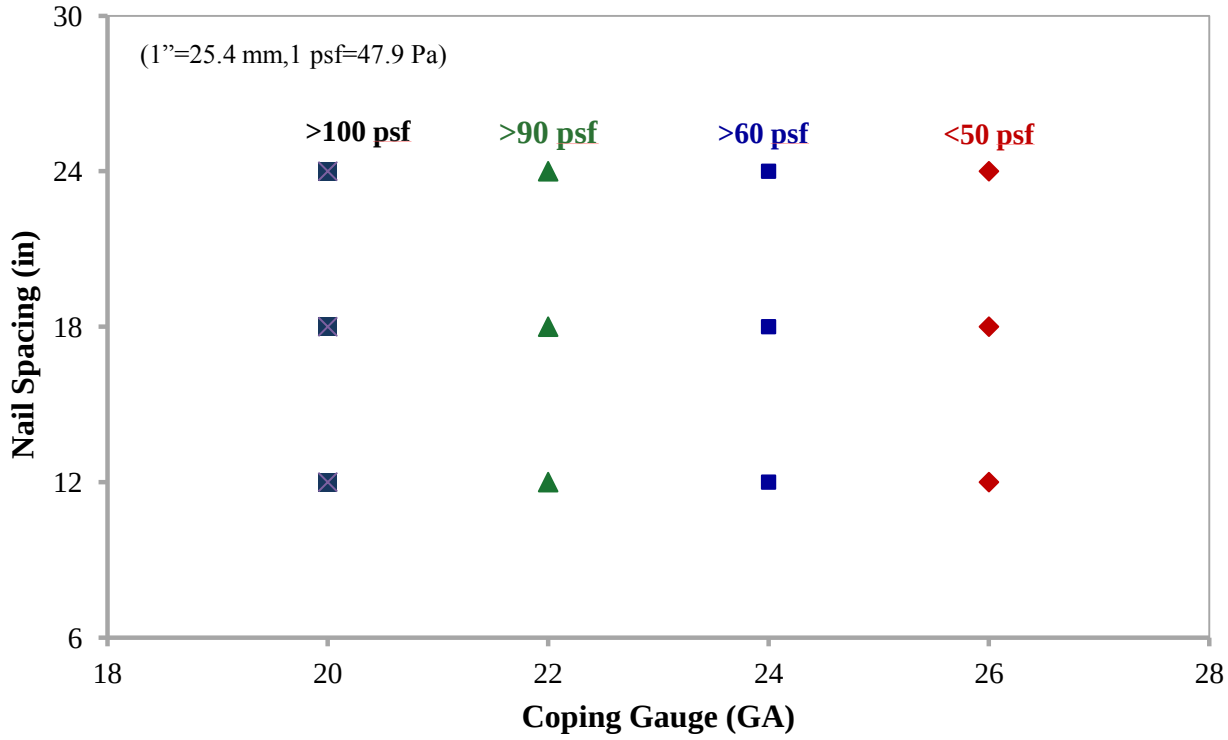

Figure 5.43 Maximum pressure for nail spacing-coping gauge relationship for the continuous cleat configuration subjected to a one-plane pressure against the coping

Figure 5.44 presents the maximum pressure that the discontinuous cleat configuration can resist when subjected to a one-plane pressure against the coping. The maximum pressure the system can resist decreases at a particular coping gauge as the nail spacing increases. For example, at a coping gauge of 24 GA and 12” (305 mm) nail spacing, the maximum pressure is more than 60 psf (2,873 Pa). When the nail spacing is increased to 24” (610 mm) the maximum pressure is reduced to a value less than 50 psf (2,394 Pa). In addition, at a coping gauge of 26 GA and 12” (305 mm) nail spacing the maximum pressure is less than 50 psf (2,394 Pa). Contrary to the continuous cleat configuration, the nail spacing does influence the maximum pressure the system could resist, as the cleat here is discontinuous. Likewise, Figure 5.45 presents the maximum pressure that the discontinuous cleat configuration can resist when subjected to a one-plane pressure against the cleat. At a coping gauge of 26 GA and 12” (305 mm) nail spacing the maximum pressure is more 60 psf (2,873 Pa); however, when the nail spacing is increased to 24”

(610 mm) the maximum pressure is reduced to less than 50 psf (2,394 Pa). From Figure 5.44 and Figure 5.45 it is evident that the cleat plate experiences less deflection than the coping plate when subjected to a one-plane pressure as was established previously.

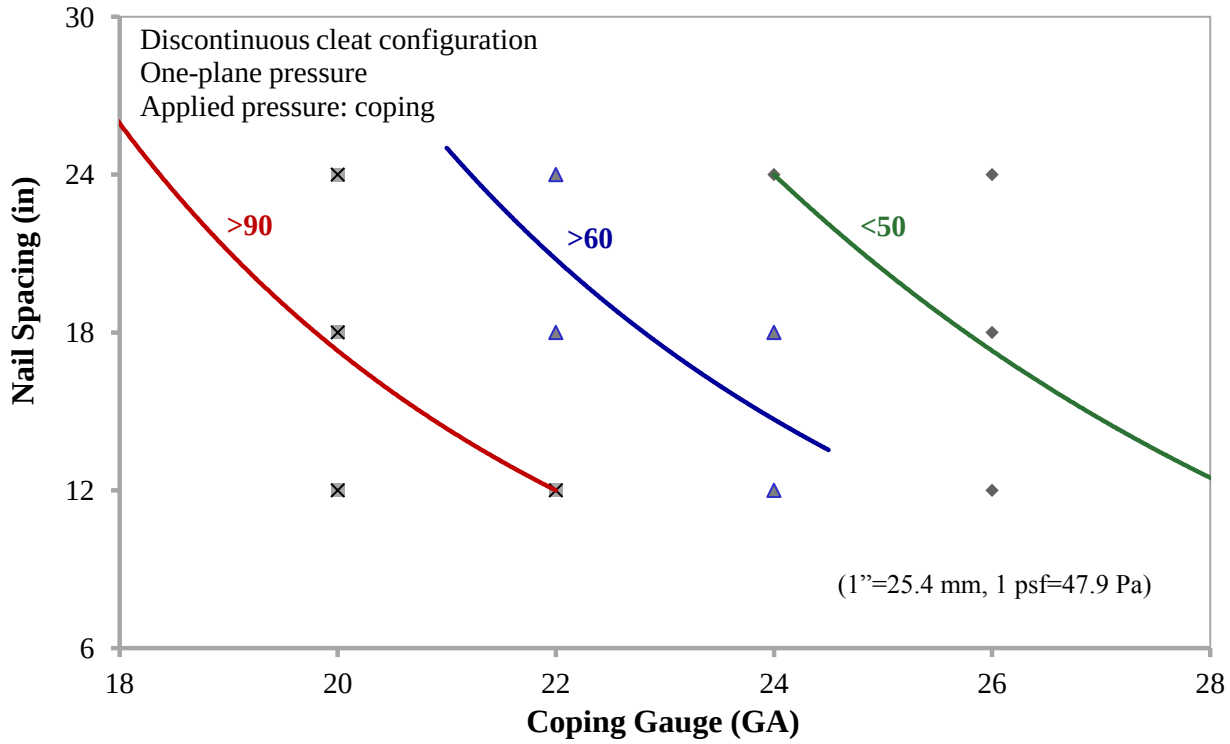

Figure 5.44 Maximum pressure curves for nail spacing-coping gauge relationship for the discontinuous cleat configuration subjected to a one-plane pressure against the coping

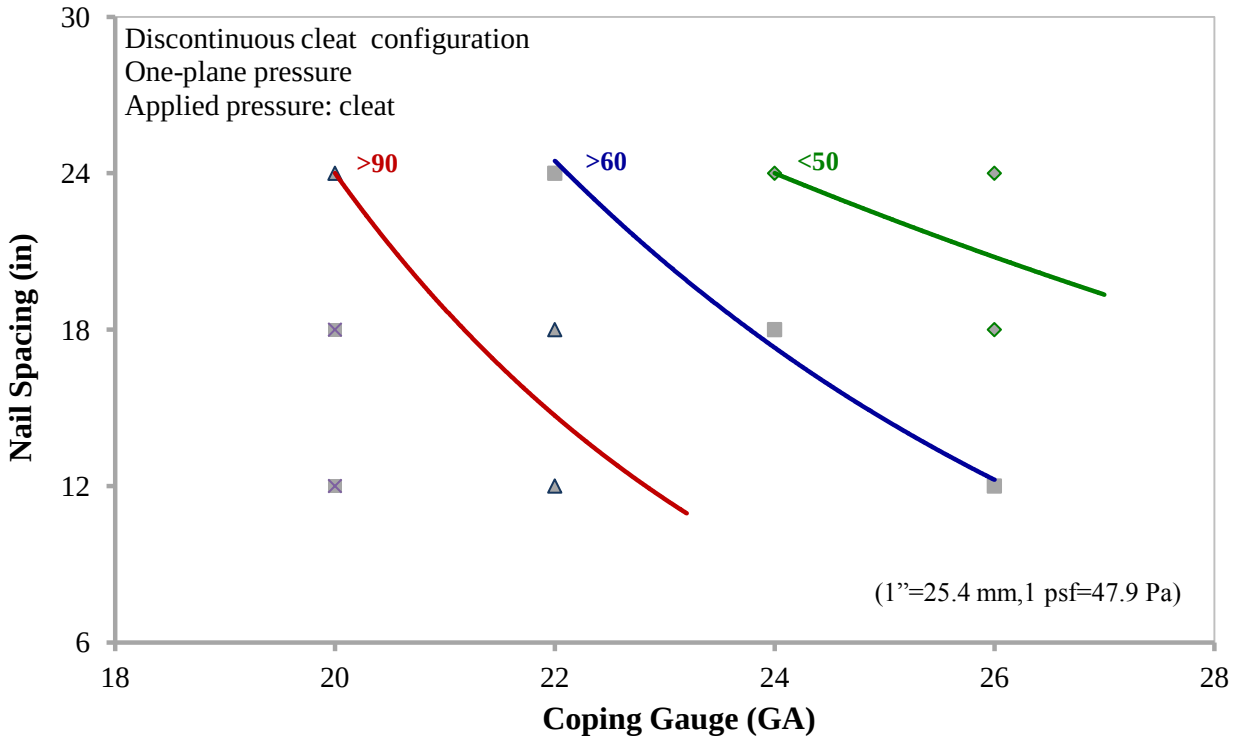

Figure 5.45 Maximum pressure curves for nail spacing-coping gauge relationship for the discontinuous cleat configuration subjected to a one-plane pressure against the cleat

Figure 5.46 illustrates the relationship between the coping length and the coping gauge for the discontinuous cleat configuration subjected to a one-plane pressure against the coping. It is observed that at a particular coping gauge, the maximum pressure the system can resist without exceeding the deflection limit decreases as the coping length increases. For example, at a coping gauge of 26 GA and a coping of 8' (2.4 m) long, the maximum pressure is 60 psf (2,873 Pa); however, for a 16'-long coping the maximum pressure is reduced to less than 60 psf (2,873 Pa). Figure 5.47 illustrates the relationship between the cleat length and the coping gauge for the discontinuous cleat configuration subjected to a one-plane pressure against the coping. It is observed that at a particular coping gauge as the cleat length increases from 40" to 16' (1 m to 4.86 m respectively) the maximum pressure that the system can resist based on the 5% deflection limit is increased. For example, for a 40" (1 m) length of the cleat at 26 GA, the maximum

pressure is less than 50 psf (2,394 Pa) while for 12’ (3.7 m) and 16’ (4.86 m) length of the cleat at the same coping gauge the maximum pressure is more than 50 psf (2,394 Pa).

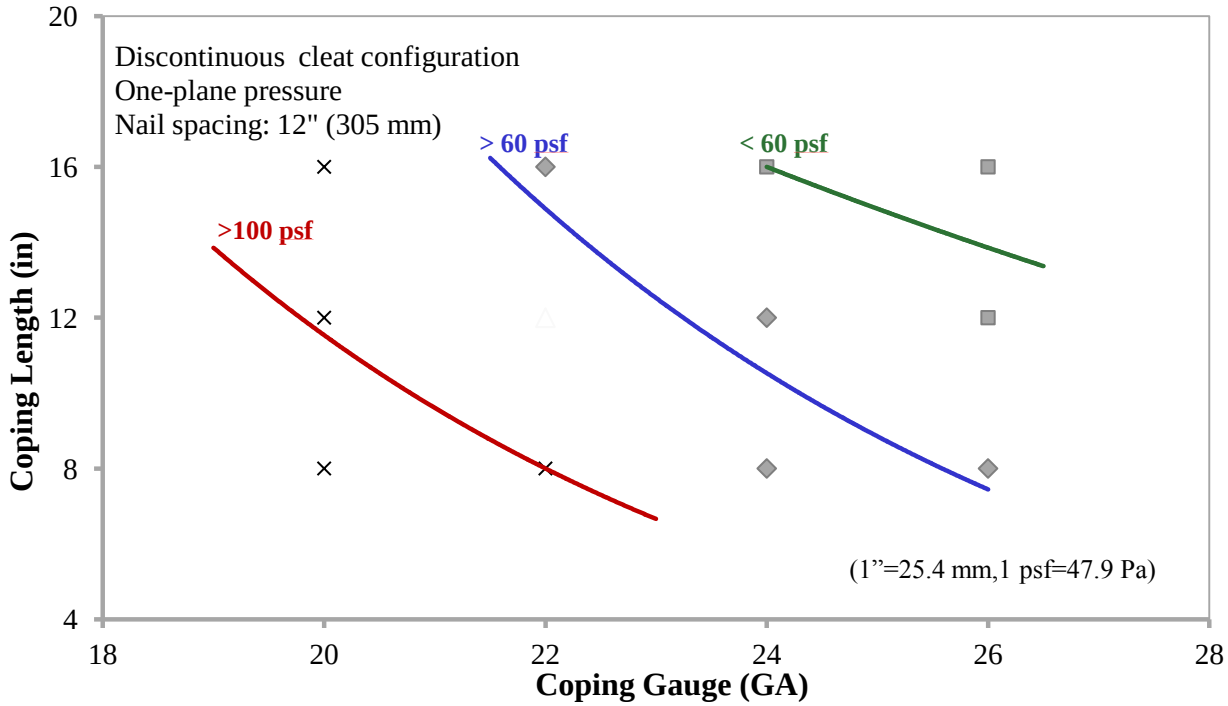

Figure 5.46 Maximum pressure curves for coping length-coping gauge relationship for one-plane pressure for discontinuous cleat configuration

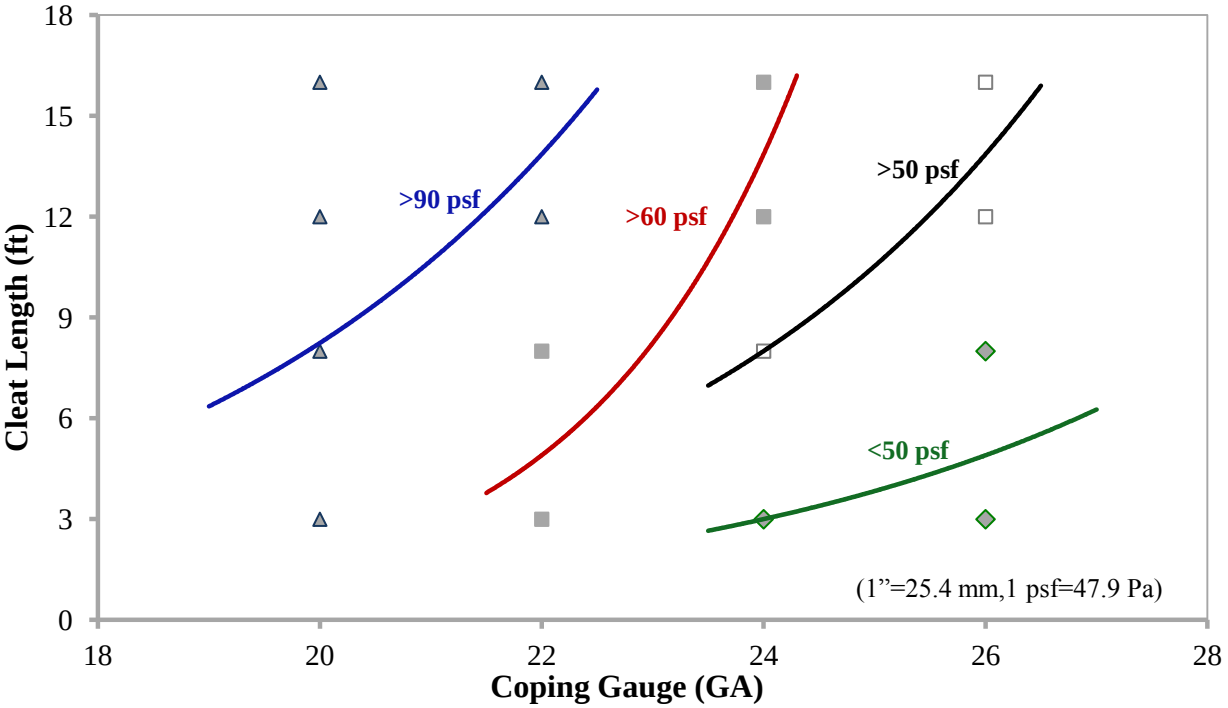

Figure 5.47 Maximum pressure curves for cleat length-coping gauge relationship for one-plane pressure for discontinuous cleat configuration

The previous design curves are useful to determine the maximum pressure based on the maximum deflection limit; nevertheless, they do not account for the nail pull-out force. And, since every component of the roof edge system contributes to the wind-uplift resistance; each component of the roof edge must remain intact to ensure the structural integrity of the system (Chapter 1). Therefore, it is significant to ensure that the nails serve their intended function as a component part of the overall system by eliminating pull-out and disengagement of the nails from their attachments. This is accomplished when the maximum nail reaction (F_{Nmax}) does not exceed the overall nail resistance (F_R), i.e. $F_{Nmax} \leq F_R$. The resistance force of the nail can be estimated from experimental nail pull-out tests, while the reaction forces are calculated using finite element analysis.

To account for the nail pull-out force in the design of the roof edge, additional design figures are developed, for which the maximum nail reaction can be estimated for a given geometry at a particular pressure value. This is achieved by selecting the appropriate value of the normalized value of the nail reaction (k) with respect to the system geometry and the applied pressure. The normalized value (k) of the nail force (F_N) represents the fraction of the force transmitted to the cleat nail due to an applied wind pressure against the coping plate. The normalized nail force (k) is used to determine the maximum nail reaction (F_{Nmax}) of the cleat plate at different pressure points for a given coping height (H_f) and nail spacing (f_s). The value of k yields a good approximation of the maximum nail reaction as long as the relationship between the increase of the nail reactions to the increase of the applied pressure remains linear. This relationship was established in Chapter 4 for a pressure applied against the coping plate for both continuous and discontinuous cleat configurations as shown in Figure 4.30, Figure 4.36 and Figure 4.48. The normalized nail force (k) is therefore calculated as follows:

$$k = \frac{F_N}{P * A_t} \qquad (5\text{-}1)$$

Where

F_N = Nail force (lbf)

P = Applied pressure (psf)

A_t = Tributary area (ft^2) for the cleat nail, $H_f \times f_s$

From equation (5-1) the contour lines of Figure 5.48 and Figure 5.49 are developed using DPlot software (Hyde 2012). From those figures the maximum nail reaction can be determined by selecting the appropriate k value for a given nail spacing for different values of coping depth or cleat length. For example, to estimate the maximum nail reaction (F_{Nmax}) for Set A (H_f=12") for a continuous cleat configuration nailed with 12" (305 mm) spacing and subjected to a uniform pressure of P_w= 90 psf (4.3 kPa) applied against the coping plate, the tributary area is calculated as A_t =1*1=1 ft^2 (0.09 m^2) and k=0.47 is found using Figure 5.48; hence, F_{Nmax}= 42 lbf (187 N). Similarly, for the same pressure of 90 psf (4.3 kPa) for Set B (H_f=6") nailed at 12" (305 mm) spacing, A_t =0.5*1=0.5 ft^2 (0.05 m^2) and k=0.58; hence, F_{Nmax}= 26 lbf (116 N). For both Set A and B, the nail reaction maintains a linear relationship with respect to the applied pressure. From this, it can be observed that the nail reaction increases as the depth of the coping plate increases from 6" to 12" (150 to 305 mm) as concluded earlier in this chapter in section 5.4. In Figure 5.49 the normalized nail force (k) can be selected for a given nail spacing at different cleat lengths from 8 to 16 ft (2.4 to 4.86 m) in order to determine the maximum nail reaction of the cleat plate. The discontinuous cleat configuration of 40" (1 m) cleat length was not included in this figure since the nail reaction force does not follow a linear behaviour. For example, for a cleat length of 12 ft (3.7 m) nailed at 12" (305 mm) nail spacing at 90 psf (4.3 kPa), k= 0.56 and F_N=50 lbf (222

N). On the other hand, at the same pressure of 90 psf (4.3 kPa) for a cleat length of 16 ft (4.86 m) nailed at 12" (305 mm) nail spacing k and F_N are 0.47 and 42 lbf (187 N) respectively. Subsequently, using Figure 5.49 the maximum nail reaction force can be determined at different pressure point for a given geometry as long as the nail reaction force follows a linear behaviour. Also, it can be observed that the nail reaction decreases as the length of the cleat plate increases.

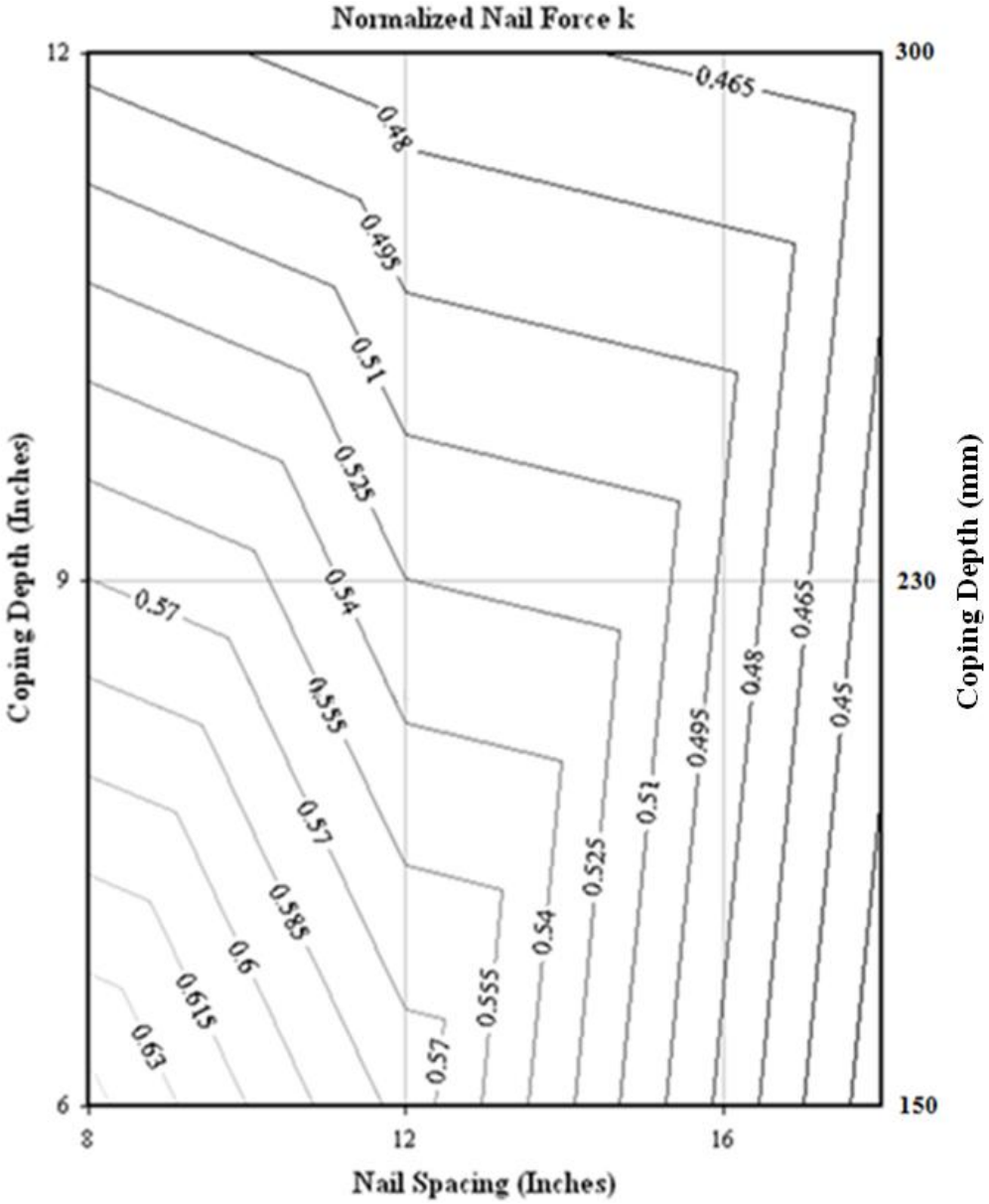

Figure 5.48 Normalized nail force k for a continuous cleat configuration for different values of coping depth H_f and nail spacing (f_s)

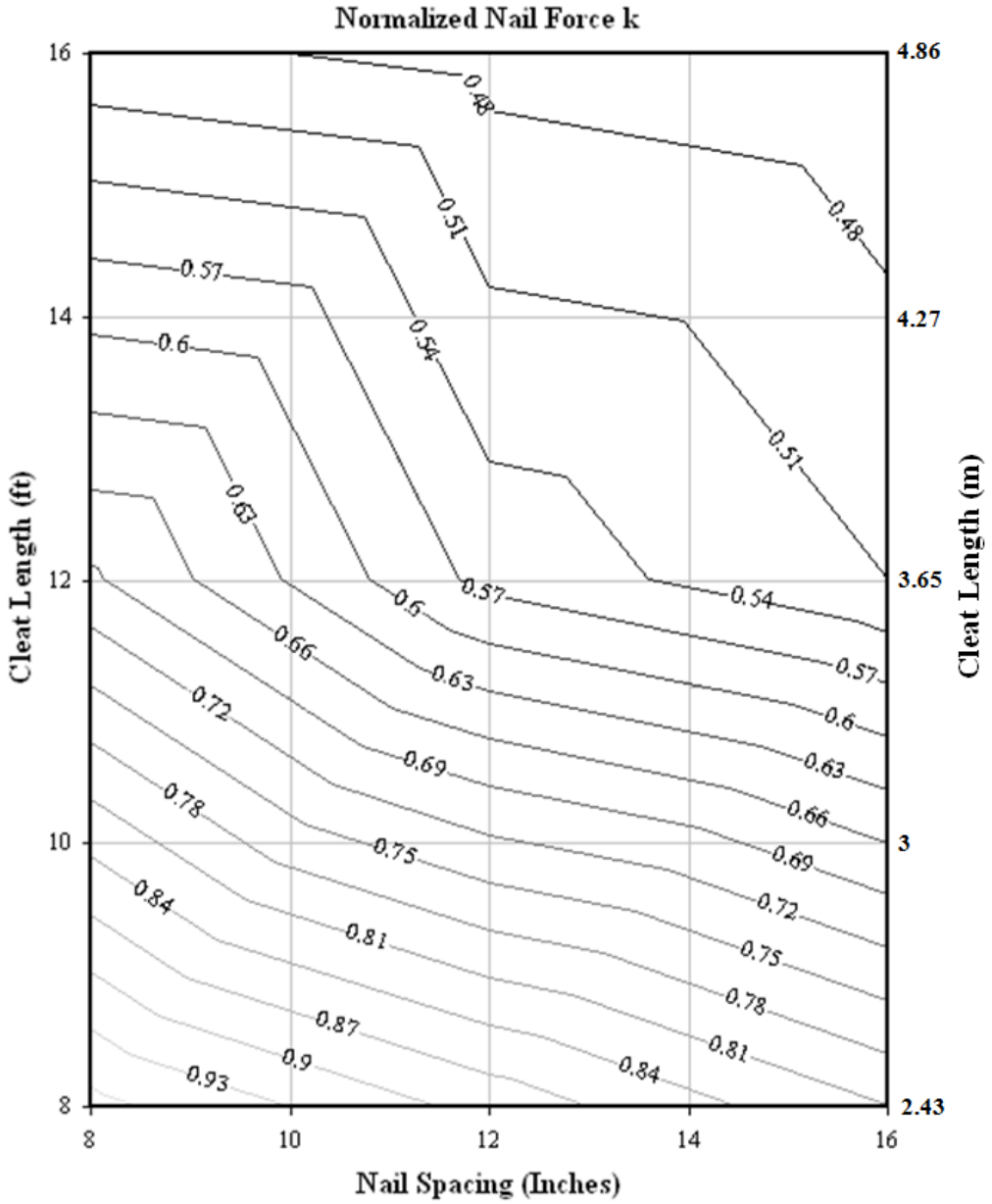

Figure 5.49 Normalized nail force (k) for Set A at different values of cleat length and nail spacing (f_s)

Chapter 6 **Concluding Remarks**

6.1 Conclusions

This study has successfully predicted the behaviour of roof edge subjected to wind-induced loads using the ABAQUS finite element software. ABAQUS allowed the modelling and simulation of the roof edge system and permitted 3D visualization of the roof edge system behaviour. Furthermore, following verification of the system, finite element analyses provided detailed information about the system behaviour under the effect of several parameters in terms of stresses, displacements and reaction forces. From this parametric analysis, preliminary design curves were developed to aid in the design of the roof edge. Finally, the system response under the effects of temperature changes was also assessed.

A finite element model was developed for two system configurations: 1) Continuous cleat configuration, and 2) Discontinuous cleat configuration. Two cross-sectional details, referred to as Set A and Set B, were simulated for the continuous cleat configuration. The finite element mesh was comprised of shell and truss elements. Symmetrical boundary conditions were imposed and static linear and non linear analyses were performed. In general, it was determined that a linear analysis was sufficient for the static analysis of the continuous cleat configuration subject to pressure against the cleat, where the system does not experience material or geometry changes. On the other hand, a non-linear analysis was required for the continuous cleat configuration subject to pressure applied against the coping plate and for the discontinuous cleat configuration, both of which lead to a significant change in geometry.

To better predict the system behaviour, three modelling approaches were used to simulate the coping and cleat interface: vertical parallel edges, continuous connection and drip-edge

connection. The interaction between the coping and cleat plates for the case when the load is applied against the cleat plate or for the drip-edge connection modelling approach was accounted for by a contact mechanism (a general contact-surface-to-surface interaction specific to the ABAQUS software). This allows the transmission of moments and forces between the interacting surfaces. Among the three modelling approaches of the coping/cleat connection, approaches 2 and 3 give more reasonable results in comparison to approach 1. This is because the connection between the coping and cleat plates stiffens the overall system and restrains the coping plate at the bottom edge, creating a parabolic deformation pattern as observed in experimental tests. On the other hand, in approach 1 the vertical edges are not connected, which render the system more flexible with the coping plate completely deflecting outwardly. Consequently, approaches 2 and 3 were used for the validation of the roof edge finite element model. For the finite element validation, two roof edge configurations were used: continuous cleat and discontinuous cleat configurations. For both system configurations, the pressure was applied at one or three planes against either the coping or cleat plates. Finite element analysis deflection results of the coping plate were verified with those obtained from experimental tests and showed very close agreement for all tests in which modelling approach 3 was mostly used. On the other hand, approach 2 yielded slightly stiffer deflection results than the experimental ones.

For the continuous cleat configuration, there is no significant displacement of the drip-edge connection. Hence, it is safe to assume that no connection disengagement occurs, which is in agreement with experimental findings. The system experiences moderate deformations of the coping plate when the pressure is applied against the cleat plate. However, the coping plate deformations are more severe and the maximum reaction force was 52 lbf (231 N) when a

pressure of 90 psf (4,309 Pa) was applied against the coping plate. The system with a discontinuous cleat configuration yields at 60 psf (2,873 Pa) with severe deformations of the coping plate and a maximum reaction force of 77 lbf (343 N). Also, the drip-edge connection does experience lifting and displacement. The continuous cleat configuration with cross section Set B experiences minor deformation of the coping plate and low reaction forces at the nails when subjected to wind pressure of 90 psf (4,309 Pa). A summary of the roof edge finite element model validation observations and results are provided in Table 6.1.

Table 6.1 Summary of the system validations

Configuration / Parameter	**Discontinuous cleat**	**Continuous cleat**	
		Set A	**Set B**
Coping plate deflection	Plate yielded at 60 psf (2,873 Pa) Drip-edge connection displacement is observed	Significant coping deflection at 90 psf (4,309 Pa)	Minor coping deflection at 90 psf (4,309 Pa)
Nail reaction	At 60 psf (2,873 Pa), F_N =77 lbf (343 N)	At 90 psf (4,309 Pa), F_N =52 lbf (231 N)	At 90 psf (4,309 Pa), F_N =28 lbf (125 N)

A parametric analysis was conducted to determine the effect of various design variables in the roof edge performance. The roof edge system was analyzed by varying several parameters which included coping gauge, nail spacing, coping plate depth, coping and cleat plate length, and load application. The followings findings are concluded from the parametric analysis, also summarized in Table 6.2:

- The deflection of the coping plate increases as the coping gauge increases,

- The coping plate thickness has no significant effect on the nail reaction force,
- The nail reaction increases as the nail spacing increases,
- The coping plate deflection and nail reaction force decrease as the coping depth decreases,
- The coping plate deflection increases as the coping plate length increases,
- The coping plate deflection increases as the cleat plate length decreases,
- The coping plate experiences higher deflections when the pressure is applied against the coping plate than when the pressure is applied against the cleat plate.

Table 6.2 Summary of the parametric analysis

<table>
<tr><th colspan="2">Parameter \ Configuration</th><th rowspan="2">Discontinuous cleat</th><th colspan="2">Continuous cleat</th></tr>
<tr><th></th><th></th><th>Set A</th><th>Set B</th></tr>
<tr><td rowspan="3">Coping plate deflection</td><td>Gauge</td><td colspan="3" rowspan="2">Coping plate deflection increases as each parameter is increased</td></tr>
<tr><td>Nail spacing</td></tr>
<tr><td rowspan="3">Nail reaction</td><td>Depth</td><td colspan="3" rowspan="2">Nail reaction does not significantly change under the effect of coping gauge increase; and,

Nail reaction increases as nail spacing, coping depth and length is increased.</td></tr>
<tr><td>Length</td></tr>
</table>

A comparison between the roof edge response, in terms of coping deflection and nail reaction force, when the pressure is applied on one or three planes against the coping plate is illustrated in Table 6.3. From this table, it is evident that for the discontinuous cleat configuration the deflection at ¼ of the coping length and reaction force for both cases are in close agreement, with a tendency of the deflection to be slightly higher at ½ L when a three-plane pressure is

applied, as illustrated in Figure 5.37. However, the continuous cleat configuration, the roof edge response leads to higher nail reaction forces when the load is applied on a three-plane pressure.

Table 6.3 Coping plate deflection and nail reaction results for both continuous and discontinuous cleat configurations subjected to a uniform pressure applied against the coping plate

	Continuous cleat configuration		**Discontinuous cleat configuration**	
	*Coping Plate Deflection at ¼ L (δ_{max}) Inches (mm)	*Nail Reaction (F_{Nmax}) lbf (N)	**Coping Plate Deflection at ¼ L (δ_{max}) Inches (mm)	**Nail Reaction (F_N) lbf (N)
One – plane Pressure	1 (26)	52 (231)	1.2 (29.4)	77 (343)
Three – plane Pressure	1.1 (27.9)	74 (329)	1.1 (29.4)	69 (307)

* Coping plate deflection and nail reaction at 90 psf (4,309 Pa)
** Coping plate deflection and nail reaction at 60 psf (2,873 Pa)

Based on the results of the parametric analyses, preliminary design curves were developed to aid in the design of the roof edge. Figure 5.43 to Figure 5.47 provide detailed information about the maximum pressure the roof edge can resist without exceeding the coping deflection limit of 5% of the coping depth. Additional design curves were developed based on the maximum nail force F_N to ensure that the cleat nails act as an integral part of the overall system without experiencing pull-out or disengagement from its attachment, i.e., $F_{Nmax} \geq F_R$. The maximum nail force F_N can be estimated from Figure 5.48 and Figure 5.49 by selecting the normalized nail force k for a given geometry at a particular pressure point.

Finally, it is predicted that based on a thermal-stress analysis there is a minimum of a 25% increase in the coping deflection due to a temperature increase in the continuous cleat configuration. Therefore, it is important to consider thermal effects on a roof edge that experiences severe temperature fluctuations during the year.

6.2 Future Work

Refinement of the preliminarily design curves developed in chapter 5 to be used as design guidelines for the roof edge design in the roofing industry. In general, testing of fastener resistance under static or dynamic tests were carried out for commercial roofs and it was determined that the pull-out force of fasteners and deflection of the roof components are much significant under the effect of the dynamic loading in comparison to the effect of static loading (Baskaran 2006). This raises the importance of studying, in the future, the behaviour of the roof edge under dynamic loading.

References

Abaqus / CAE (2012). "User's manual, v 6.11."< http://abaqus.ethz.ch:2080/v6.11/>. (December 5, 2012). Dassault Systèmes Simulia Corp. USA.

Alassafin, W. (2012). "Wind uplift resistance of roof edge components." MASc thesis. University of Ottawa. Ottawa, Canada.

ASCE. (2010). "Minimum design loads of buildings and other structures." ASCE07-2010, American Society of Civil Engineers. USA

Baskaran, A. (2011). "Wind uplift standard for roof edge systems and technologies REST project." Tentative agenda. National Research of Canada. Ottawa, Canada.

Baskaran, A., Molleti, S., and Roodvoets, D. (2007). "Understanding flat roofs under Hurricane Charely from field to practice." Journal of ASTM International, v. 4, no. 10, pp. 1-13.

Baskaran, A. (2006). "10 questions and answers on static vs. Dynamic wind testing for commercial roofs." Journal of Roof Consultant Institute, v. 24, no. 9, pp. 5-13.

CBC News (2012). "Power returning to Toronto in the wake of a storm". http://www.cbc.ca/news/canada/toronto. (November 15, 2012).

CRCA. (2007). "Perimeter edge flashing and wind resistance." Advisory Bulletin. Canadian Roofing Contractors' Association. Ottawa, Canada.

Fish, J., and Beyltsschko, T. (2007). "First course in finite element." John Willey & Sons Ltd, England. Chapter 9, pp. 215-217.

Holmes, J.D. (2001). "Wind loadings of structures." Spon Press. Canada.

Hyde, D. (2012). "DPlot graph software for engineers and scientist – DPlot User Manual". http://www.dplot.com/evaluation.htm (December 14, 2012), HydeSoft Computing, LLC. USA

Jiang, H. (1995). "Wind effects on metal edge flashing." B.S.E thesis. Texas Tech University. USA.

Johnson, K. L. (1985). "Contact mechanics." Cambridge University Press. UK. Chapter1. pp. 1-9.

Liu, .G.R., and Quek, S.S. (2003). "Finite element method: a practical course." Elsevier. Ltd. ISBN: 978-0-7506-5866-9. Chapter 1, 8, 11 and 13, pp. 1-11, 180-193, 324-341.

McDonald, .J.R., Sarkar, .P.P., and Gupta, H. (1997). “Wind-induced loads on metal edge flashing.” Journal of Wind Engineering and Industrial Aerodynamics.72 (1997) 367 377.

Molleti, S. (2012). “Wind uplift standard for roof edge systems and technologies REST project.” Tentative agenda. National Research of Canada (NRC). Canada.

Reddy, .J.N. (2004). “An introduction to non-linear finite element analysis.” Oxford United Press Inc. USA.

RGC. (2012). RCABC Roofing Practices Manual (RPM online), Section 10: construction details. <http://rpm.rcabc.org/index.php?title=Main_Page>. (Nov 20, 2012). RCABC, British Columbia, Canada.

Rowlett, R. (2002). “Sheet metal thickness gauges.” <http://www.unc.edu/~rowlett/units/scales/sheetmetal.html>. (December 1, 2012). University of North Carolina, USA.

SIMULIA. (2010). “ABAQUS 6.10: getting started with ABAQUS, Keyword edition.” Dassault Systèmes Simulia Corp. USA.

SPRI. (2011). Wind design standard for edge system used with low slope roofing systems, ANSI/SPRI/FM 4435/ES-1. <http://nationalestesting.com/newcontact.html>. (November 22, 2012). Single-ply and Roofing Industry (SPRI). NESTS, Inc. Georgia, USA.

Valentin, L.P. (2010). “Contact mechanics and friction: physical principles and applications.” Springer. USA. Chapter 2, pp. 9-20.

Wang, W., James, R. MacDonald, and Jiang, H. (1995). “Field experiments for wind loading on metal edge flashings.” 11th Conference on Roofing Technology. Gaithersburg, Md. 60-66.

APPENDIX

***Sample of an Input file generated for the modeling of Set B for continuous cleat configuration

```
*HEADING
ROOF EDGE MODELLING- CONTINUOUS CLEAT CONFIGURATION (SET B)

*****COPING PLATE NODE GENERATION
*NODE, NSET=COPING
1, 0, 0, 0
977, 0, 0.12, 0
1139, 4.86, 0.12, 0
1221, 0, 0.137, 0
1383, 4.86, 0.137, 0
163, 4.86,0,0
*NODE, NSET=NAILS
11091, 0.18, 0.015, 0.23
11092, 0.48, 0.015, 0.23
11093, 0.78, 0.015, 0.23
11094, 1.08, 0.015, 0.23
11095, 1.38, 0.015, 0.23
11096, 1.68, 0.015, 0.23
11097, 1.98, 0.015, 0.23
:
:
:
11105, 4.38, 0.015, 0.23
11106, 4.68, 0.015, 0.23
*NODE, NSET=CPLATE
3417, 0, 0.137, 0.24
3579, 4.86, 0.137, 0.24
*NODE, NSET=CPLATE1
4637, 0, -0.015, 0.24
4799, 4.86, -0.015, 0.24
*NODE, NSET=COPING
8391, 1.92, -0.015,-0.01
8425, 2.94,-0.015,-0.01
*NODE, NSET=CORNERS
8065, 1.92,-0.015,-0.011
8099, 2.94,-0.015,-0.011

*****CLEAT PLATE NODE GENERATION
*NODE, NSET=CORNERS1
8717, 1.92, 0, 0.001
8751, 2.94, 0, 0.001
9377, 1.92, 0.12, 0.001
9411, 2.94, 0.12, 0.001
```

```
9542, 1.92, 0.137, 0.001
9576, 2.94, 0.137, 0.001

****GENERATION OF CLEAT NAILS
*NODE, NSET=CNAILS
11180, 1.98, 0.03, 0.01
11181, 2.28, 0.03, 0.01
11182, 2.58, 0.03, 0.01
11183, 2.88, 0.03, 0.01
:
:
*NODE, NSET=CPLATE2
9872, 1.92, 0.137, 0.031
9906, 2.94, 0.137, 0.031

*****NODE GENERATION FOR COPPING
*NGEN, NSET=EDGE1
1, 163, 1
*NGEN, NSET=EDGE2
977, 1139, 1
*NFILL, NSET=WALL
EDGE1, EDGE2, 4, 244
*NGEN, NSET=EDGE3
1,977,244
*NGEN, NSET=EDGE4
163, 1139, 244
*NSET, NSET=EDGE
EDGE1, EDGE2, EDGE3, EDGE4
:
:
:
*NGEN, NSET=E1
1221, 1 383, 1
*NGEN, NSET=E2
3417, 3579, 1
*NFILL, NSET=WALLT
E1, E2, 9, 244
*NGEN, NSET=E3
1221, 3417, 244
*NGEN, NSET=E4
1383, 3579, 244
*NSET, NSET=EE
E1, E2, E3, E4
*NGEN, NSET=EDG111
3417, 3579, 1
*NGEN, NSET=EDG222
4637, 4799, 1
:
:
:
*NSET, NSET=T1, GENERATE
```

```
3417, 3579, 1
3173, 3335, 1
2929, 3091, 1
2685, 2847, 1
2441, 2603, 1
2197, 2359, 1
9872, 9906, 1
9542, 9576, 1
*NSET, NSET=T2, GENERATE
3661, 3823, 1
3905, 4067, 1
4149, 4311, 1
*NGEN, NSET=VR1
8065, 8099, 1
*NSET, NSET=VR2, GENERATE
65, 99, 1
*NFILL
VR2, VR1, 1, 8000
*NGEN, NSET=VR11
8391, 8425, 1
*NSET, NSET=VR22, GENERATE
8065, 8099, 1
*NFILL
VR22, VR11, 2, 163
*NGEN, NSET=VR111
8717, 8751, 1
*NSET, NSET=VR222, GENERATE
8391, 8425, 1
*NFILL
VR222, VR111, 2, 163

*****NODE GENERATION FOR CLEAT PLATE
*NGEN, NSET=CEDGE1
8717, 8751, 1
*NGEN, NSET=CEDGE2
9377, 9411, 1
*NFILL, NSET=CWALL
CEDGE1, CEDGE2, 4, 165
*NGEN, NSET=CEDGE3
8717, 9377, 165
*NGEN, NSET=CEDGE4
8751, 9411, 165
*NSET, NSET=CEDGE
CEDGE1, CEDGE2, CEDGE3, CEDGE4
*NGEN, NSET=Z1
9542, 9576, 1
*NSET, NSET=Z2, GENERATE
9377, 9411, 1
*NFILL
Z2, Z1, 1, 165
*NGEN, NSET=CHZ1
```

```
9872, 9906, 1
*NSET, NSET=CHZ2, GENERATE
9542, 9576, 1
*NFILL, NSET=CD
CHZ2, CHZ1, 1, 330

*****ELEMENT GENERATION
*ELEMENT, TYPE=S4, ELSET=PLATE
1, 1, 2, 246, 245
*ELGEN, ELSET=PLATE
1, 162, 1, 1, 4, 244, 244
*ELEMENT, TYPE=T3D2, ELSET=FRAME
11180,8884,11180
11181,8894,11181
11182,8904,11182
11183,8914,11183
*ELEMENT, TYPE=S4, ELSET=C
977, 977, 978, 1222, 1221
*ELGEN, ELSET=C
977,162,1,1,1,244,244
*ELEMENT, TYPE=S4, ELSET=CX
1221, 1221, 1222, 1466, 1465
*ELGEN, ELSET=CX
1221, 162, 1, 1, 9, 244, 244
*ELEMENT, TYPE=S4, ELSET=C1
3417, 3417, 3418, 3662, 3661
*ELGEN, ELSET=C1
3417, 162, 1, 1, 5, 244, 244
*ELEMENT, TYPE=S4, ELSET=CURVEE
8065, 8065, 8066, 66, 65
*ELGEN, ELSET=CURVEE
8065, 34, 1, 1, 1, 8000, 8000
*ELEMENT, TYPE=S4, ELSET=CURVEE1
8228, 8065, 8066, 8229, 8228
*ELGEN, ELSET=CURVEE1
8228, 34, 1, 1, 2, 163, 163
*ELEMENT, TYPE=S4, ELSET=CURVEE2
8554, 8391, 8392, 8555, 8554
*ELGEN, ELSET=CURVEE2
8554, 34, 1, 1, 2, 163, 163

*****ELEMENT GENERATION FOR CLEAT
*ELEMENT, TYPE=S4, ELSET=CPLATE
8882, 8717, 8718, 8883, 8882
*ELGEN, ELSET=CPLATE
8882, 34, 1, 1, 4, 165, 165
*ELEMENT, TYPE=T3D2, ELSET=CFRAME
11091,4399,11091
11092,4409,11092
11093,4419,11093
11094,4429,11094
```

```
11095,4439,11095
11096,4449,11096
:
:
:
:
*ELEMENT,TYPE=S4,ELSET=CC
9542,9377,9378,9543,9542
*ELGEN,ELSET=CC
9542,34,1,1,1,165,165
*ELEMENT,TYPE=S4,ELSET=CC1
9872,9542,9543,9873,9872
*ELGEN,ELSET=CC1
9872,34,1,1,1,330,330

*****SECTION GENERATION
*SHELL SECTION, MATERIAL=STEEL, ELSET=PLATE
0.0007,
*SOLID SECTION, MATERIAL=STEEL2, ELSET=FRAME
0.005,
*SHELL SECTION, MATERIAL=STEEL, ELSET=C
0.0007,
*SHELL SECTION, MATERIAL=STEEL, ELSET=CX
0.0007,
*SHELL SECTION, MATERIAL=STEEL, ELSET=C1
0.0007,
*SHELL SECTION, MATERIAL=STEEL, ELSET=CC1
0.0007,
:
:
:
*****MATERIAL DEFINITION
*MATERIAL, NAME=STEEL
*ELASTIC
210.0E9, 0.3
*PLASTIC
350.0E6, 0
*DENSITY
7800.0,
*MATERIAL, NAME=STEEL2
*ELASTIC
800.0E9, 0.3
*PLASTIC
810.0E6, 0
*DENSITY
7800.0,

*****BOUNDARY CONDITIONS
*BOUNDARY
11091, PINNED
11092, PINNED
```

11093, PINNED
11094, PINNED
11095, PINNED
11096, PINNED
11097, PINNED
11098, PINNED
:
:
:
11183, PINNED
T1, YSYMM
T2, ZSYMM
163, ENCASTRE
245, ENCASTRE
:
:
EDGE4, ENCASTRE

*****LOAD STEPS
***UNIFORM PRESSURE IN (Pa)
*STEP, NAME=STEP1
*STATIC
*DLOAD
PLATE, P,-478.8
*END STEP
*STEP, NAME=STEP2
*STATIC
*DLOAD
PLATE, P,-1436.4
*END STEP
*STEP, NAME=STEP3
*STATIC
*DLOAD
PLATE, P,-2394
*END STEP
*STEP, NAME=STEP4
*STATIC
*DLOAD
PLATE, P,-3351.6
*END STEP
*STEP, NAME=STEP5
*STATIC
*DLOAD
PLATE, P,-4309.2
*END STEP
Note: Contact interaction was applied using CAE user interface.